Doctoral Thesis

Polish Academy of Sciences
Institute of Physical Chemistry

Iryna Voloshchuk

HYDROGEN ENTRY INTO IRON THROUGH POROUS SOL-GEL COATINGS

Dissertation completed at the
Institute of Physical Chemistry
Polish Academy of Sciences
Within International Ph.D. Studies

Supervisor:
Prof. dr hab. Tadeusz Zakroczymski

Warsaw 2011

First and foremost I would like to express my deepest gratitude to my supervisor Prof. Tadeusz Zakroczymski, whose sincere and valuable guidance helped me bring this thesis research to a successful completion. I am particularly grateful for the degree of freedom he left me.

Many thanks go to all my colleagues from the Department of Electrochemistry, Corrosion and Applied Surface Science for fine and warm working atmosphere.

I am grateful to prof. Robert Nowakowski for AFM examination.

Finally, I would like to thank my husband Roman and my sonny Oleksyk for being my source of inspiration, support and motivation.

TABLE OF CONTENTS

This work was financially supported by
the Ministry of Science and Higher Education
Research project Nr N N507 419936

1. INTRODUCTION

Hydrogen interaction with metals and alloys has been for many years a topic of considerable scientific studies and interests in various industrial branches. This interaction is manifested, among others, in deterioration of the mechanical properties of the metals. As they become more brittle, this type of corrosion is often referred to as hydrogen embrittlement. In recent years, interest in this subject has not diminished. This is due to the challenges that faced by the industrial societies, involving the replacement of the traditional energy sources by hydrogen. In such a scenario, production, storage, transportation and use of hydrogen in fuel cells become necessary. Since these hydrogen technologies are based on metallic materials, problems caused by hydrogen damage could limit the progress in the hydrogen economy.

Among various methods of avoiding or alleviating the hydrogen embrittlement problems, the surface modification of the metal seems to be especially promising. Generally, the surface modification involves chemical and metallurgical changes of the surface/near surface region and, therefore, it can prevent or reduce the entry of hydrogen into the metal, and consequently, the amount of hydrogen absorbed by the metal. For instance, electrodeposited metals [1-5], plasma nitriding [6-10] or ion implantation [11,12] markedly decrease hydrogen absorption. Another promising way to modify the metal surface is a sol-gel technology. Applying the sol-gel process, it is possible to produce a wide range of thin films and coatings of ceramic or glass materials [13,14]. Since in general, the ceramic materials are more resistant to oxidation than metals, they provide corrosion protection by forming a physical barrier between the metallic substrate and the environment. Pure and mixed oxide coating, such as ZrO_2 [15-25], SiO_2 [27-31], TiO_2-SiO_2 [13,19,34], ZrO_2-SiO_2-TiO_2 [35], ZrO_2-TiO_2 [36] were widely studied as potential corrosion-resistance coatings. Among these coatings, ZrO_2 and ZrO_2-based coatings are especially attractive not only because of their inertness, but also of high hardness and thermal expandability close to that of many metals [37,38,39].

The zirconia sol-gel coatings were mainly considered for the improving of corrosion resistance of stainless steels and other metals that naturally form a passive layer on their surface [37,40]. The applying of those coatings on mild steels or the other active, corroding metals remains questionable [41,42]. The role of sol-gel coating in preventing hydrogen absorption is even more unexplored. So far there are no literature reports on the application of sol-gel coatings, including zirconia, to counter hydrogen

absorption. However, one can expect that the presence of any sol-gel coatings, even in spite of its porous nature, should impede, at least in some extent, the entry of hydrogen into the substrate metal. Hence, the objective of this work was to study how the sol-gel coatings, based on zirconia, influence the entry of hydrogen into a metal, specifically into iron.

2. LITERATURE REVIEW

2.1. Hydrogen in iron

Studying the possible effect of the sol-gel coatings on hydrogen entry into and on hydrogen absorption inside the substrate metal, it is worthy to outline these processes in relation to the uncoated metal. There has been a great amount of works devoted to these processes, and a lot of valuable information were collected in conference proceedings [43-50] and in monographs [51-53]. Nevertheless, the interaction of hydrogen with metals, especially with iron and steels, still surprises its complexity. The main reasons for this state are the ubiquity of the sources of hydrogen and the unique properties of the iron-hydrogen system.

2.1.1. Hydrogen entry and hydrogen evolution

Small size of hydrogen atom and its simple electronic structure cause that this element easily enters into metals, especially into those having relatively loose lattice structure, e.g. iron. The entry of hydrogen into the metal may occur from both gaseous environments and electrolyte solutions. It is commonly believed that regardless of the environment, hydrogen entry (HE) is preceded by adsorption of hydrogen atoms on the metal surface. Thus, the entry process can be expressed as follows [54,55]:

$$MH_{ads} \rightarrow MH_{abs} \qquad (1)$$

where MH_{ads} is hydrogen atom adsorbed on the metal surface, and MH_{abs} is hydrogen atom already inside the metal, just beneath its surface. Depending on the type of environment, the formation of MH_{ads} is a result of different processes. In the experiments of this work, hydrogen was generated on iron during its cathodic polarization in an aqueous NaOH solution. Thus, the entry of hydrogen was directly related to the hydrogen evolution reaction (HER) in alkaline solutions and this process will be described below.

In aqueous, alkaline solutions, the HER can be represented by the overall equation

$$2H_2O + 2e \rightarrow H_2 + 2OH^- \qquad (2)$$

The first step of HER is discharging of water molecules and consequently the adsorbed hydrogen atoms MH_{ads} are produced on the metal surface

$$H_2O + M + e \rightarrow MH_{ads} + OH^- \quad (3)$$

The discharge step is followed by either a chemical desorption (recombination) step

$$MH_{ads} + MH_{ads} \rightarrow H_2 + 2M \quad (4)$$

or an electrochemical desorption step

$$MH_{ads} + H_2O + e \rightarrow H_2 + OH^- + M \quad (5)$$

Alternatively to the desorption stages (4) and/or (5), some of the adsorbed atoms MH_{ads} can enter into the sub-surface layer of the metal according to Eq. (1). Thus the processes (1) and (4) or (5) compete with each other. Bockris et al. [54]. have studied the HER on iron in 0.1 M NaOH and have concluded that the reaction mechanism is coupled discharge-chemical desorption at low extent of adsorption of hydrogen atoms , i.e. at low coverage θ, with the discharge step being rate determining.

2.1.2. Hydrogen forms in iron

After entering into the metal, hydrogen atoms occupy the interstitial sites in the iron lattice forming a solid solution. This is a basic and clearly defined form of hydrogen in the metal. However, it appears that this is not the only form of hydrogen in iron, as it is evidenced by the experimental data on hydrogen diffusivity and solubility [56-58]. It is characteristic that measurements of the diffusion coefficient for hydrogen in iron at room temperature often give much lower values (in range from 10^{-5} to 10^{-9} cm^2/s), than those expected by extrapolation from higher temperatures data (near 10^{-4} cm^2/s). On the other hand, a relatively strong hydrogen charging, e.g. using cathodic polarization, involves introduction into the iron of much greater amounts of hydrogen (even 100 wt. ppm) than those corresponding to the saturated interstitial solid solution (only about 5×10^{-4} wt. ppm).

It is generally acknowledged that the above anomalies are due to the retention of hydrogen at defects in the metallic structure. These defects act as traps for hydrogen atoms, ions and molecules, slow down the transport of hydrogen and increase the amount of absorbed hydrogen. Thus, one can assume that at low and moderate temperatures, hydrogen can occur in iron in at least three different forms [59]:

a) as the above mentioned interstitial solid solution;
b) as atoms attached to the structure defects, especially to dislocations;
c) as molecular hydrogen accumulated in the internal microcracks and blisters.

At the lowest concentrations, the all absorbed hydrogen exists in the form (a), at medium concentrations, both the forms (a) and (b) are present, and at the highest concentrations, all three forms of hydrogen coexist.

Strictly speaking, only hydrogen as a component of the interstitial solid solution (a) is able to move inside the metal according to the laws of diffusion. Therefore this form of hydrogen is often called as the "diffusible" hydrogen and it is denoted as H_d. In turn, hydrogen attached to the structural defects is more tightly bound with the metal and it shows lesser mobility. Hence, this form of hydrogen is generally called as the "trapped" hydrogen and it is designated as H_t. The variety of defects in metal structure makes the binding energy of hydrogen with traps, and hence the release energy of hydrogen from traps is different. The relatively week hydrogen traps are dislocations, grain and interphase boundaries. These defects are considered as more or less reversible traps. Finally, the strong bound form of hydrogen in the metal is the molecular (gaseous) hydrogen accumulated in the closed blisters and microcracks. The latter form of hydrogen may be considered at room temperature as hydrogen irreversibly trapped.

2.2. Hydrogen permeation and desorption techniques

The electrochemical permeation technique by Devanathan and Stachurski [60] and its adaptation [61-64], relating to hydrogen desorption, have proved to be very useful in studies of hydrogen in metals and alloys. Since these both techniques are based on the electrochemical detection of hydrogen, they are simple, convenient, high sensitive, and flexible with regard to experimental condition. While the permeation technique allows to characterize the diffusible hydrogen, the desorption one provides information on the trapped hydrogen [65-69].

2.2.1. Hydrogen permeation

In the electrochemical permeation technique, here adapted for the experimental conditions of this work (Fig. 1), a thin metal (iron) membrane of thickness L is mounted between two independent electrochemical cells. The entry side of the membrane ($X = 0$) is brought into contact with a hydrogen source. For example, it is cathodically polarized in the appropriate electrolyte solution at a current density i_c or potential E_c. In the case of iron and steels, the major part of adsorbed hydrogen atoms MH_{ads}, produced on the cathode surface (equation (3)), usually undergoes chemical desorption (equation (4). However, a part of MH_{ads} enters into the membrane according to equation (1), diffuses through the membrane and leaving its opposite, exit side ($X = L$). This exit side is anodically polarized in an alkaline solution at a suitable, constant potential E_a, allowing the electrochemical oxidation of MH_{ads}

$$MH_{ads} + OH^- \rightarrow H_2O + M + e \qquad (6)$$

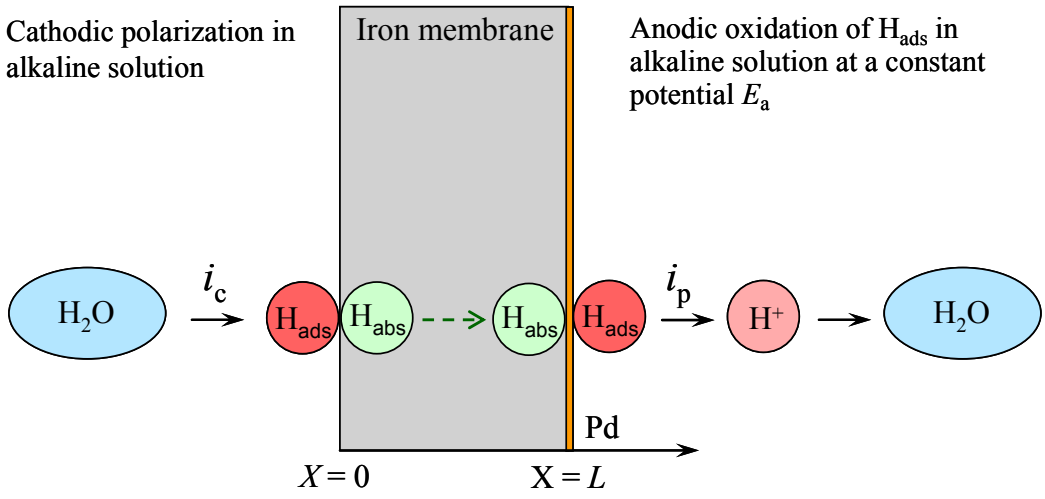

Fig. 1. Diagram showing the electrochemical hydrogen permeation technique.

The measured anodic current density (i_a), minus the background current density, i.e the steady-state anodic current density for the hydrogen-free membrane, is a measure of the permeation rate of hydrogen through the membrane (i_p). It is worthy to note that the electrochemical detection of hydrogen is very accurate - the current density i_p of

1 μA/cm^2 corresponds to the hydrogen flux of 1.04×10^{-11} mol H/cm^{2}s. In the case of iron membranes, to maximize the efficiency of the oxidation of hydrogen atoms according to equation (6), as well as to minimize the background current, in fact the passivation current of iron in alkaline solutions, the membrane exit side is often coated with a thin layer of palladium, e.g. by electroplating.

The practical use of the permeation technique is based on the assumption that well defined conditions controlling hydrogen entry are established at the entry side of the membrane. It means that the measured hydrogen permeation rate of hydrogen is fully controlled by its transport in the membrane. In this case, the hydrogen permeation may be described by a relatively simple mathematical model [61]. Namely, when the transport of hydrogen atoms consists in the lattice diffusion with a constant coefficient D (i.e. the diffusible hydrogen is considered), the diffusion paths are identified with the membrane thickness L, and the concentration of hydrogen beneath the entry side of the membrane C_0 changes rapidly according to Fig. 2a, the permeation rate is described by the following equations:

Build-up

$$\frac{i_\mathrm{p}-i_\mathrm{p}^\mathrm{o}}{i_\mathrm{p}^\infty-i_\mathrm{p}^\mathrm{o}}=\frac{2L}{\sqrt{\pi Dt}}\sum_{n=0}^{\infty}\exp\left(-\frac{(2n+1)^2L^2}{4Dt}\right) \tag{7}$$

Decay

$$\frac{i_\mathrm{p}-i_\mathrm{p}^\infty}{i_\mathrm{p}^\mathrm{o}-i_\mathrm{p}^\infty}=1-\frac{2L}{\sqrt{\pi Dt}}\sum_{n=0}^{\infty}\exp\left(-\frac{(2n+1)^2L^2}{4Dt}\right) \tag{8}$$

where i_p is the measured permeation rate at time t, i_p^o is the initial steady-state permeation rate ($t=0$), i_p^∞ is the new steady-state permeation rate ($t\to\infty$). For the build-up $i_\mathrm{p}^\infty>i_\mathrm{p}^0$, and for the decay $i_\mathrm{p}^\infty<i_\mathrm{p}^0$. The permeation transients are represented by the suitable curves shown schematically in Fig. 2b. The fitting of pertinent permeation equation (7) or (8) to the experimental permeation transients leads to the determination of the diffusion coefficient D.

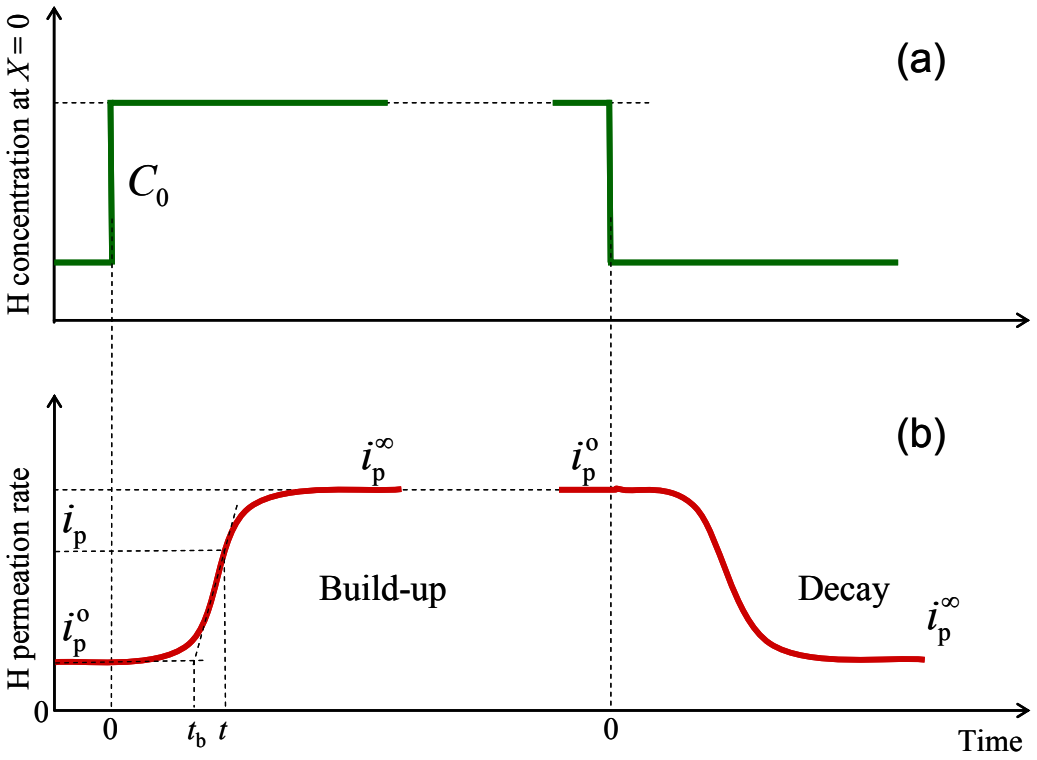

Fig. 2. Schematic presentation of the ideal permeation transients; C_0 = const, fully diffusion control.

The fitting of the permeation equation to the whole experimental permeation curve seems to be the most correct way to determine the diffusivity of hydrogen. The other, even simpler way is based on the chosen, characteristic points of the permeation transient. One of these characteristic points is that corresponding to the so called breakthrough time t_b, which resulted from the intersection of the tangent at the inflection point of the permeation rate-time curve with the initial permeation level [60,70]. In the linear time scale, the appropriate relationship between D and t_b is as follows

$$D = \frac{0.051L^2}{t_b} \tag{9}$$

while for the logarithmic time scale

$$D = \frac{0.064L^2}{t_b} \tag{10}$$

Knowing D one can calculate, for a given steady state permeation rate i_p^∞, the concentration of hydrogen in the membrane at its entry side C_0, using the following equation for the steady state hydrogen flux:

$$i_p^\infty = \frac{FDC_0}{L} \tag{11}$$

hence

$$C_0 = \frac{i_p^\infty L}{FD} \tag{12}$$

Since it was assumed that D is constant, independent on hydrogen concentration, the steady-state distribution of the diffusible hydrogen in the membrane is represented by a linear gradient

$$C = C_0\left(1 - \frac{X}{L}\right) \tag{13}$$

and the steady state amount of the diffusible hydrogen in the membrane (in mol H per unit area of the membrane) equals

$$q = \frac{C_0 L}{2} \tag{14}$$

For iron membranes, the above ideal picture, taking into account only the diffusible hydrogen, is rather rare, especially with reference to the first charging of the fresh ($i_p^o = 0$), hydrogen-free membrane, as well as to the complete decay ($i_p^\infty = 0$), after removing the hydrogen source - Fig. 3. In the first case, the permeation rate is not

controlled by diffusion only, but also by slow surface processes (involving hydrogen entry) and/or hydrogen trapping (involving hydrogen transport). For these reasons, the concentration of hydrogen C_0 at the entry side does not increase suddenly (Fig. 3a, left) and/or hydrogen atoms are stopped by traps and, consequently, the permeation rate of hydrogen may be delayed and it increases slowly (Fig. 3b, left). In the second case, in spite of the sudden drop of the concentration C_0 to zero, after removing the hydrogen source at the membrane entry side (Fig. 3a, right), the permeation rate decreases slowly (Fig. 3b right). Moreover, after some time, the permeation rate practically reflects the release of hydrogen from traps.

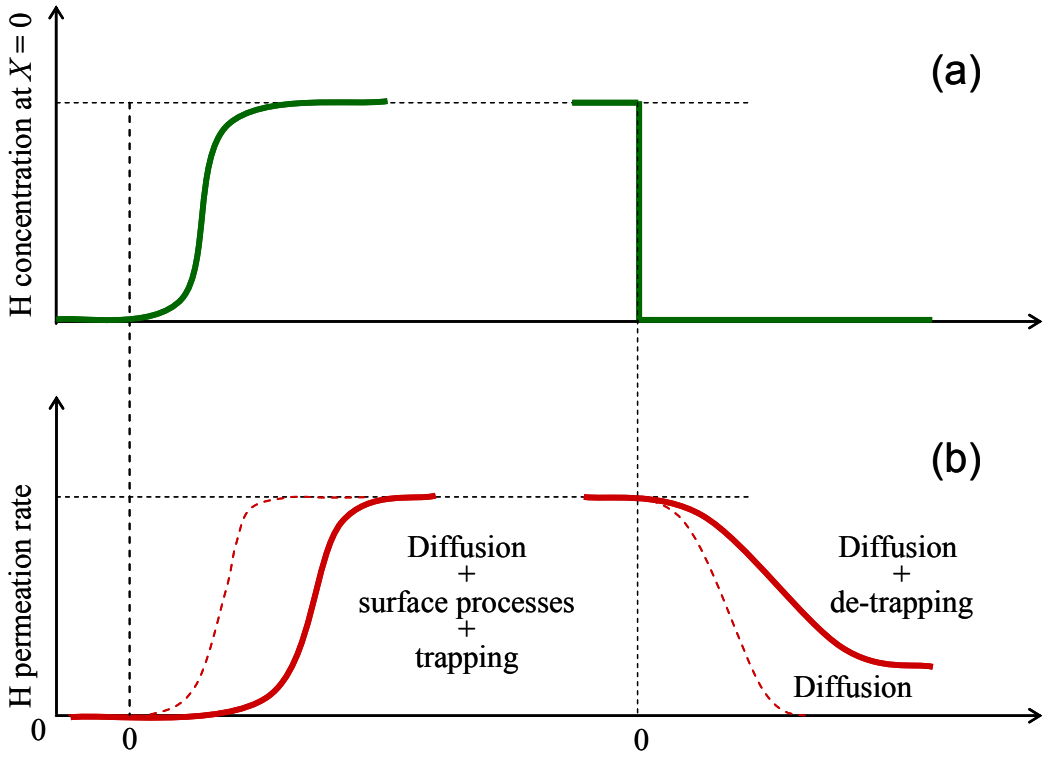

Fig. 3. Schematic presentation of the real permeation transients: first build-up (a) and complete decay (b).

In the above circumstances, it is obvious that there are no exact fitting of the equations (7) or (8) to the suitable permeation transients shown in Fig. 3, and the resulted values of D can be treated only as values of the effective (apparent) hydrogen diffusivity D_{eff}. Values of the effective diffusivity can be significantly, even two order of magnitude lower than that of the real, lattice diffusion coefficient [56,57].

However, as it was found earlier [71,72], the undesirable effects of slow surface processes (involving hydrogen entry) and trapping (involving hydrogen transport) are not observed for the pre-charged membrane during the partial build-up or decay transients caused by a relatively small increase or decrease of hydrogen concentration C_0. In this case, the permeation transients are described by the equations (7) or (8) and their courses are like that shown earlier in Fig. 2b. Consequently, the fitting procedure leads to values of D which can be considered as the real diffusivity of hydrogen.

Considering the permeation of hydrogen through the membrane charged with cathodically produced hydrogen, it is worthy to note that the steady-state permeation rate is at the most proportional to the square root of the cathodic current density

$$i_{\mathrm{p}}^{\infty} = k\sqrt{i_{\mathrm{c}}} \tag{15}$$

where k is a coefficient characteristic of a given metal and hydrogen charging conditions. The above dependence, first observed by Bodenstein [73], has been confirmed in many experiments and it is considered as a characteristic feature of the cathodic charging. It is also explicit evidence that the entry of hydrogen into the metal is preceded by adsorption of hydrogen atoms on its surface.

2.2.2. Hydrogen desorption

Using the electrochemical permeation technique, under some experimental conditions, it is possible to characterize the mobility (D) and solubility or concentration (C) of the diffusible hydrogen, because only this form of hydrogen is "visible" by the measured hydrogen flux (i_{p}). The other hydrogen forms comprising the reversibly trapped hydrogen may be characterized using the electrochemical desorption technique [62,63]. A practical approach for the effective use of this technique is described in paper [64].

The desorption of hydrogen is carried out when hydrogen permeation rate through the membrane achieved a steady-state permeation rate i_{p}^{∞}. The hydrogen charging at the entry side of the membrane ($X = 0$) is switched off and a suitable anodic

potential (usually the same like that at the membrane exit side ($X = L$)) is immediately applied. Subsequently, the anodic currents are measured at both sides of the membrane.

The anodic current density at the membrane exit side $i_{a,L}$ practically equals to the desorption rate of hydrogen at this side $i_{H,L}$, because the background current density i.e. the passivation current density of iron in NaOH after long time is negligible. However, the applied anodic potential at the entry side causes also the significant oxidation of the cathodically treated metal. Therefore, to obtain the desorption rate of hydrogen at the entry side $i_{H,0}$, the measured current density $i_{a,0}$ must be corrected by a current density i_{Me}, measured in the separate experiment with a hydrogen-free membrane.

In turn, the desorption rates of hydrogen $i_{H,L}$ and $i_{H,0}$ are sums of the suitable desorption rates of the diffusible hydrogen ($i_{Hd,L}$ and $i_{Hd,0}$) and reversibly trapped one ($i_{Ht,L}$ and $i_{Ht,0}$), escaping from the membrane its exit and entry side, respectively. Knowing D and assuming that the steady state permeation rate $i_{p,\infty}$ is at the same time the initial desorption rate of the diffusible hydrogen $i^{o}_{Hd.L}$ at the membrane exit side, one can reconstruct the desorption rate-time curves for the diffusible hydrogen. For the membrane exit side, the following equation, similar to the equation (8) can be used

$$\frac{i_{Hd,L}}{i^{o}_{Hd,L}} = 1 - \frac{2L}{\sqrt{\pi Dt}} \sum_{n=0}^{\infty} \exp\left(- \frac{(2n+1)^2 L^2}{4Dt} \right) \tag{16}$$

while for the membrane entry side the suitable equation is as follows [62,74]

$$\frac{i_{Hd,0}}{i^{o}_{Hd,L}} = -1 + \frac{L}{\sqrt{\pi Dt}} \left\{ \sum_{n=0}^{\infty} \exp\left(- \frac{n^2 L^2}{Dt} \right) + \sum_{n=0}^{\infty} \exp\left(- \frac{(n+1)^2 L^2}{Dt} \right) \right\} \tag{17}$$

Then, subtracting the desorption rates $i_{Hd,L}$ and $i_{Hd,0}$ from the measured desorption rates $i_{H,L}$ and $i_{H,0}$, the suitable desorption rates of the trapped hydrogen $i_{Ht,L}$ and $i_{Ht,0}$ are determined.

Finally, integration of the individual desorption rate-time curves with respect to time leads to the amounts of the diffusible hydrogen $q_{Hd,L}$ and $q_{Hd,0}$, the trapped hydrogen $q_{Ht,L}$ and $q_{Ht,0}$, their sum $q_{H,L}$ and $q_{H,0}$ leaving the membrane its exit and entry side,

respectively, and the total amount of hydrogen in the membrane $q_H = q_{H,L} + q_{H,0}$. With reference to the diffusible hydrogen, an analytical integration is possible. Taking equations (16) and (17), the final amounts of the diffusible hydrogen, i.e. for $t \to \infty$, are

$$q_{Hd,L} = \frac{i^{o}_{Hd,L} L^2}{6FD} = \frac{C_0 L}{6} \tag{18}$$

and

$$q_{Hd,0} = \frac{i^{o}_{Hd,L} L^2}{3FD} = \frac{C_0 L}{3} \tag{19}$$

Hence, the total amount of the diffusible hydrogen in the membrane equals

$$q_{Hd} = \frac{i^{o}_{Hd,L} L^2}{2FD} = \frac{C_0 L}{2} \tag{20}$$

which is consistent with the previous equation (14).

An important conclusion from the above relationships is that the fraction of the diffusible hydrogen escaping at the membrane exit side is $q_{Hd,L}/q_{Hd} = 1/3$, while the fraction leaving the membrane its entry side is $q_{Hd,0}/q_{Hd} = 2/3$. These ratios correspond to the linear concentration gradient of the diffusible hydrogen (equation (13)). Therefore, it can be inferred by analogy that for the ratios $q_{Ht,L}/q_{Ht}$ and $q_{Ht,0}/q_{Ht}$ different than 1/3 and 2/3, respectively, the distribution of the trapped hydrogen (or strictly speaking, the filling of traps) cannot be linear across the membrane.

2.3. Sol-gel chemistry

For many years, researchers have become increasingly interested in the sol-gel processing. Ebelman was the first (1845) to report the formation of a transparent material as a result of slow hydrolysis of an ester of the silicic acid. Today sol-gel methods are reaching their full potential, enabling the preparation of new generations of advanced materials. In the field of corrosion, the sol-gel materials as protective coatings have been extensively studied in recent years.

In order to discuss the using of zirconia sol-gel coatings for corrosion protection (including its possible application against hydrogen embrittlement), it is worth to review briefly the sol-gel chemistry. In this chapter, the main idea of the sol-gel technique, factors that influence on the final properties of sol-gel coatings, and their applications for corrosion protection will be described.

2.3.1. Basic principles of sol-gel process

The sol-gel process is a chemical synthesis method. Initially it was used for the preparation of inorganic materials such as glasses, ceramics and thin films. Generally, the sol-gel process is based on the evolution of the sol (colloidal suspension of very small, 1-100 nm particles in a liquid medium) into the form of gel that is defined as a colloidal system. The sol-gel chemistry is based on creating the oxide network through hydrolysis and condensation of metal alkoxides in organic solvents [75-77]. As known [75,78], there are two methods of preparing the sol-gel coating: inorganic and organic. The difference is based on the nature of precursors: metals salts in aqueous solution or metal alkoxides in organic solvents. In both cases, the result of condensation of „sol" and formation of clusters or colloids is the final network in continuous liquid phase - „gel".

The initial materials used in the preparation of the sol are mainly metal organic compounds, such as metal alkoxides $M(OR)_z$, where, M represents the network-forming elements, for example Al, Si, Ti, Zr etc.; R is typically an alkyl group ($-CH_3$, $-C_2H_5$, etc.); and z is the oxidation state of the metal atom M^{z+} [78,79]. Generally, the formation of sol-gel occurs in six stages: hydrolysis, condensation, gelation, ageing, drying and densification [77,80].

1. Hydrolysis

The first step is the hydrolysis of the metal alkoxide (for example zirconium alkoxide) and it can occur by acid or base-catalysed processes, as shown in the following reactions

$$Zr(OR)_4 + nH_2O \rightarrow Zr(OR)_{4-n}(OH)_n + nROH \qquad (21)$$

$$Zr(OR)_{4-n}(OH)_n + (4-n)H_2O \rightarrow Zr(OH)_4 + (4-n)ROH \quad (22)$$

During the hydrolysis stage, the alkoxide groups (−OR) are replaced with hydroxyl groups (−OH) due to the interaction of alkoxide molecules with water. The mechanism of reactions (reactions (21) and (22)) proceeds in three stages [13,76]. First, the metal atom from the alkoxide molecule undergoes nucleophilic attack by the oxygen atom from the water molecule. While the zirconium atom is in the penta-coordinated state, a proton is transferred from the water molecule to a −OR group on the same Zr atom. Finally, the ROH molecule is released from the zirconium atom [76].

2. Condensation

Two partially hydrolyzed molecules can link together in a reversible condensation reaction, such as:

$$Zr(OR)_3OH + HOZr(OR)_3 \rightarrow (RO)_3ZrOZr(OR)_3 + HOH \quad (23)$$

$$Zr(OR)_3OR + HOZr(OR)_3 \rightarrow (RO)_3ZrOZr(OR)_3 + ROH \quad (24)$$

During the condensation reactions, two −OH groups (23) or −OH with −OR group (24) produced the same ≡Zr−O−Zr≡ bridge, and low-molecular weight by-products (water and alcohol) produced. The hydrolysis and condensation reactions occur simultaneously.

3. Gelation

With time, the colloidal particles and condensed zirconia species link together to become a three-dimensional network. In this structure Zr atom is joined to neighbouring Zr atoms by oxygen bridges. Hydroxide or functional groups are attached to some zirconium atoms. The gel network depends greatly upon the size of particles and on the extent of cross-linking prior to gelation.

As known [81], the acid or base catalysts can influence both the hydrolysis and condensation rates and the structure of the condensed products. Thus, the newly formed gel structure depends on the selected catalyst (Fig. 4). Basic catalysis leads to the formation of more highly branched polymeric networks. In addition, the highly cross-

linked large sol particles are initially formed, which later link to gel with large pores between interconnected particles. In the case of the acid-catalyzed hydrolysis-condensation, the primary linear or randomly branched polymers with the open network structure are formed [75,81].

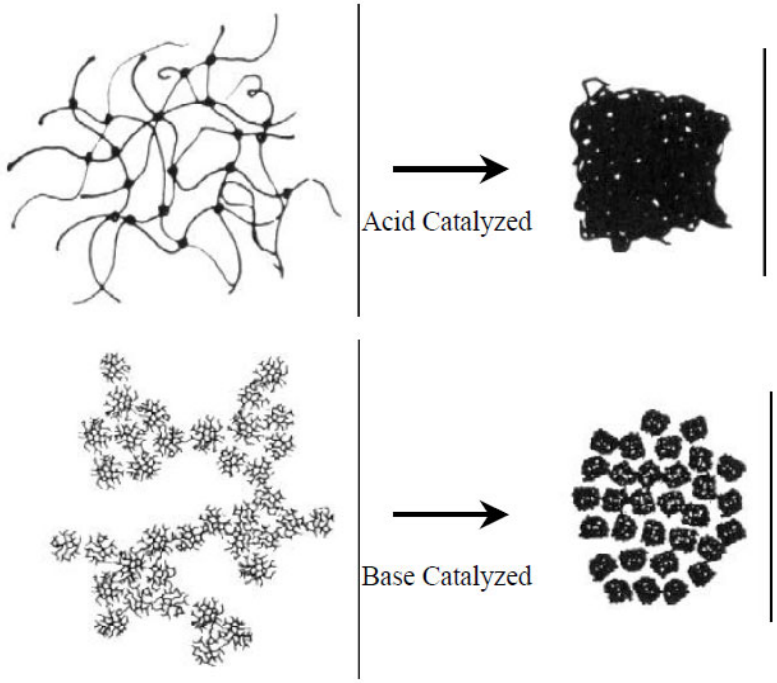

Fig. 4. Scheme of the gel structure for acid and base catalyzed reactions [75].

4. Ageing

Gel aging is an extension of the gelation and during this stage the gel network is reinforced through further polymerization, possibly at different temperature and solvent conditions. During the ageing the expulsion of solvent from the pores leads to the gel matrix shrinkage. As a result, the size of pores, which are under the stress, is changed.

5. Drying

The drying consists of evaporation of small molecules (water, alcohol and other volatile components), and as a consequence the shrinkage of gels occurs. These processes are basically affected by the initial reaction conditions, such as pH, temperature, molar ratios of reactants, solvent compositions, etc.

6. Densification

Heat treatment at above 500° C is necessary for the production of dense glasses and ceramics from gels.

As known [81], the hydrolysis and condensation reactions occur concurrently, but one reaction can be favoured over the other depending on circumstances. The physicochemical properties (transparency, porosity, pore size, surface functionality) of sol-gel derived materials depend on the composition of sol and processing conditions. The main variables that will play a significant role on the preparation of sol-gel coating and strongly influence on the final morphology and structure are: the nature of the precursors (hydrophilic/hydrophobic) [77], type of catalyst (acid or base) [82,83], pH [76,77], nature of the solvent and ratio of solvent to precursor [77,84], temperature [76,85], humidity and aging (storage) conditions, and another factors. It is the most important advantage of the sol-gel process that the desired characteristics of the resulting materials can be obtained by the change of preparation procedure. In addition, the sol-gel materials have other very important advantages, such as:

- compatibility with many organic and inorganic reagents,
- the pore size and shape of sol-gel materials can be controlled,
- the synthesis can be performed (except densification stage) under mild (atmospheric) conditions,
- the sol-gel method give opportunity to obtain not only one layer coating but also multilayer and multicomponents coatings,
- the sol-gel method is relatively simple and not very expensive,
- sol-gel coatings can be prepared with high degree of chemical purity and with easy control of stoichiometry.

However, there are some disadvantages of the sol-gel methods. They are: sensitivity to the moisture of precursors, time-consuming, changing the dimensions of coatings as a result of their densification and shrinkage, and stress cracking during drying [75-77].

2.3.2. Deposition of sol-gel coatings by spin technique

Sol-gel coatings can be deposited on the metal substrate through various techniques. The most widely used are the spin-coating and dip-coating [86-89]. The other applied methods are: spraying [90-92] and electrochemical deposition [93-95]. In

this work, the sol-gel coatings were obtained using the spin-coating technique and, therefore, this technique will be described in detail.

Generally the spin coating is carried out in four basic stages: deposition of the sol, spin up, spin off, and gelation by solvent evaporation (Fig. 5).

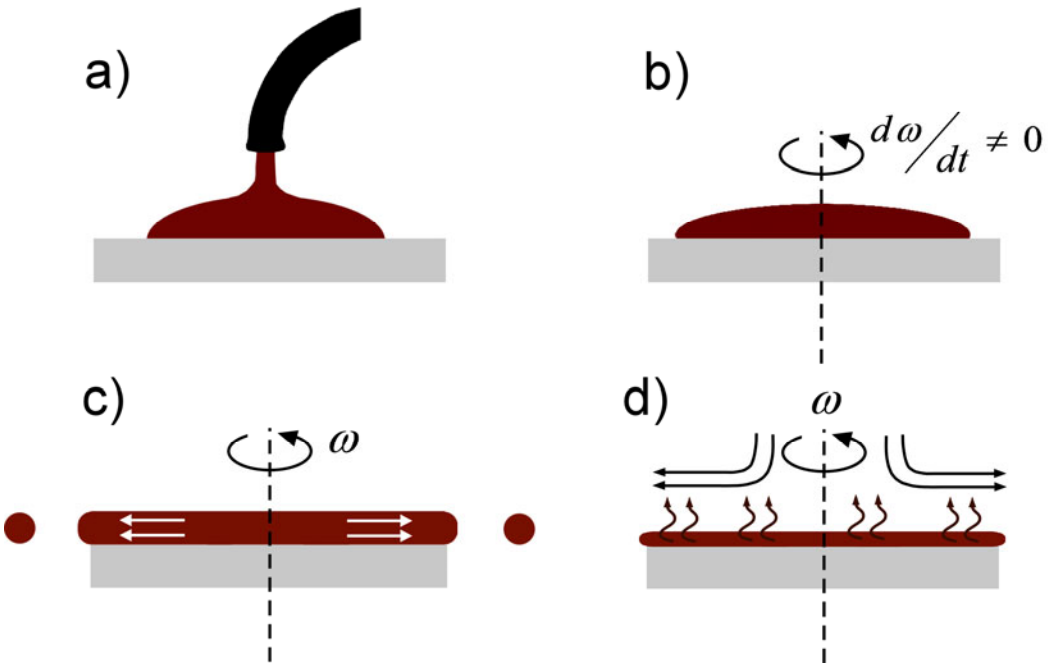

Fig. 5. Typical stages of the spin coating [89].

The first step of spin-coating involves deposition a small amount of sol solution onto the centre of a substrate. Then the substrate is rotated at a relatively high speed in order to spread the fluid by centrifugal force. Rotation is continued for some time, with fluid being spun off the edges of the substrate, until the desired film thickness is achieved. The solvent is usually volatile, providing for its simultaneous evaporation. The film-forming is primarily driven by two independent parameters - the sol viscosity and the spin speed of substrate. In general, lower viscosity, higher spin speeds and longer spin times produce thinner films.

2.3.3. Applications of sol-gel materials

The sol-gel coatings are interesting from both the scientific and application's point of view. These coatings are often used in the various industrial branches. An outline of the current and potential applications of the sol-gel materials is given below.

Using the sol-gel technology, a wide range of materials can be produced, such: thin films and coatings, monoliths, powder, fibres, composites, porous gels and membranes, and it is not the last of this long list (Fig. 6).

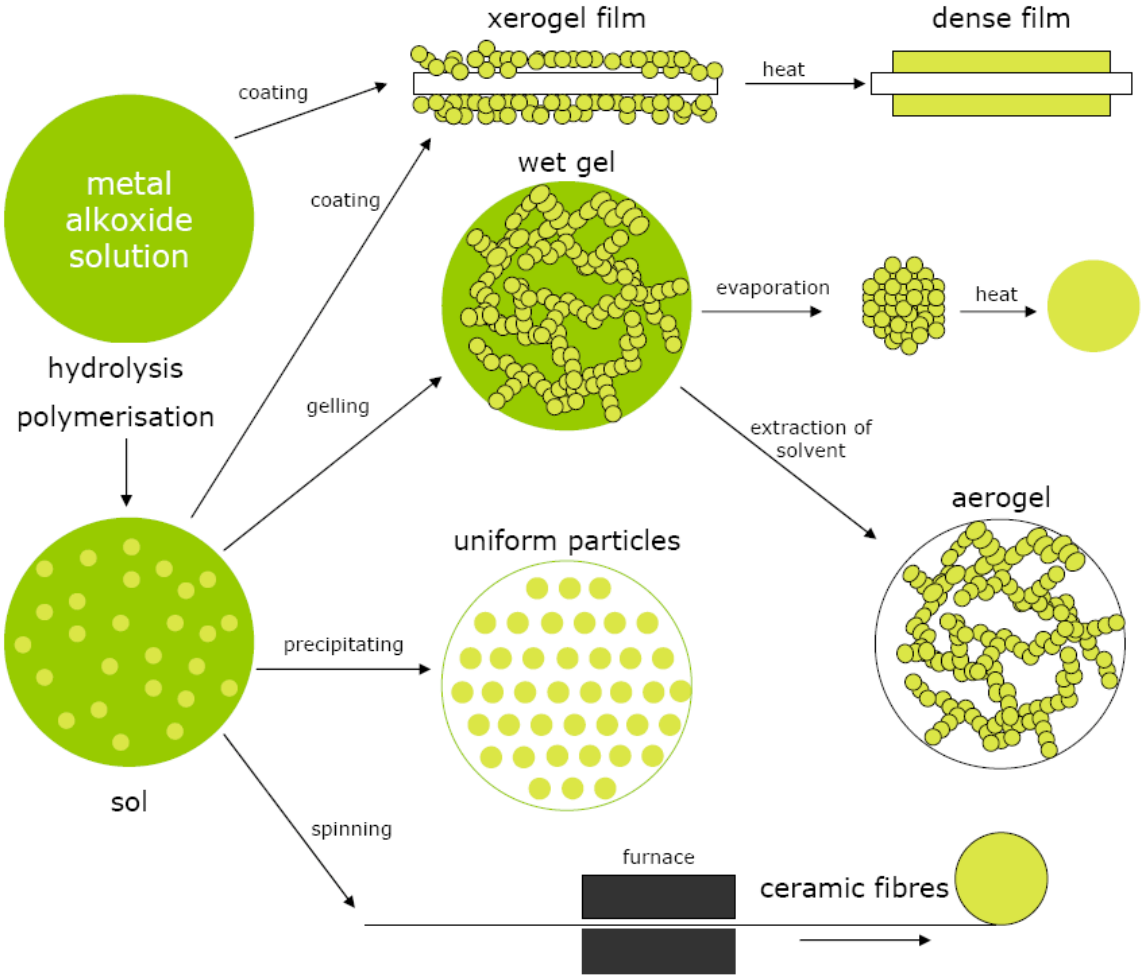

Fig. 6. Sol-gel preparing and its products [96].

The sol-gel materials are applied in electrotechnics, electronics, chemical technologies, biochemistry etc. (Table 1).

Table 1. The application of sol-gel materials [13,96].

Optical and photonic functions	Fluorescence solar collector, solar cell. Laser element, light guide, optical switching, light amplification, antireflecting coatings, non-linear optical effect (second generation).
Electronic functions (ferroelectricity, electronic and ionic conduction)	Capacitor, piezoelectric transfer. Non-volatile memory, transparent semiconductors. Solid electrolyte (battery, fuel cell).
Thermal function	Refractory ceramics, fibers wood, aerogels. Low expansion ceramics.
Mechanical functions	Protection with hard coat, strong ceramics abrasive.
Chemical functions	Catalyst, membrane, gas barrier, repellent film.
Biomedical functions	Entrapment of enzyme, cell, coated implant, medical tests.

2.4. Zirconia sol-gel coatings

In this chapter the application of zirconia (ZrO_2) sol-gel coatings for corrosion protection of metals and alloys are considered. Zirconia sol-gel coatings are well known materials which has excellent properties, such as high mechanical strength, ionic conductivity and chemical durability. Hence, zirconia coatings are highly promising for use as thermal and diffusion barriers and as barriers against oxidation of the metal substrate. In addition, ZrO_2 coatings are very hard and they are potentially useful as wear resistant coatings, especially in environments where heat and corrosion resistance are required [97].

Porous ZrO_2 sol-gel coatings as membranes can be applied in aqueous filtration with much better alkali durability than other ceramic membranes, particularly at high temperature and in chemically harsh conditions [37]. Zirconia coatings are also very interested as catalysts for some selected reaction [98]. Zirconia sol-gel coatings, owing to their excellent chemical stability in aqueous solutions (including basic and alkaline) are often used as corrosion-resistance coatings [99].

One of the important applications of zirconia coatings is improving the corrosion resistance of some metals and alloys, including stainless steels years [21,97,99,100]. Stainless steels, in spite of their natural, high corrosion resistance have a tendency to corrode in extraordinary aggressive environments. That is why, in recent years, researches have become increasingly interested in preparing the adhesive, stable, chemically resistance, inert and long lasting coatings for efficient preventing of corrosion. Unlike the stainless steels, there are only a few reports dedicated the effect of ZrO_2 coatings to corrosion protection of mild steels [21,101,102].

Some studies on the protection effect of ZrO_2 coatings on metals and alloys against high temperature corrosion [16,17], acid attack [17-19,22,23], and corrosion in aqueous NaCl solutions [20,24] are described in more detail below.

2.4.1. High temperature corrosion

Some studies have focused on the using of zirconia sol-gel coating for corrosion protection of metals and its alloys in high temperature conditions. Most of that reports comes from Atik's group [16-20,29]. The anticorrosion properties of ZrO_2 coatings on 316L steel at high temperatures was studied by M. Atik and Aegerter [17]. The coatings were deposited by the dip technique. The oxidation resistance of the ZrO_2 coatings was determined by measurements of weight gain (Fig. 7). The experimental results show that the weight of the coated membranes remains almost unchanged with time, whereas for uncoated membranes a significant weight increasing was observed. The anticorrosion properties of zirconia coatings were associated with their thickness. The samples with coating less than 40 nm thick had good chemical durability and resistance against oxidation. However, the coatings thicker than 40 nm were destroyed and their protective effect was lower.

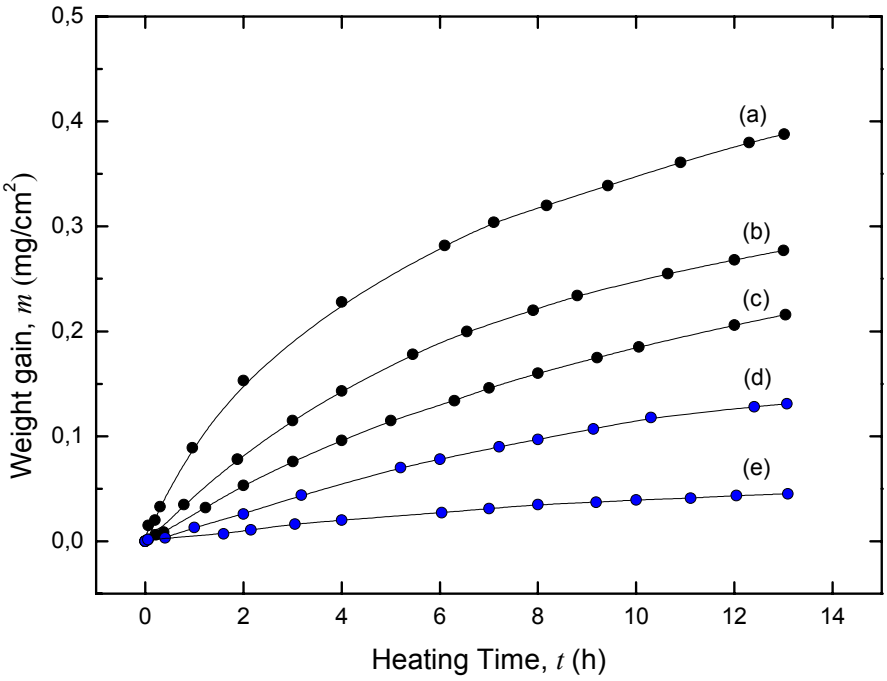

Fig. 7. Weight gain (mg/cm^2) of 316L stainless steel sheets measured as a function of the time of isothermal oxidation treatment in air at different temperatures. (a)-(c) Uncoated substrates tested at 950, 870 and 800 °C, respectively. (d)-(e) ZrO_2 coated substrates tested at 800 ^oC: (d) Film thickness 35 nm, (e) film thickness 5.5 nm and rapid heating process (samples inserted at 800 ^oC [17]).

The similar situation was observed in the case of ferritic stainless steel [16]. It was also noted, that the anticorrosion properties of ZrO_2 coating were mainly depends on the heating temperature and the thickness of coating. The total corrosion rate was evaluated by measuring the weight gain as a function of heating time, and ellipsometry measurements were performed to asses the thickness of coatings.

As it was mentioned, the use of zirconia coatings on mild steel paid less attention. As it was shown [101], the corrosion protection effect depended strongly upon the thickness of the coatings. The deposited one and three layers of zirconia were not effective, because of holes and cracks present in the coatings (Fig. 8). In addition, it was noted that the oxidation kinetics is controlled by a uniform diffusion of the reactant through a growing dense scale. Namely, the thicker coating is more effective in delaying oxidation of the metal substrate. As expected, the single-layer and three-layer coatings

were less protective due to short diffusion paths and a few holes, whereas the thickest samples coated by six depositions exhibited excellent protective effect.

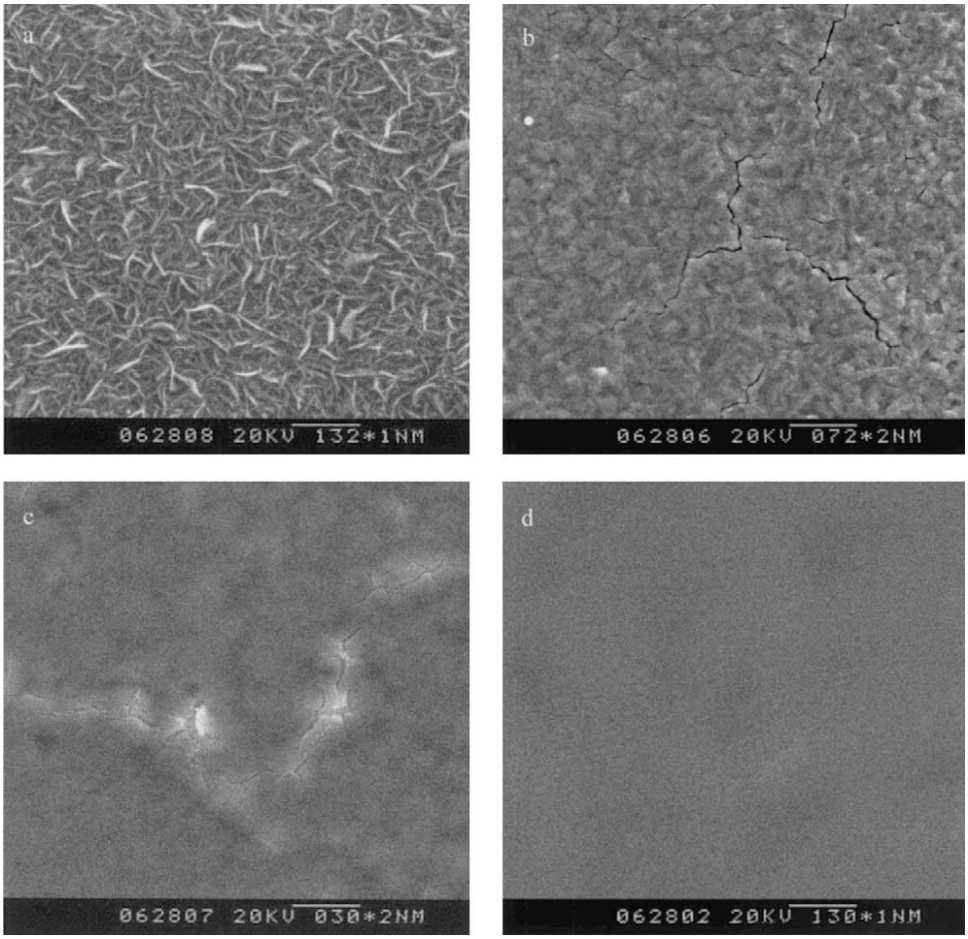

Fig. 8. SEM micrographs of samples of mild steels without and with zirconia sol-gel coatings after oxidation in air at 500 °C for 8h: (a) as received; (b) one layer; (c) three layers; and (d) six layers [101].

2.4.2. Corrosion in acid solutions (H_2SO_4)

The anticorrosion protection of 316L steel by the ZrO_2 coatings was studied in 15% H_2SO_4 solution by potentiodynamic measurements at different temperature up to 50 ^oC [19]. The results obtained are shown in Fig. 9. The ZrO_2 coatings with thickness less than 0.5 μm effectively protected the steel, whereas thicker coatings were less effective because of cracks in the coating. The coatings influence on the cathodic and anodic branches of the potentiodynamic curves. The slope of the cathodic curves was practically the same for the uncoated and zirconia coated specimens. However, the

cathodic current for the coated specimen was lower than that observed for the uncoated one. The coating had also a strong influence on the anodic parts of the polarization curves in the passive region - the suitable current decreased. The obtained results indicate that corrosion mechanism for coated and uncoated samples remains unchanged and ZrO_2 sol-gel coatings act as geometric blocking layers against the corrosion media.

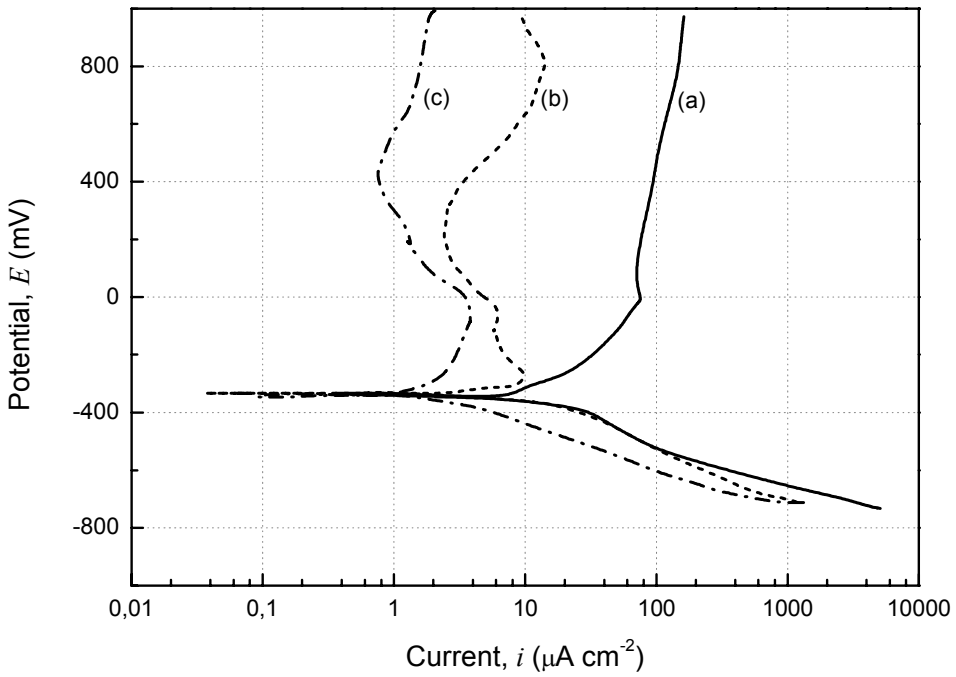

Fig. 9. Potentiodynamic polarization curves measured in deareated 15 % aqueous H_2SO_4 at 25 °C for 316L stainless steels: (a) uncoated sample and heat-treated at 800 °C for 2 h; (b) coated with ZrO_2 (800 °C/2h); and (c) coated with ZrO_2 (800 °C/10h) [19].

A similar situation was observed for zirconia coated 304L stainless steels [18,22]. The sol-gel coatings showed excellent barrier and enhanced corrosion protection of stainless steels in aqueous sulphuric acid solution at room temperature (Fig. 10). Again it was concluded, that mechanism for hydrogen evolution reaction remains unchanged for the uncoated and coated samples, and the zirconia coating act as physical barrier.

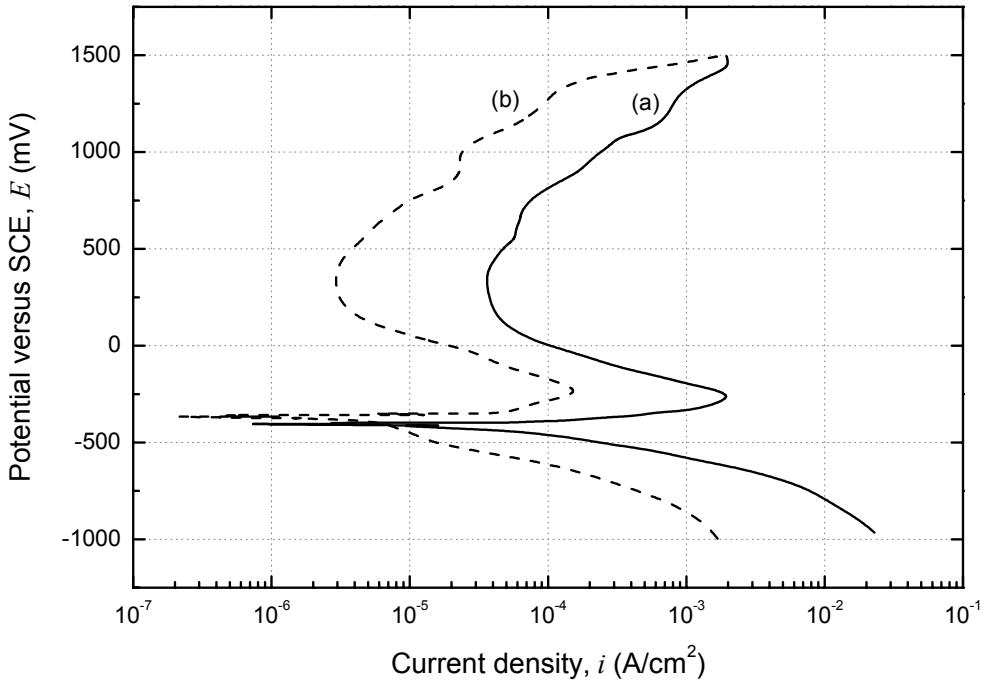

Fig. 10. Potentiodynamic polarization curves measured in deareated 15 % aqueous H_2SO_4 for 304L stainless steels: (a) uncoated and heat-treated at 800 °C for 2 h; (b) coated with ZrO_2 (800 °C/2h) at 25 °C [18].

2.4.3. Corrosion in chloride solutions (pitting corrosion)

Quinson et al. [24] has deposited the ZrO_2 sol-gel coatings on 304L stainless steel. Aside the deformation capability, the protection effect of the coatings in 0.5 M NaCl solution was studied by the potentiodynamic polarization measurements and electrochemical impedance spectroscopy. The anticorrosion properties were evaluated from the rest and pitting potentials.

It was recorded that for the zirconia coated samples the rest potential insignificantly vary with immersion time in the chloride solution. In addition, it was proved that the rest potential for the coated steel was close to that determined for the uncoated one. However, the applied zirconia coating influenced on the pitting potential. This potential of the coated sample before ageing in chloride solution was much higher (more anodic) in comparison with the potential of the uncoated steel, and after ageing the pitting potential had a tendency to decrease [24].

The corrosion behaviour of ZrO_2 sol-gel coatings on stainless steel was also studied by Atik et al. [20]. The potentiodynamic polarization measurements were performed in aqueous 3% NaCl solution and it was shown that zirconia has a great effect on the anodic and cathodic polarization curves Fig. 11. In the presence of ZrO_2 coating the corrosion potential shifted toward the anodic direction. Thus, this work also revealed that zirconia coating act as geometric blocking layer against exposure to the aggressive corrosion media.

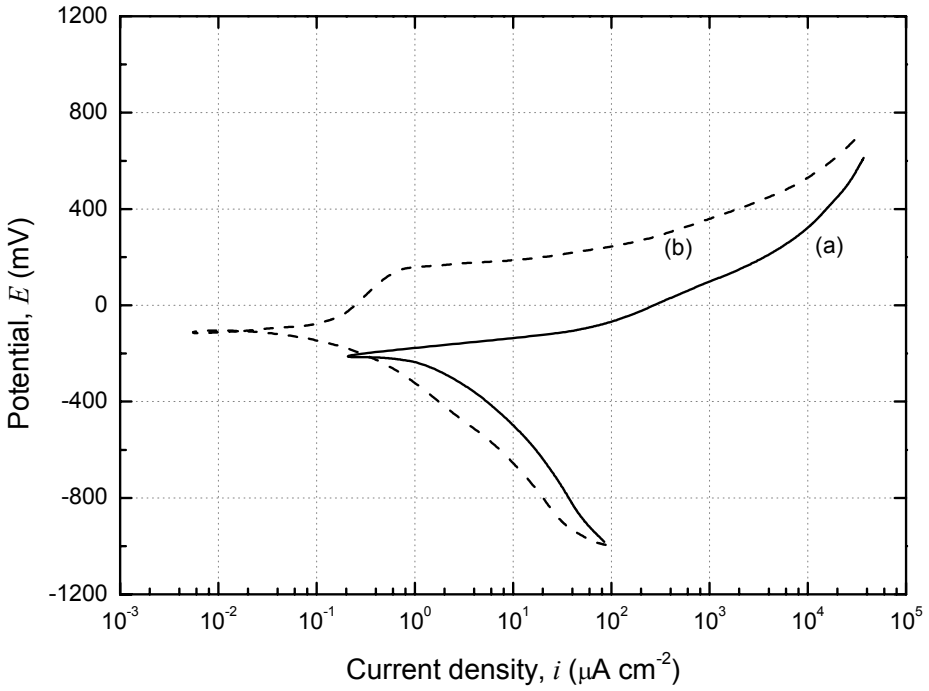

Fig. 11. Potentiodynamic polarization curves obtained at room temperature in aqueous 3 % NaCl for stainless steels (a) uncoated, heat treated at 800 °C for 2h; (b) coated with ZrO_2 (800 °C /2h) [20]

3. THE AIM AND SCOPE OF WORK

As shown in the literature chapter, zirconia coatings were mainly studied as corrosion resistant coatings on stainless steels. Fewer reports are related to the use of zirconia for corrosion protection of mild steels. So far, there are no literature reports on the study and application of sol-gel coatings, including zirconia, to counter hydrogen embrittlement. However, the results of the works discussed above seem to be interesting also for this type of corrosion. In particular, they indicated for the hindrance of hydrogen evolution reaction by blocking the surface of bare metal. One can expect that the ZrO_2 coatings should also affect the entry of hydrogen into the metal and in this way influence on the intensity of hydrogen embrittlement. This issue seems to be important and since it was not yet examined, its closer understanding is desirable from both the scientific and practical point of view. This is a general objective of this work.

Any layer on the metal surface, including the ZrO_2 coating on iron, in the first place influence on the entry of hydrogen into the metal. Therefore, an explanation of this process is the main purpose of this study. The point is to reveal not only to what extent, but also how (mechanism) the coating affects the entry of hydrogen. In this context, an important challenge will be the determination of the effective coverage of the iron surface by ZrO_2 coatings.

As it was also mentioned in the literature chapter, the relationship between the flux of diffusible hydrogen entering the metal and the amounts of various forms of hydrogen absorbed inside the metal is not simple. One may expect that in the presence of coating, the picture is even more complex. Namely, the concentration of diffusible hydrogen beneath the metal surface may be locally disturbed by the coating and, consequently, the trapping of hydrogen may change. Hence, the study of hydrogen trapping inside the ZrO_2 coated iron, including the distribution of the trapped hydrogen in the metal, is also the important purpose of the work.

In order to achieve these goals, the ZrO_2 sol-gel coatings were prepared on the surface of iron membranes. The coatings were characterized using SEM, XPS, AFM as well as the electrochemical polarization and impedance spectroscopy techniques. Then the electrochemical studies of hydrogen permeation and desorption were carried out. An analysis of the obtained experimental results was an essential part of the work.

4. EXPERIMENTAL

In this chapter, detailed information about the materials used, the preparation of zirconia sol-gel coatings on iron membranes, and the characterization of the obtained coatings using the surface analysis techniques (XPS, SEM and AFM) are described. Then, the main points of experimental conditions for the electrochemical measurements, including the essential hydrogen permeation/desorption measurements, potentiodynamic polarization curves and electrochemical impedance spectroscopy (EIS) are given.

4.1. Material

The material used was a commercial Armco iron with the chemical composition presented in Table 2. The samples in the form of 1-mm thick disc-membrane were sliced from a hot drawn, 25-mm diameter rod, perpendicularly to the rod axis. Owing to such orientation, in the hydrogen permeation measurements, the flux of hydrogen was directed along the layers o fibers of nonmetallic inclusions and there was no formation of blisters filled with gaseous hydrogen. Consequently, the permeation of hydrogen was not restrain and there was no irreversibility of the behaviour of membranes in permeation measurements [103,104]. This condition is very important, because changes in the steady state permeation rate can be attributed to the entry rate of hydrogen into the metal. The entry of hydrogen can be, in particular, affected by the surface coating.

Table 2. Chemical composition of Fe-Armco (wt%).

C	Mn	Si	P	S	Cr	Ni	Cu	Al	Fe
0.02	0.097	0.009	0.021	0.019	0.009	0.028	0.068	0.041	balance

Both sides of the membranes were mechanically polished using successively 400, 800 and 1200 grit SiC abrasive paper. Finally the samples were degreased ultrasonically in acetone. The one (entry side of iron membrane) was coated with zirconia sol-gel coatings.

4.2. Chemicals

The following chemicals were use to prepare a base electrolytic solution and a sol-gel solution:

- sodium hydroxide (NaOH), pure p. a. (Chempur);
- zirconium (IV) n-propoxide ($Zr(n\text{-}OC_3H_7)_4$), pure p. a., 70 % w/w in n-propanol, (Alfa Aesar);
- 1-propanol ($n\text{-}C_3H_7OH$), pure p. a. (Chempur);
- acetylacetone $(CH_3CO)_2CH_2$, 99 %, (Aldrich);
- acetone ($CO(CH_3)_2$), pure. p. a. (Chempur);
- filtered and demineralised water with an ELIX system (Millipore).

4.3. Preparation of zirconia sol-gel coatings

The zirconia sol-gel was prepared according to a procedure described in detail by Li et al. [101]. Zirconium n-propoxide was used as a source of zirconia. The sol precursor was prepared at room temperature by dissolving the n-propoxide in n-propanol, and then acetylacetone and deionised water were added. The molar ratio of zirconium n-propoxide: acetylacetone: water: n-propanol was 1: 2: 2: 60. The solution was stirred for homogenization during 3 h.

The prepared sol was deposited onto one side of the iron membrane by spin-coating at a rate 20 rev/s during 30 s. The resulting gel film on the iron surface was initially dried in air for 12 h and then densified at 70 ºC for 15 min. Then, the above procedure was repeated two and five times to obtain two-layer and five-layer coatings, respectively. Finally, the coated membranes were annealed in vacuum at gradually rising temperature up to 800 ^oC at a rate of 5^oC/min, with isothermal holding at 350^oC, 550^oC and 800^oC for 30 min, and then furnace cooled. The annealed coating was visible as a transparent, straw colour film.

4.4. Surface characterization of sol-gel coatings

Surface composition of the coated and uncoated iron samples was determined by X-Ray Photoelectron Spectroscopy (XPS). The measurements were carried out using VG Microtech spectrometer and X-ray source with Al Kα radiation at 10 kV and 10 mA. An

ion gun with Ar^+ sputtering of about 10 μA /cm^2 at 3.0 kV was used for surface cleaning. The obtained XPS spectra were analyzed using the NIST XPS Database [105].

Scanning Electron Microscopy (SEM) was used to characterize the morphology of the coated and uncoated surfaces. These surfaces were compared before and after prolonged hydrogen charging to evaluate the deleterious effect of hydrogen.

4.5. Electrochemical studies

All electrochemical measurements were conducting using a double electrochemical cell, especially designed for the electrochemical permeation measurements with the electrochemical detection of hydrogen, like in the classical permeation method by Devanathan and Stachurski [60]. The prepared membrane was mounted between two electrochemical cells (Fig. 12) using a convenient, connecting holder made of methyl polymethacrylate (Perspex), having flanges and rubber gaskets in the form of flat ring with inner diameter of 8 mm. The geometric area of the membrane exposed to solution was 0.5 cm^2.

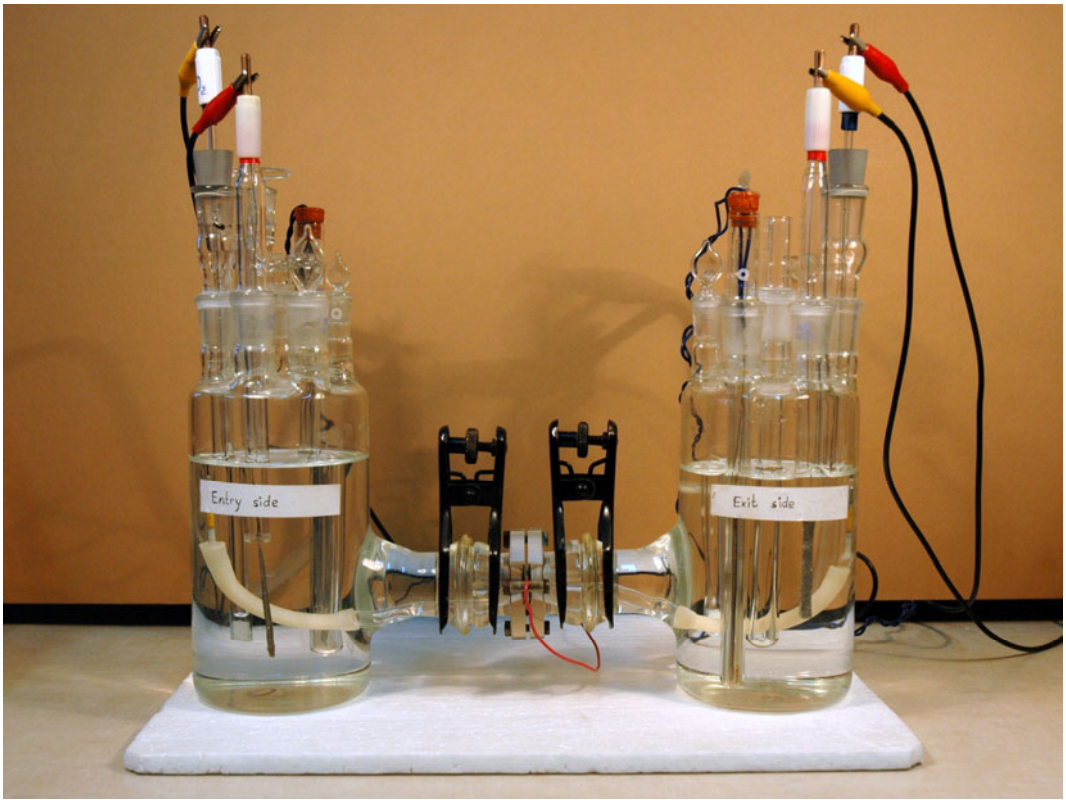

Fig. 12. Double electrochemical cell used for hydrogen permeation experiments.

The solution used in both cells was 0.1 M NaOH freshly prepared from NaOH of analytical grade and demineralised water. The solutions in both electrolytic cells were de-aerated with argon; the deaeration was continued during measurements. Both cells were equipped with the Pt wire as a counter electrode, and a mercury-mercuric oxide electrode Hg|HgO|0.1 M NaOH (~ +0.17 V versus NHE) as a reference electrode. The individual membrane sides worked as separate working electrodes.

4.5.1. Hydrogen permeation and desorption measurements

During the permeation measurements, the entry side ($X = 0$) of the membrane, sol-gel coated or uncoated, was subjected to galvanostatic cathodic charging in 0.1 M NaOH at a constant current density i_c; most often it was 10 mA/cm^2 in relation to geometric area. The other, exit side ($X = L$) of the membrane, previously electroplated with a thin layer of palladium, was continuously polarized in 0.1 M NaOH at a constant potential of 0.15 $V_{Hg|HgO|0.1\ M\ NaOH}$ (~ +0.32 V versus NHE). Under this potential, hydrogen atoms escaping from the membrane were instantaneously oxidized and the measured anodic current corresponded to the permeation rate of hydrogen through the membrane. As it was mentioned earlier, the steady state permeation rate informs about the entry rate of hydrogen.

The hydrogen permeation measurements were also used for the determination of the hydrogen diffusion coefficient (apparent or real, depending on the membrane used). To this end, the non-stationary permeation rate was taken into account. When the permeation rate achieved a steady-state level (after approximately 96 h of hydrogen charging), the successive permeation build-up and decay transients were recorded by a rapid change of the cathodic current density from 10 to 20 mA/cm^2, and then back to the previous value of 10 mA/cm^2.

Finally, after 5-6 days of the uninterrupted hydrogen charging, the complete desorption of hydrogen was examined to determine the amount of hydrogen in the membrane. The cathodic current at the membrane entry side was switched off and this side was polarized immediately at the same potential of 0.15 $V_{Hg|HgO|0.1\ M\ NaOH}$ as the exit side. From this moment, the anodic currents were recorded at the both sides of the membrane. After subtraction of the suitable background currents, the desorption rate of hydrogen at each side was obtained.

4.5.2. Electrochemical polarization curves and impedance spectroscopy

In addition, to the main hydrogen permeation measurements, the polarization curves and the electrochemical impedance spectroscopy measurements were performed at the membrane entry side. These measurements provided valuable information for comparable characterization of the electrochemical behaviour of coated and uncoated iron.

Polarization curves were recorded after 1 min holding at a potential of -1.8 V versus NHE, applied for standardizing the surface conditions. The curves were measured at a potential scan rate 2 mV/s, starting from a potential of -1.8 to 0.9 V versus NHE. The measurements were performed using the Electrochemical Measurement System CMS100/CMS105, manufactured by Gamry Instruments, Inc.

The EIS measurements were performed using the Solartron 1255 Frequency Response Analyser in conjunction with the Solatron 1286 Electrochemical Interface. The amplitude of the sinusoidal interference signal was 40 mV, and the frequency range of 1000 kHz to 0.1 Hz was applied. The impedance measurements were performed periodically (every 24 h), simultaneously with cathodic polarization at the constant current density i_c= 10 mA/cm^2. ZPLOT software was used for control and analysis of the impedance measurements. EIS data were plotted in terms of Nyquist and Bode diagrams.

All the electrochemical measurements were carried out at 30 ^{o}C. All experiments were repeated 3-4 times, and the average values of the measured parameters are shown and they were taken into account for further transformation.

5. RESULTS AND DISCUSSION

The main topic of the work, concerning the effect of the sol-gel coatings on the entry of hydrogen into iron, is directly related to the results of the hydrogen permeation experiments. However, it seems to be reasonable to discuss in the first place that results and observations which characterize the uncoated and coated iron surface.

5.1. Surface characteristic of uncoated and coated iron membranes

5.1.1. SEM analysis

SEM observations of the morphology of the entry side of iron membranes, without and with the zirconia sol-gel coatings, were performed before and after a long-lasting hydrogen charging (~5 days) to compare the coated surface with the uncoated one (micrographs 1a vs. 2a and 3a in Fig. 13) and to estimate the level of hydrogen degradation (micrographs 1b, 2b and 3b in Fig. 13).

Comparing the micrograph 1a with the micrographs 2a and 3a can be seen that the ZrO_2 coatings obscured to a certain extent the scratches on the iron surface produced during its previous grinding and polishing. There were also some cracks visible on the coated surfaces (more distinct on the five-layer coating), presumably formed during cooling because of different thermal expansion coefficients for iron and ZrO_2.

The micrographs 1b, 2b and 3b in Fig. 13 show that the long-lasting hydrogen charging caused significant changes in both the uncoated and coated iron. Moreover, the changes of the uncoated iron surface seem even greater than those observed for the coated iron, especially in regard to that for five-layer coating (Fig. 13, 3b).

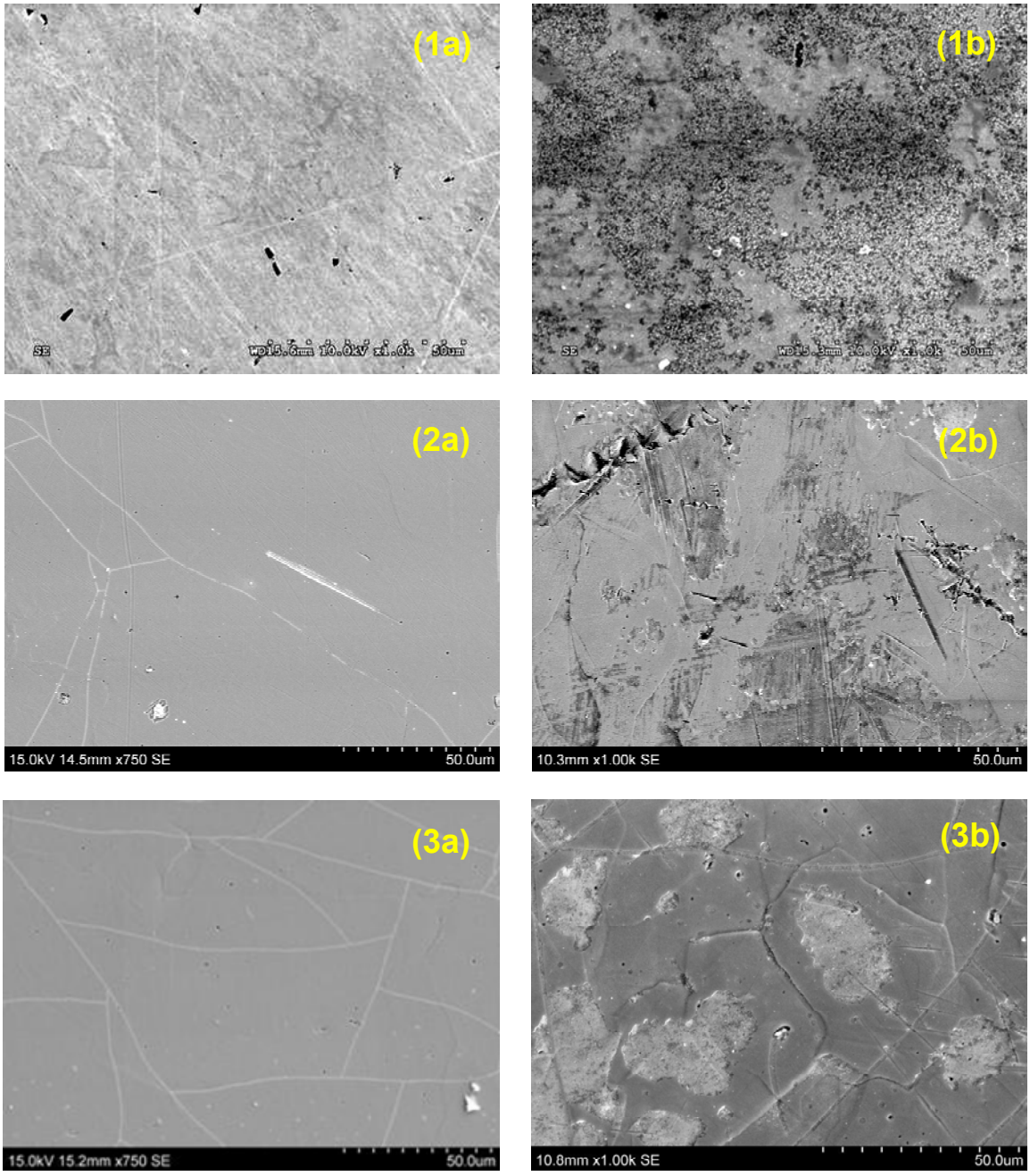

Fig. 13. SEM images of uncoated (1) and zirconia sol-gel coated iron membranes with different number of layers: (2) two-layers, (3) five-layers; (a) – before and (b) after hydrogen permeation measurements.

As it was found earlier [71], a long cathodic polarization of iron in NaOH resulted in the formation of some alien layer on its surface. The longer the cathodic polarization the thicker layer was. After a few dozen hours of cathodic treatment, this surface layer became visible even to the unaided eye. It was supposed, therefore, that by a long hydrogen charging, disintegration of a subsurface iron layer occurred. It was also

assumed that the new formed surface layer consisted of a inner sublayer of elemental iron and an outer sublayer of some kind of iron hydroxide $Fe_x(OH)_y$. Comparing the micrograph 1b with the micrograph 2b, and especially 3b, one can conclude that the zirconia coated iron was less susceptible to the disintegration caused by hydrogen. Undoubtedly, it can not be indifferent to the hydrogen evolution reaction and to the entry of hydrogen into the metal.

5.1.2. Thickness of ZrO_2 sol-gel coatings

The coating thickness was estimated using the AFM technique working in the contact (repulsive) mode. For this purpose, the surface of the coated iron membrane was scratched and the scanning was performed along the straight line intersecting the scratch. As an example, the AFM image of the annealed, one-layer of ZrO_2 sol-gel coating on the iron membrane is shown in Fig. 14a, whereas the resulting, relative cantilever deflection curve is shown in Fig. 14b. On the basis of this curve, one can estimate the thickness of the one-layer ZrO_2 coating as about 60 nm. Consequently, one can assume that the thickness of the two- and five-layers coatings was about 120 nm and 300 nm, respectively.

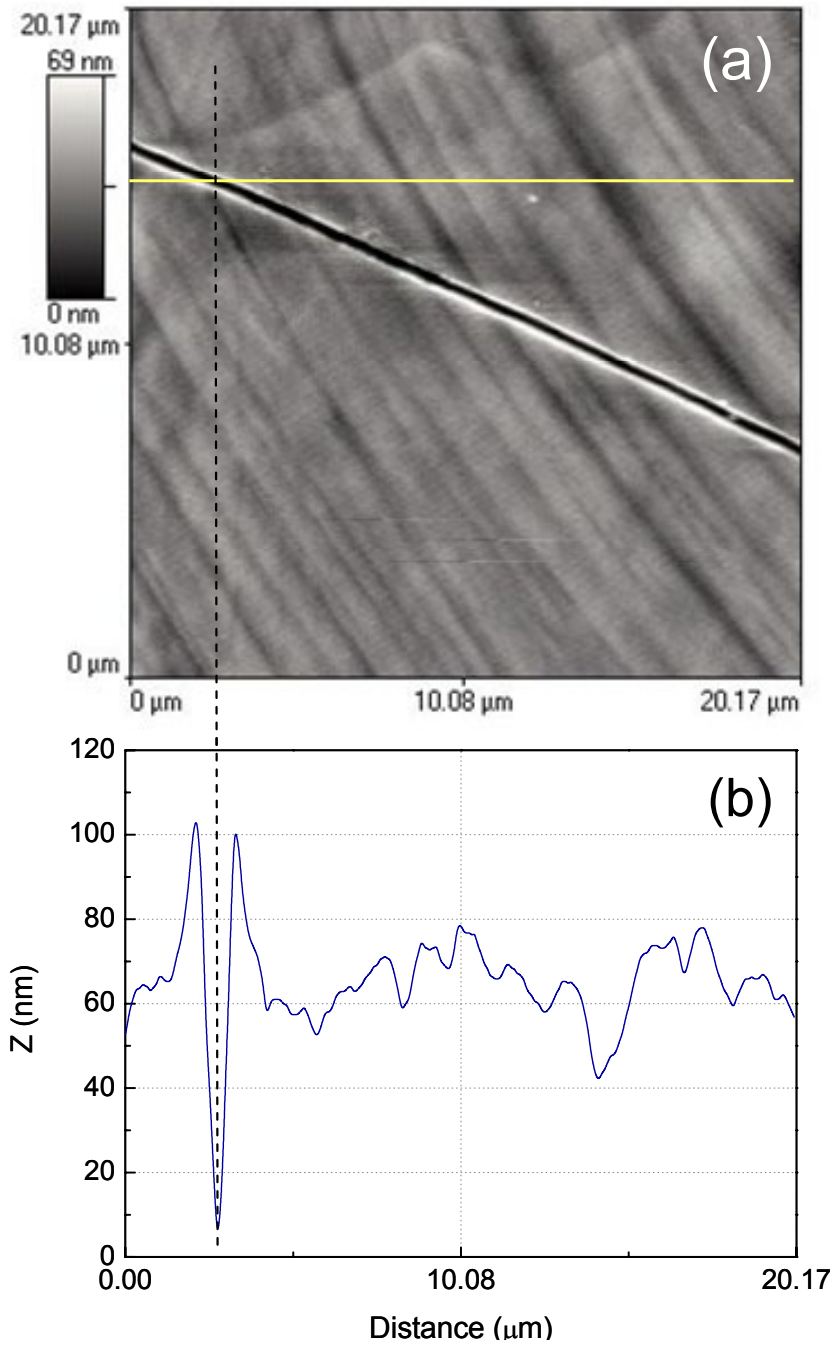

Fig. 14. AFM image of the annealed ZrO_2 sol-gel coating on the iron membrane with the marked yellow line (a), along which the thickness was measured (b).

5.1.3. XPS spectra

A comparison of the XPS spectrum for the uncoated iron surface with those for the ZrO_2 coated iron are shown in Fig. 15a and Fig. 15b, respectively. The XPS spectrum for the uncoated iron surface was typical. It indicates only for the presence of Fe and

traces of O, which in spite of cleaning (Ar sputtering) are usually detectable in XPS measurements.

The XPS spectra for the ZrO_2 coated iron membrane surface (Fig. 15b) include mainly characteristic peaks coming from Zr and O, whereas there are no peaks coming from iron. It means that the coatings consisted mainly of ZrO_2. However, the lack of peaks characteristic for iron did not determine of the complete tightness of the obtained coatings. More likely, the coatings were porous but their thickness was enough to restrain the photoelectrons coming from the iron substrate.

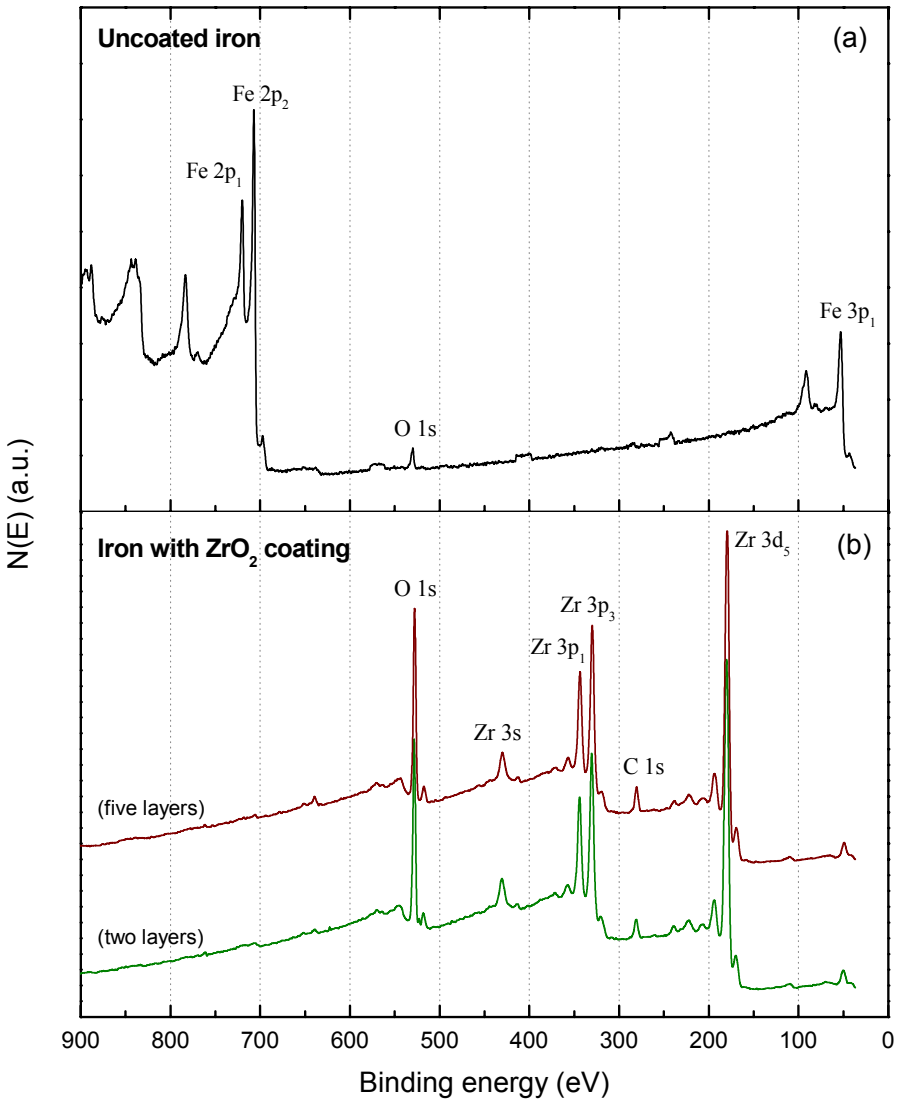

Fig. 15. XPS spectra for the uncoated iron surface (a) and for the iron surface coated with two and five layers of ZrO_2.

Analysing the XPS spectra for the coated membranes (Fig. 15b), one can see a characteristic pick for carbon (C 1s). It is rather unexpected, since the applied annealing of the sol-gel coating up to 800 ^{o}C should be effective not only for the complete removal of water and organic solvents, but also for organic parts of zirconium n-propoxide (Zr(n-$OC_3H_7)_4$), used as a source of zirconia. Probably, it was not true in the latter case and during the annealing of the coated membranes under vacuum, a part of hydrogen atoms derived from the propyl groups remained in the coating.

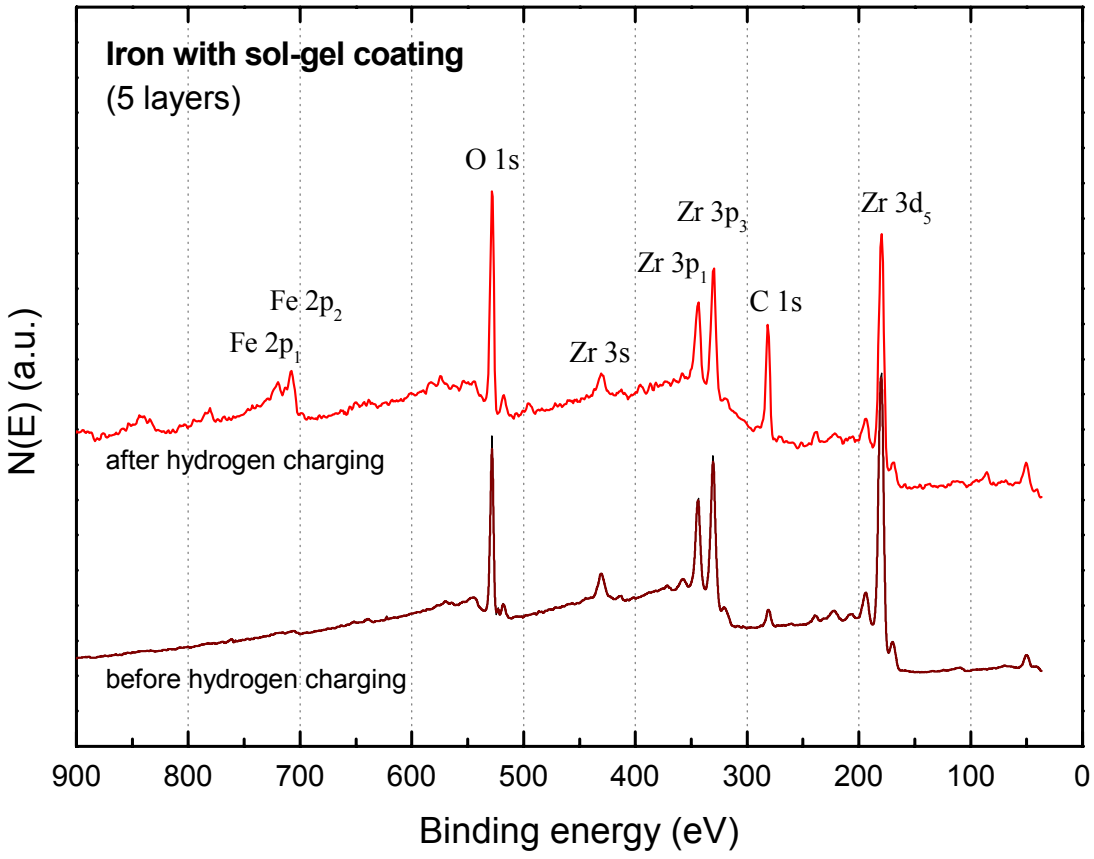

Fig. 16. XPS spectra for the coated iron membrane surface before and after 5 days of hydrogen charging.

The interaction of hydrogen with the coated iron surfaces was reflected in the XPS spectra. After 5 days of the uninterrupted hydrogen charging, the XPS spectrum revealed the presence of iron on the coated surface (Fig. 16). However, the peaks derived from Zr and O remain the most pronounced. Thus, the ZrO_2 coating was quite resistant to the damaging effect of hydrogen.

5.2. Electrochemical characteristic of uncoated and coated iron membranes

5.2.1. Electrochemical polarization curves

The potentiodynamic polarization curves for the membrane's entry sides were performed to compare the electrochemical-corrosion behaviour of the coated and uncoated iron and to examine the stability of the ZrO_2 coating. Fig. 17 shows the polarization curves for the fresh, i.e. before hydrogen charging, uncoated and coated iron membranes. The zero-current (corrosion) potentials of the coated iron were nobler than that of the uncoated iron. At the same time, in the presence of coating, both the cathodic and anodic polarization curves were shifted towards lower values of current density. Consequently, the resulting corrosion current density for the coated iron was also lower than that for the uncoated one. As can be expected, the five-layers coated membrane showed a better protective properties than the two-layers coated one.

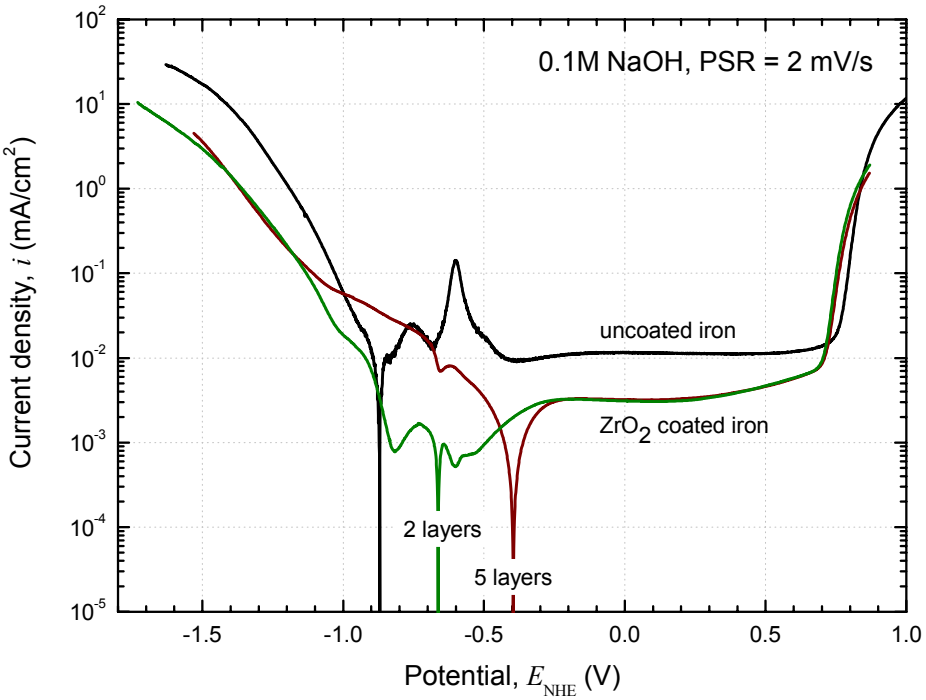

Fig. 17. Potentiodynamic polarization curves for the entry side of iron membranes without and with ZrO_2 coatings (2 and 5 layers), measured before hydrogen charging.

The most important, however, is that the potentiodynamic polarization curves for the uncoated and coated iron membranes had a similar shape. It suggests that the mechanism of electrode processes, in particular the mechanism of the hydrogen evolution reaction was the same for both the uncoated and coated iron. This is consistent with the previously presented data [18,19,22] suggesting that the ZrO_2 coatings, blocking the metal surface, provided a mechanical barrier for the electrode processes.

The following figures illustrate the effect of a prolonged hydrogen charging on the potentiodynamic polarization curves for the uncoated (Fig. 18) and coated iron (Fig. 19 and Fig. 20 for two and five layers of ZrO_2, respectively). Generally, one can note that the long-lasting cathodic polarization influenced to a greater extent on the uncoated iron than on the coated one. It means that the ZrO_2 coated iron surface was less prone to change under the influence of hydrogen charging.

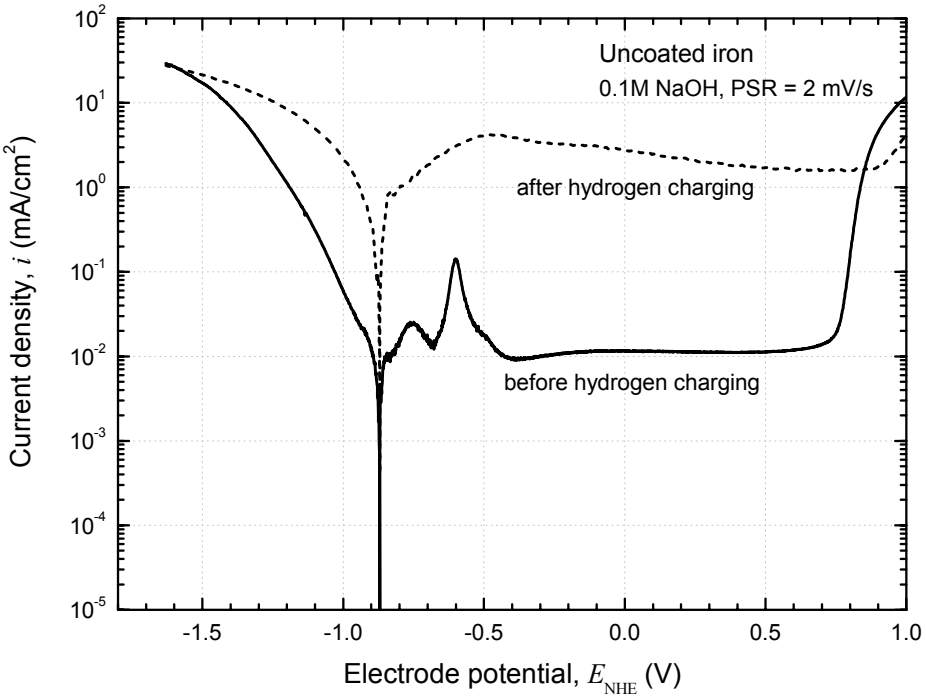

Fig. 18. Potentiodynamic polarization curves for the entry side of the uncoated iron membranes before and after hydrogen charging (i_c = 10 mA/cm^2, t_{char} = 120 h).

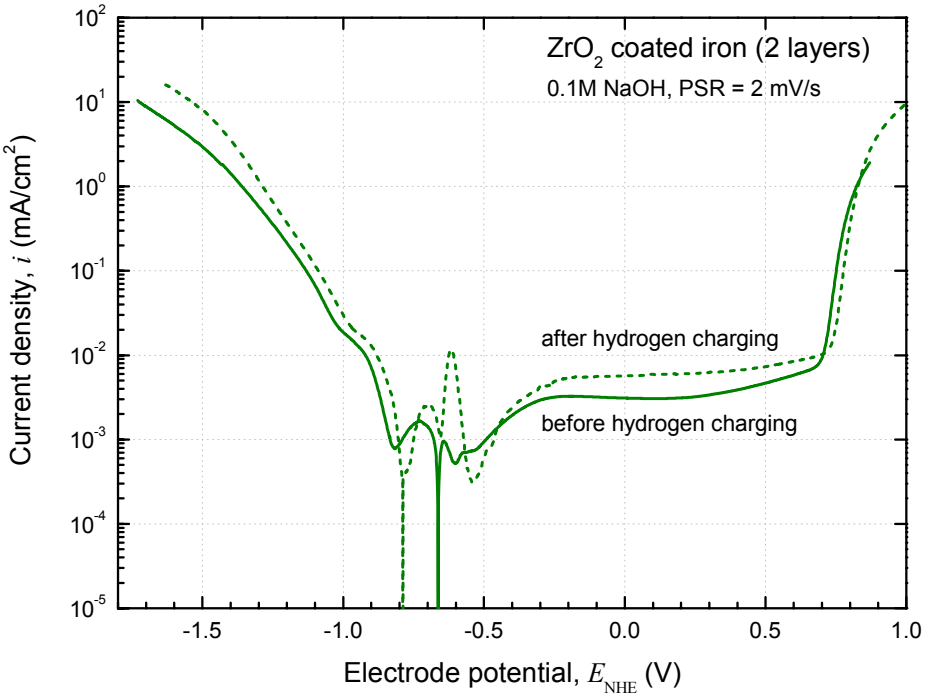

Fig. 19. Potentiodynamic polarization curves for the entry side of the ZrO_2 coated iron membranes (two-layers), before and after hydrogen charging (i_c = 10 mA/cm^2, t_{char} = 120 h).

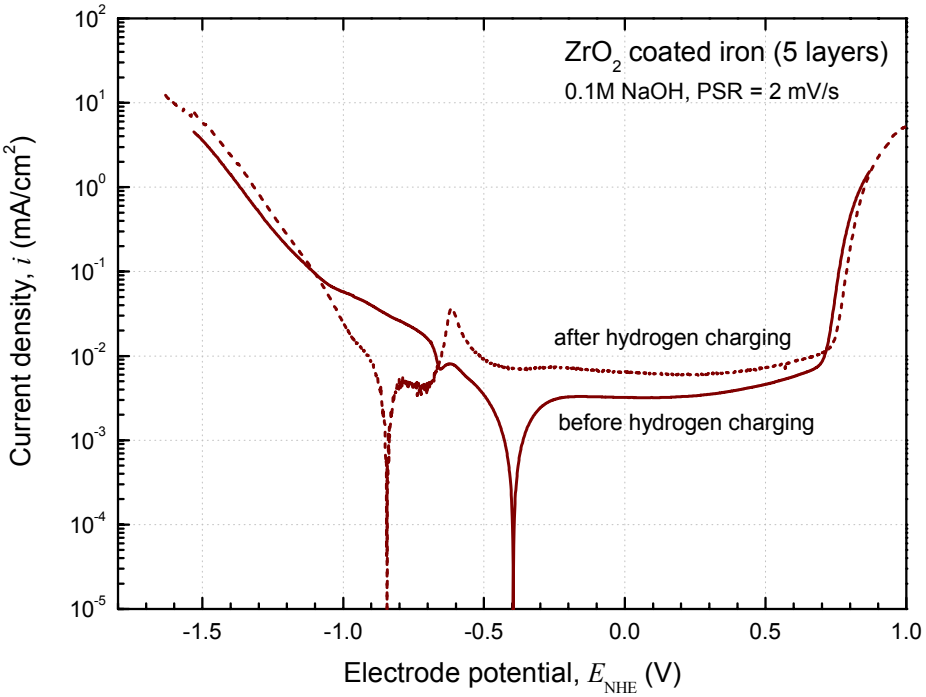

Fig. 20. Potentiodynamic polarization curves for the entry side of the ZrO_2 coated iron membranes (five-layers), before and after hydrogen charging (i_c = 10 mA/cm^2, t_{char} = 120 h).

5.2.2. EIS characteristics

Electrochemical impedance spectroscopy (EIS), being the technique for versatile characterization of electrochemical responses of interfacial processes and structures, has been successfully applied to the study of many corrosion systems, including those comprising the protective coatings. So it was natural to use it in this work to characterize and compare the behaviour of the uncoated and ZrO_2 coated iron membranes.

The EIS spectra for the uncoated and zirconia sol-gel coated iron membranes (entry side) were recorded simultaneously with hydrogen charging at the constant applied current density (i_c = 10 mA/cm^2). Thus, the obtained results shown below inform about the hydrogen evolution reaction at a given time, as well as about the changes that have occurred on the electrode surface during hydrogen charging.

The EIS spectra acquired after a given time of hydrogen charging are presented in the form of Nyquist plots in Fig. 21 for the uncoated iron, and in Fig. 22 and Fig. 23 for the coated iron with two and five layers of ZrO_2, respectively.

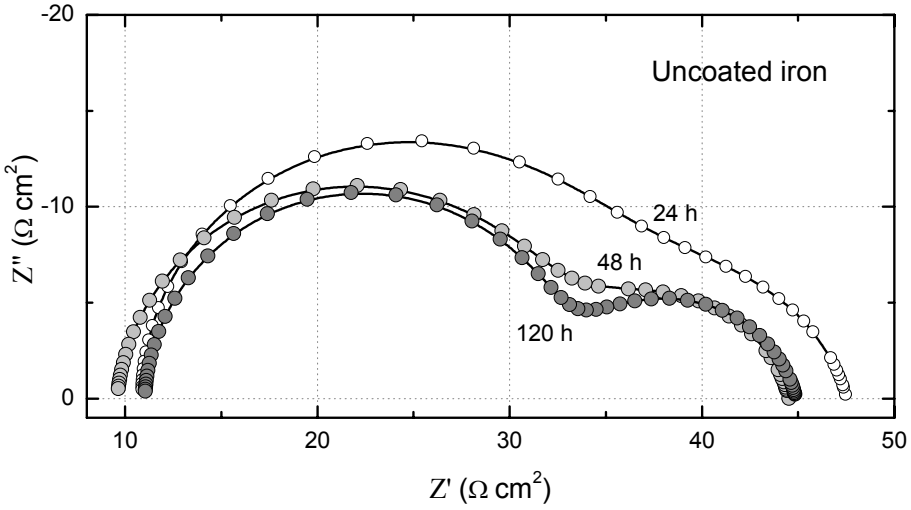

Fig. 21. Nyquist plots for the entry side of the uncoated iron membranes, recorded after a given time of hydrogen charging (0.1 M NaOH, i_c = 10 mA/cm^2).

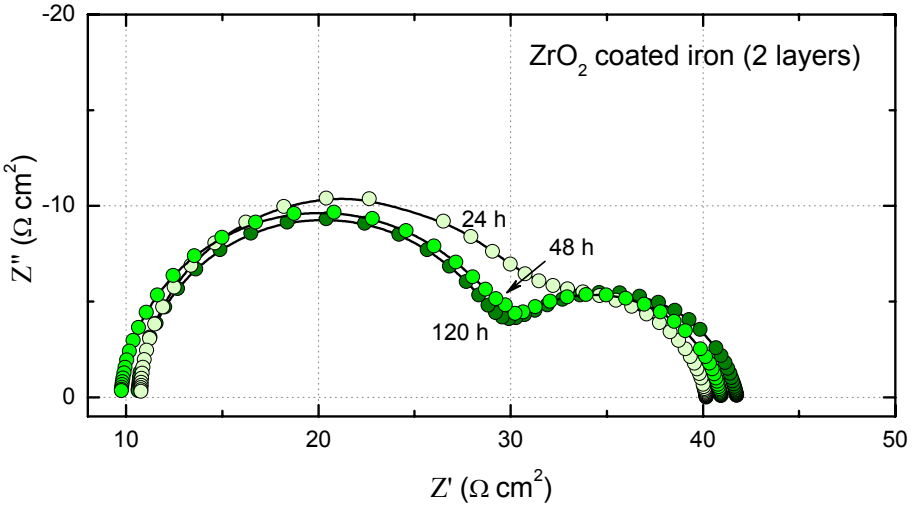

Fig. 22. Nyquist plots for the entry side of the ZrO_2 coated iron membranes (two layers), recorded after a given time of hydrogen charging (0.1 M NaOH, i_c = 10 mA/cm^2).

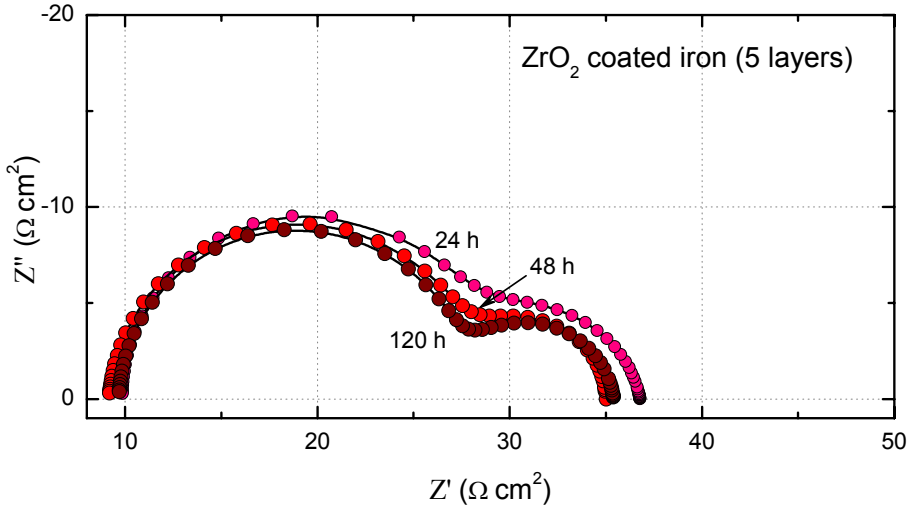

Fig. 23. Nyquist plots for the entry side of the ZrO_2 coated iron membranes (five layers), recorded after given time of hydrogen charging (0.1 M NaOH, i_c = 10 mA/cm^2).

Although generally, the impedance spectra for the uncoated and ZrO_2 coated membranes had similar shape, especially those recorded after a long time (e.g. after 5 days) of hydrogen charging, there was some difference between them during the initial

period of charging. Admittedly, it was not possible to obtain regular spectra shortly after the start of hydrogen charging because of large scatter of impedance data caused by the hydrogen gas bubbles. Namely, at the beginning of hydrogen charging, the evolution of gaseous hydrogen was very irregular; since the relatively small number of sites on the membrane surface was engaged in this process and quite large bubbles blocked intermittently a part of the electrode area. However, during prolonged cathodic polarization more sites became available for the evolution of gaseous hydrogen and the evolved gaseous bubbles were relatively small and they did not have very big influence on the registered impedance data. Nevertheless, the Nyquist plot for the uncoated membrane, recorded after 24 h, distinctly departed from the others plots observed for longer times (Fig. 21). Thus, the EIS spectra for the uncoated iron membrane confirm previous reports on the surface changes of iron during its cathodic polarization in alkaline solutions, consisting in the formation of a new surface layer [71,106,107]. This layer was porous and it probably composed of disintegrated iron and hydrated iron oxides. As opposed to the unmodified iron, the EIS spectra for the ZrO_2 coated membranes (Fig. 22 and Fig. 23), especially those for the five layers coated membranes, were practically independent on the charging time. It means that the ZrO_2 coating was quite resistant to hydrogen.

EIS characteristics for the uncoated and ZrO_2 coated membrane entry sides, after 5 days of the uninterrupted cathodic polarizations, are depicted in Fig. 24, Fig. 25, and Fig. 26, containing the Nyquist, Bode-phase, and Bode-magnitude plots, respectively. It is seen that both the uncoated and coated iron surface were characterized by two time constants.

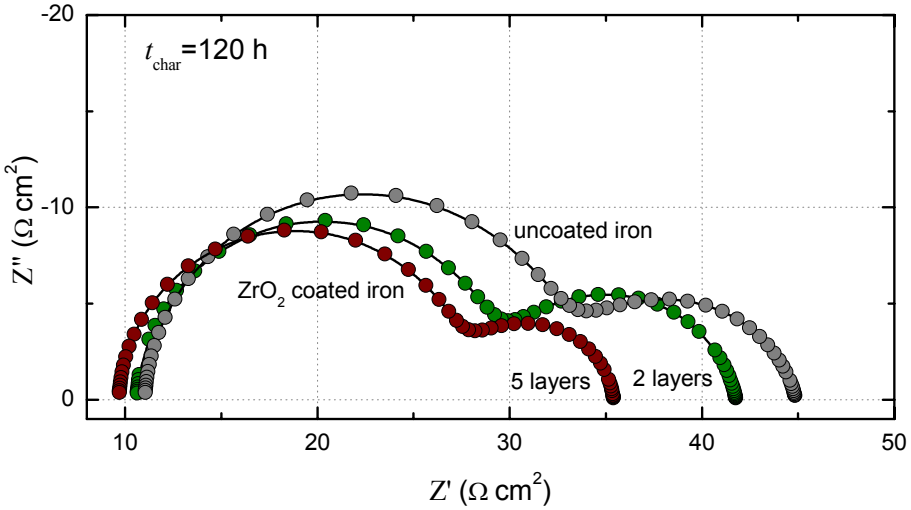

Fig. 24. Nyquist plots for the entry side of iron membranes without and with ZrO_2 coatings (2 and 5 layers), measured after 5 days of hydrogen charging (0.1 M NaOH, i_c = 10 mA/cm^2).

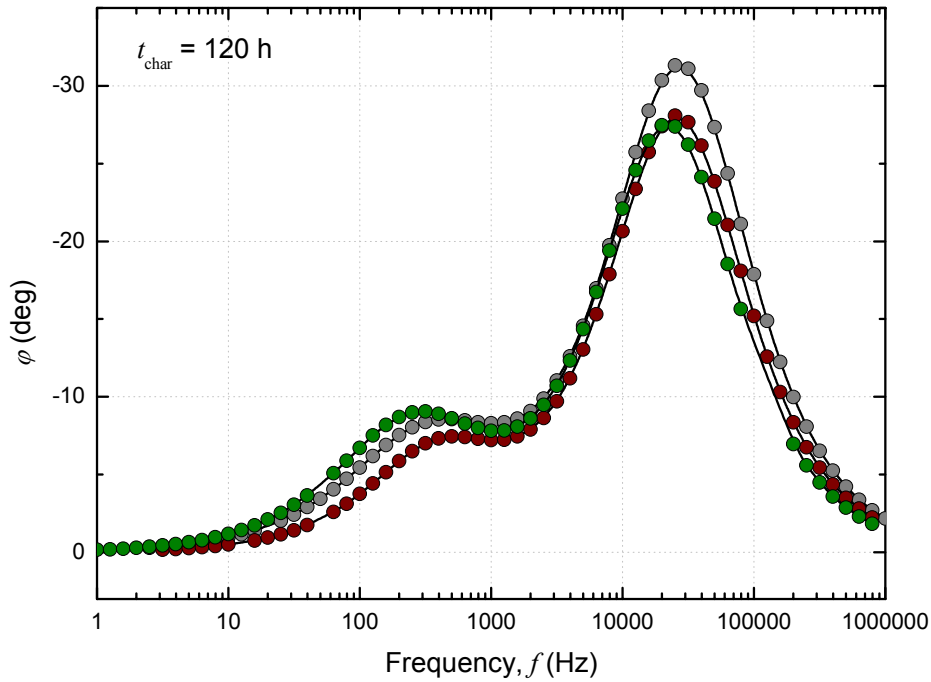

Fig. 25. Bode phase plots for the entry side of iron membranes without and with ZrO_2 coatings (2 and 5 layers), measured after 5 days of hydrogen charging (0.1 M NaOH, i_c = 10 mA/cm^2).

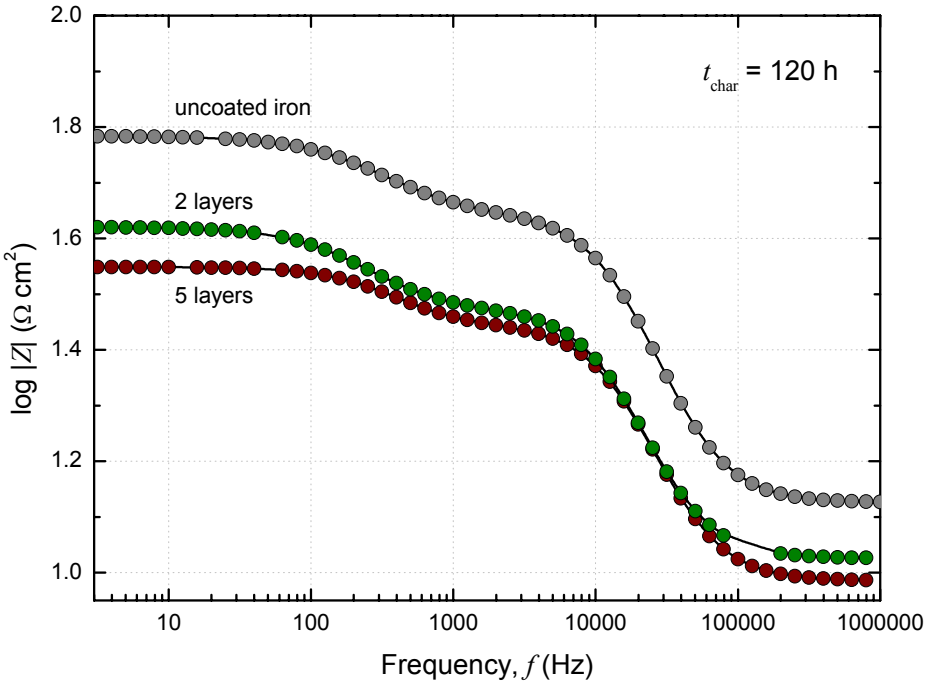

Fig. 26. Bode magnitude plots for the entry side of iron membranes without and with ZrO_2 coatings (2 and 5 layers), measured after 5 days of hydrogen charging (0.1 M NaOH, i_c = 10 mA/cm^2).

One may suppose that the first time constant (in the high frequency region) corresponded to the resistance of electrolyte in the pores or cracks of the ZrO_2 coating. It is understandable, because the sol-gel coatings are inherently porous and have other defects (cracks, etc). In the case of the uncoated iron membrane, the EIS spectra confirm the formation of a new surface layer, which was also porous. In turn, the second time constant (in the low frequency region) may be ascribed to the charge transfer resistance of the hydrogen evolution reaction on the uncoated places of the ZrO_2 coated iron membranes as well as of the bare (working) places of the uncoated iron membranes.

As it is known, the most common method used to analyse EIS spectra is equivalent circuit modelling. Usually, several cell elements and cell characteristics such as the electrode double layer capacitance, electrode kinetics, diffusion layer and solution resistance contribute to the EIS spectrum. The behaviour of each element may be described in terms of electrical components (resistors, capacitors) and specialized electrochemical elements (Warburg diffusion elements).

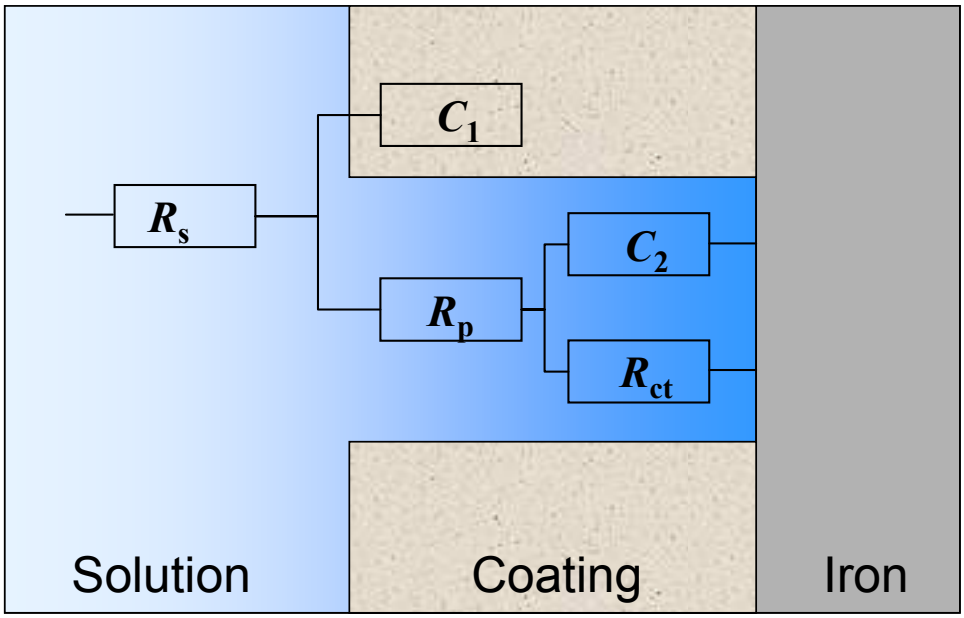

Fig. 27. Equivalent circuit used for analysis of EIS spectra of iron with ZrO_2 coatings and of iron with a porous surface layer.

To analyse the EIS spectra observed for the metal with damaged, untight or porous protective coatings, an equivalent circuit shown in Fig. 27 was often used [108,109]. However, the term coating can mean not only the intentionally produced coating, but also other kinds of layers on the metal surface, such as sediments, corrosion products etc., which can prevent the electrochemical reactions. Therefore, the above equivalent circuit was used to analyse the EIS spectra acquired for the ZrO_2 coated, as well as for the originally uncoated iron. In this circuit R_s represents the electrolyte resistance, R_p is called the pore resistance [110], C_1 is related with the non ideal capacitance of the surface layer (in particular ZrO_2 coating), R_{ct} is the charge transfer resistance, and C_2 is the corresponding capacitance.

Changes in the pore resistance R_p and charge transfer resistance R_{ct} during long-lasting hydrogen charging are shown in Fig. 28. Since in the given case, the permeation efficiency (expressed by the ratio i_p/i_c) was very low, the changes of the above resistances can be ascribed to the hydrogen evolution reaction on the membrane entry side. It is seen that the charge transfer resistance for the uncoated iron membrane was higher than that for the zirconia coated membranes. It means, that the hydrogen evolution reaction, and strictly speaking its desorption step(s) (equation (4) and/or (5)) on the

uncoated membrane run more difficult. Under the galvanostatic charging (i_c = const), the higher value of R_{ct} corresponds to higher impediment of the desorption of hydrogen atoms H_{ads} and, consequently, to enhanced hydrogen entry, as it was observed. Changes in the pore resistance are less obvious and they are hard to explain.

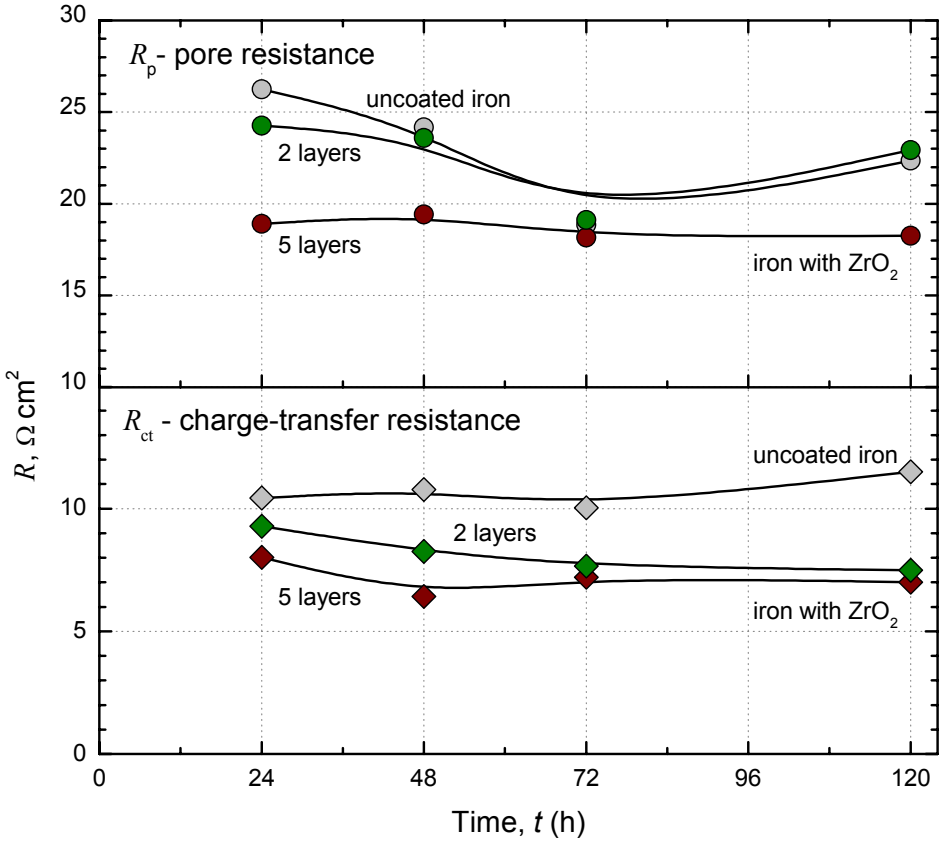

Fig. 28. Changes of the pore and charge transfer resistance for the entry side of the uncoated and ZrO_2 coated iron membranes during their hydrogen charging.

5.3. Hydrogen permeation measurements

According to the main goal of this work, the electrochemical measurements of hydrogen permeation of hydrogen performed on the uncoated and ZrO_2 coated iron membranes proved to be the most important and informative. Therefore, this chapter is a pivot of this work. The main attention was paid to examine to what extent and how the zirconia sol-gel coatings influence the hydrogen entry into.

5.3.1. Hydrogen permeation

Hydrogen permeation rate (i_p) vs. time (t) curves recorded during the first 6 min of the cathodic polarization of the iron membranes with and without the ZrO_2 coating are shown in Fig. 29. During this initial period, the effect of the applied coatings on the hydrogen permeation was not satisfactory. Initially, the permeation rate through the coated membranes was even higher than through the uncoated one. Undoubtedly, this rather unexpected effect was related to the surface processes occurring on the cathode and affecting the entry of hydrogen.

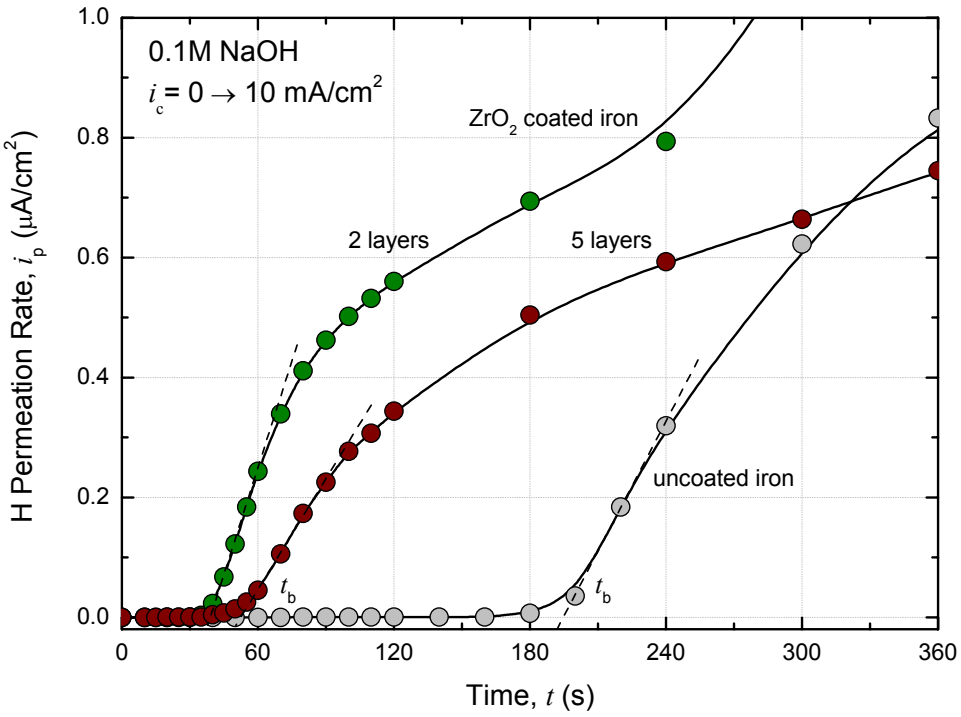

Fig. 29. Changes of hydrogen permeation rate through the uncoated and ZrO_2 coated iron membranes during the initial period of hydrogen charging.

Namely, taking into account extremely high diffusivity of hydrogen in iron, values of the so-called breakthrough time for both the coated membranes ($t_b \approx 60$ s), and especially for the uncoated membrane ($t_b \approx 180$ s) seem to be too long. Assuming that the permeation rate of hydrogen was controlled by its diffusion inside the membrane with the diffusion coefficient of hydrogen $D \approx 8\times10^{-5}$ cm^2/ s [111], an expected value of the breakthrough time for the 1-mm thick membrane equals only 6.4 s. Thus, the observed

values of breakthrough time in Fig. 29 were rather related to slow surface processes, influencing the entry of hydrogen, than to hydrogen transport through the membrane. These slow surface processes probably consisted in the cathodic reduction of the air-formed oxides and/or hydroxides formed in NaOH solution on the metal surface. In other words, at the beginning of the galvanostatic hydrogen charging, the applied current was consumed for the reduction of iron oxides and/or hydroxides. Therefore, at the initial period of charging the hydrogen evolution reaction was diminished. A much shorter breakthrough time for the coated membranes indicates that the oxidation of the coated iron was even less intense than the uncoated one. The main reason was that the oxidized iron area, and hence the amount of oxides was lesser than that for the uncoated iron.

However, the above behaviour of the zirconia coated membranes during the initial, relatively short period of the cathodic charging (Fig. 29) did not determine the beneficial effect of the coatings as a hindrance to hydrogen entry. A quite different picture was observed when the cathodic charging was continued for a long time. As shown in Fig. 30, after several hours, the permeation rate of hydrogen through the coated membranes attained almost constant level of about 7 μA /cm^2 and about 4 mA/cm^2, for two and five layers of ZrO_2, respectively.

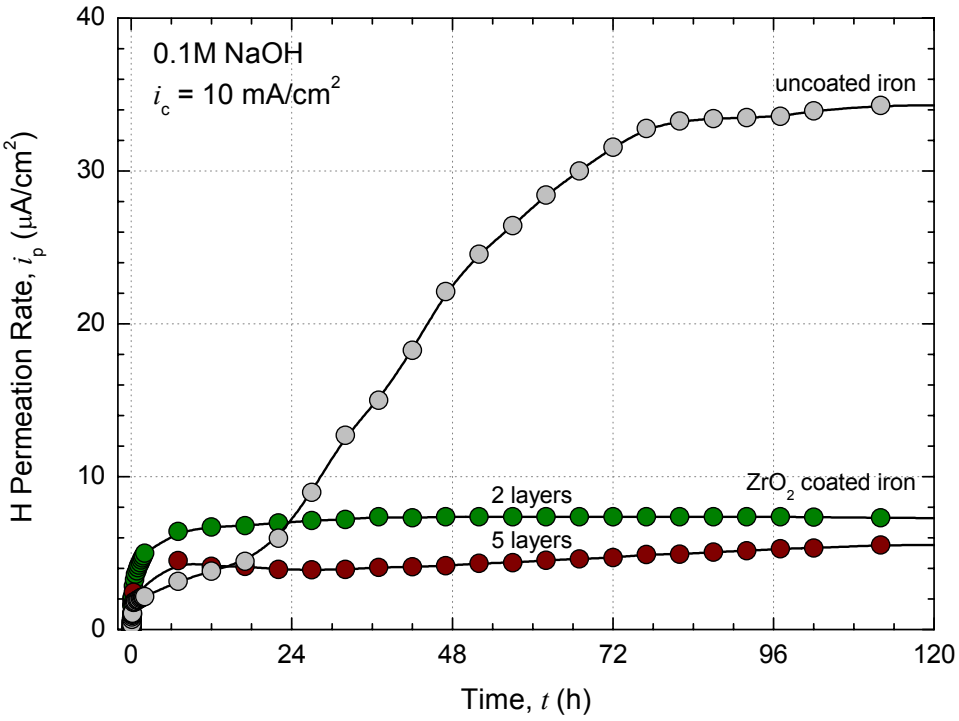

Fig. 30. Changes of hydrogen permeation rate through the uncoated and ZrO_2 coated iron membranes during their long-lasting cathodic charging.

In the case of the uncoated iron membrane, after a few hours of hydrogen charging the permeation rate was even lower than that observed for the coated membranes, but then it increased quite rapidly within approximately 3 days, attaining a much higher value of about 34 μA /cm. The detail explanation of this favourable effect observed during long-lasting hydrogen charging of iron in alkaline solutions was found many years ago [71,72] and it was studied using various experimental techniques [112-115]. Independently of its explanation, the enhanced hydrogen flux means that the working area of the iron cathode became activated, i.e. more prone to hydrogen entry into the subsurface region.

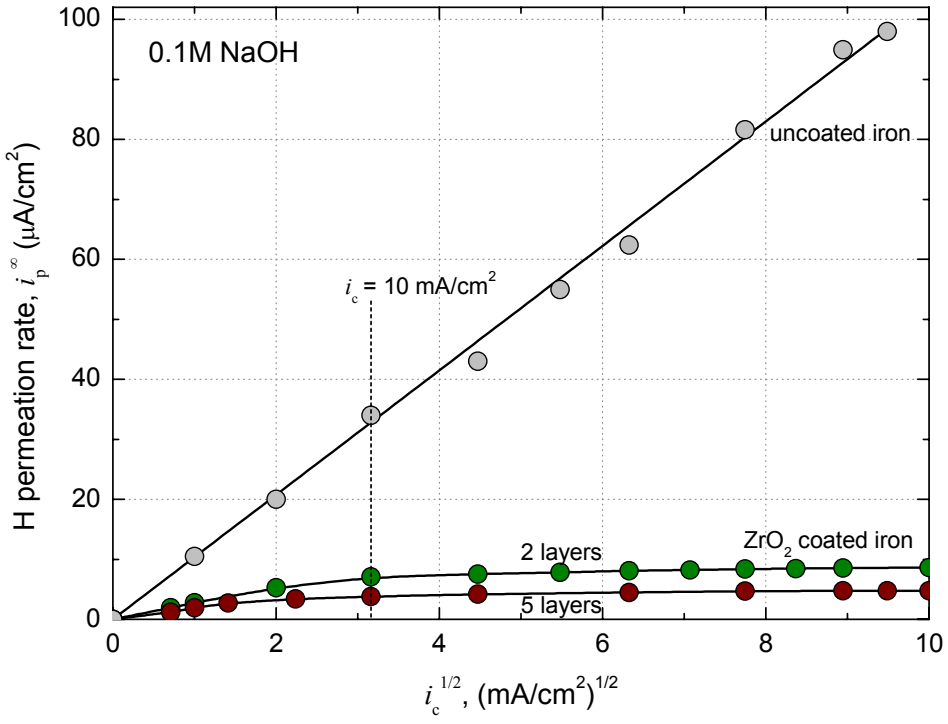

Fig. 31. Relationship between the measured hydrogen permeation rate and the square root of cathodic current density for the uncoated and ZrO_2 coated iron membranes.

One of the most significant, experimentally proved relationships, characterizing the hydrogen charging of metallic membranes, cathodically polarized in aqueous solutions, is a linear relationship between the steady state permeation (entry) rate of hydrogen and the square root of the applied cathodic current density. As seen in Fig. 31, this characteristic relationship was complied with the uncoated iron membranes over

whole applied range of i_c, i.e. up to 100 mA/cm^2. In the case of uncoated iron membrane, hydrogen permeation rate was a linear function of the square root of cathodic current density over its whole applied range, i.e., up to 100 mA/cm^2. However, for the ZrO_2 coated membranes this relationship was valid only for the current density up to 3-4 mA/cm^2. Then, the permeation rate increased insignificantly with increasing i_c, and further increase of i_c above about 16 mA/cm^2 do not influence on the permeation rate. An explanation of this interesting and crucial effect will be provided later in this work (Section 5.3.3).

5.3.2. Electrode potential

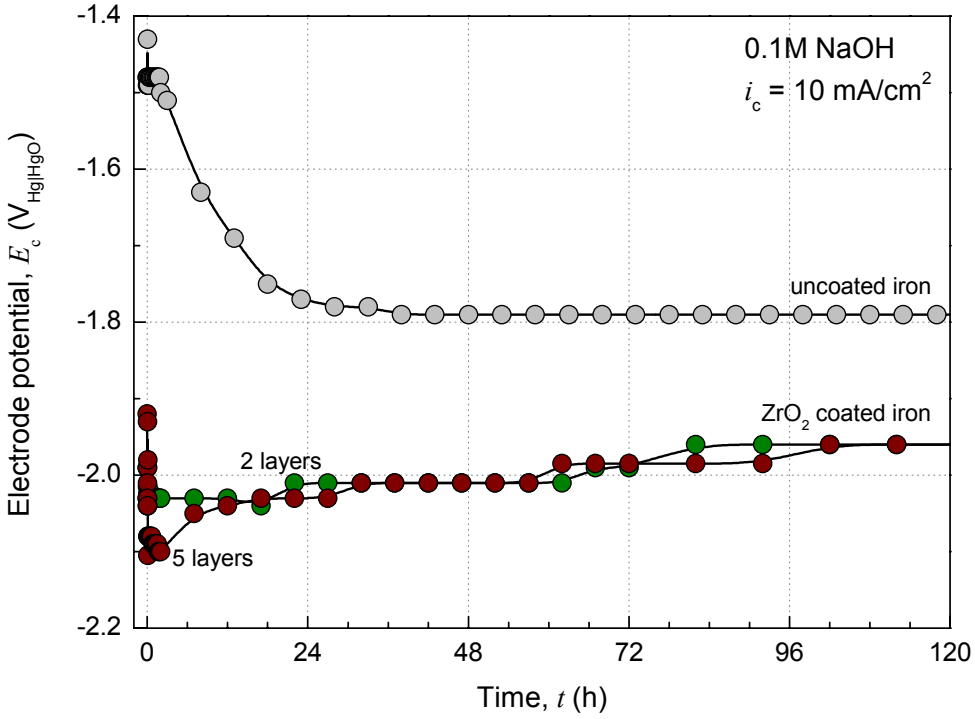

Fig. 32. Changes of the electrode potential of the entry side of the uncoated and ZrO_2 coated iron membranes during their long-lasting cathodic charging.

An important observation related to the role of ZrO_2 coating in the hydrogen evolution reaction and hydrogen entry is shown in Fig. 32, showing changes of the electrode potential of the membrane entry side with time. During the initial period of cathodic polarization, the potential of both the uncoated and coated iron membranes

shifted into the negative direction. This was presumably related to the reduction (removal) of the oxide layer. However, the most important is that during long-lasting cathodic polarization the electrode potential of the ZrO_2 coated iron was much more negative than that for the uncoated iron.

The more negative value of the cathode potential suggests that the overpotential of the hydrogen evolution reaction on the coated iron was greater than that for the uncoated iron. The greater overpotential means that the actual (real) current density on the zirconia coated iron was higher. Since the applied cathodic current (or current density in regard to the geometric area of electrode) was the same, the working area of the coated membrane had to be smaller than that of the uncoated membrane. Undoubtedly, that was because the zirconia coatings blocked the iron surface. Further considerations on this issue are given in the next section.

5.3.3. Zirconia surface coverage

As it is known, zirconia is a superior insulator. The electrical bulk conductivity of zirconia at room temperature is of the order 10^{-12} $\Omega^{-1}m^{-1}$ [116]. One may suppose that the electrical conductivity of the ZrO_2 sol-gel coatings studied in this work was low enough to exclude them from the participation in the electrode reactions, in particular in the hydrogen evolution reaction. Consequently, under the imposed cathodic current, the hydrogen evolution reaction, or strictly speaking its first step - the discharge of hydronium ions or water molecules - took place on the uncoated iron surface on the bottom of the pores. A question arises what was the effective coverage of the iron surface by the applied ZrO_2 coatings?

To solve this problem, an assumption was made that both the hydrogen evolution and hydrogen entry occurred only on the ZrO_2-free iron surface. This surface corresponds to the geometric area A of the uncoated membrane and the area A_{Fe} of the coated membrane - Fig. 33. The ZrO_2 coverage θ is defined as

$$\theta = \frac{A - A_{Fe}}{A_{Fe}} \tag{25}$$

and hence

$$A_{Fe} = A(1 - \theta) \tag{26}$$

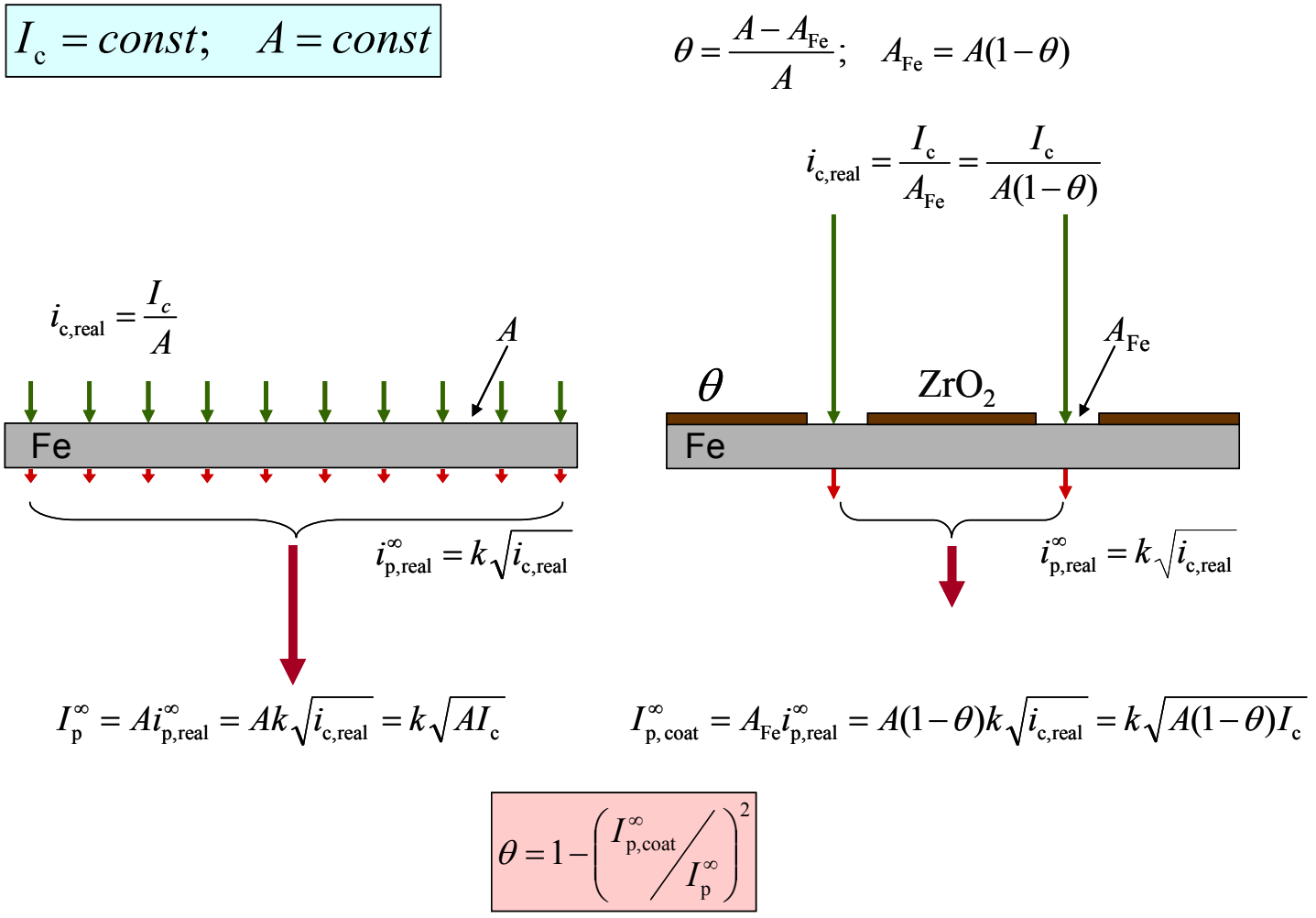

Fig. 33. Schematic presentation of hydrogen permeation through the uncoated (left) and coated (right) iron membranes, of constant geometric area A, cathodically polarized with constant cathodic current I_c).

Under the same applied cathodic current I_c (as it has just occurred in the permeation measurements), the real cathodic current density $i_{c,real}$ for the uncoated membrane is

$$i_{c,real} = \frac{I_c}{A} \tag{27}$$

and for the coated it is also a function of θ

$$i_{c,real} = \frac{I_c}{A_{Fe}} = \frac{I_c}{A(1-\theta)} \tag{28}$$

At this point, a characteristic relationship between the real steady-state permeation rate of hydrogen ($i^{\infty}_{p,real}$) and the real applied current density ($i_{c,real}$) on the uncoated iron turned out to be helpful. It is common knowledge and it was also observed in this work (Fig. 31), that the permeation (entry) rate of the cathodically produced hydrogen is at most proportional to the square root of the current density (equation (15)). It is obvious that equation (15) applies primarily to the real current densities

$$i^{\infty}_{p,real} = k\sqrt{i_{c,real}} \tag{29}$$

where k is a coefficient characteristic of a given metal and hydrogen charging conditions.

Turning to the measured steady-state permeation current I^{∞}_{p} through the uncoated membrane

$$I^{\infty}_{p} = Ai^{\infty}_{p,real} = Ak\sqrt{i_{c,real}} = k\sqrt{AI_c} \tag{30}$$

and the suitable current $I^{\infty}_{p,coat}$ for the coated membrane may be expressed as

$$I^{\infty}_{p,coat} = A_{Fe}i^{\infty}_{p,real} = A(1-\theta)k\sqrt{i_{c,real}} = k\sqrt{A(1-\theta)I_c} \tag{31}$$

The comparison of equation (30) with equation (31) leads to the following expression for the ZrO_2 coverage

$$\theta = 1 - \left(\frac{I^{\infty}_{\mathrm{p,coat}}}{I^{\infty}_{\mathrm{p}}} \right)^2 \tag{32}$$

or passing to the current densities related to the geometric area A

$$\theta = 1 - \left(\frac{i^{\infty}_{\mathrm{p,coat}}}{i^{\infty}_{\mathrm{p}}} \right)^2 \tag{33}$$

Using the last equation (33) and substituting, for example, the following steady state hydrogen fluxes for i_c = 10 mA/cm^2, read from Fig. 31: i^{∞}_{p} = 34.0 μA/cm^2 for the uncoated membrane, $i^{\infty}_{\mathrm{p,coat}}$ = 7.1 and 3.8 μA/cm^2 for the coated membranes with two and five layers of ZrO_2, respectively, the values of ZrO_2 coverage: θ = 0.956 (two layers) and θ = 0.988 (five layers) were obtained. However, these values seem to be overstated and the reason for this is rather simple. Namely, looking at Fig. 31 one can note that values of $i^{\infty}_{\mathrm{p,coat}}$ taken into account and corresponded to i_c = 10 mA/cm^2, lie beyond the initial linear part of the curves $i^{\infty}_{p} = f(i_c)^{1/2}$. This is even more visible on Fig. 34, which is the re-plotted part of Fig. 31.

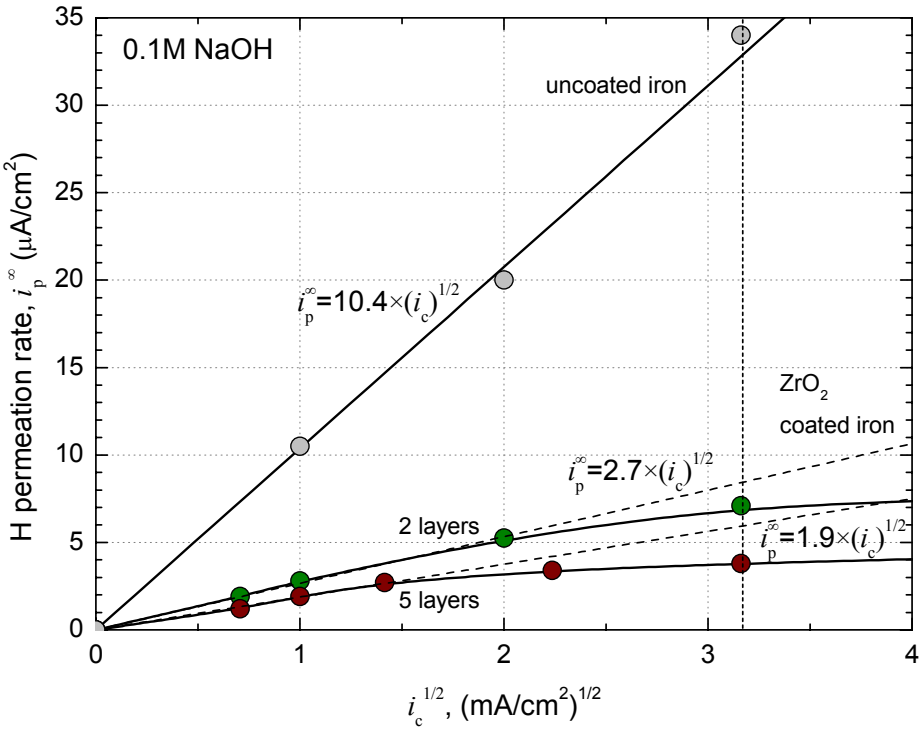

Fig. 34. An analysis of the relationship between the measured hydrogen permeation rate and the square root of cathodic current density for the uncoated and ZrO_2 coated iron membranes, as regard to low cathodic current densities (re-plotted from Fig. 31).

To obtain correct values of θ, one should take into account the values of i_p^∞ and $i_{p,coat}^\infty$ for a such value of i_c, which corresponds to the linear dependence of the steady-state permeation rate on the square root of i_c. Alternatively, and even more properly, one can take the pertinent slopes (Fig. 34), i.e. values of the factors k^* and k_{coat}^* in the following relationships for the uncoated membrane

$$i_p^\infty = k^* \sqrt{i_c} \tag{34}$$

and for the coated one

$$i_{p,coat}^\infty = k_{coat}^* \sqrt{i_c} \tag{35}$$

Thus

$$\theta = 1 - \left(\frac{k^*_{coat}}{k^*} \right)^2 \qquad (36)$$

In this way, the following values of θ were evaluated: $\theta = 0.933$ and $\theta = 0.967$ for the membranes with two and five ZrO_2 layers, respectively.

Knowing correct values of θ and using equation (26) one may calculate the uncoated area A_{Fe}, and then the real cathodic current density $i_{c,real}$ and the real permeation rate $i^{\infty}_{p,real}$. As an example, values of the pertinent parameters for the uncoated and coated membranes charged with hydrogen at i_c = 10 mA/cm^2 for 5 days are given in Table 3.

Table 3. Parameters (in evaluating order) characterizing the hydrogen evolution and permeation (entry) for the uncoated and ZrO_2 coated iron membranes cathodically charged with hydrogen. Charging conditions: 0.1 M NaOH, i_c = 10 mA/cm, t_{char} = 5 days.

Parameter	Unit	**Uncoated iron** membrane	**ZrO_2 coated iron** membrane	
			2 layers	5 layers
k^*	$\sqrt{uA}$/cm	10.4	-	-
k^*_{coat}	$\sqrt{uA}$/cm	-	2.7	1.90
θ	-	0	0.933	0.967
A_{Fe}	cm^2	0.5	0.034	0.017
i_c	mA/cm^2	10	10	10
$i_{c,real}$	mA/cm^2	10	147	294
i^{∞}_{p}	μA/cm^2	34	7.1	3.8
$i^{\infty}_{p,real}$	μA/cm^2	34	148	200

In the same way, taking the values of A_{Fe} (Table 3), the experimental relationship between the measured hydrogen permeation rate i^{∞}_{p} and the square root of cathodic current density i_c (related to the geometric area A, Fig. 31) were recalculated. The obtained dependence of the real permeation rate $i^{\infty}_{p,real}$ on the real cathodic current density $i_{c,real}$ is shown in Fig. 35.

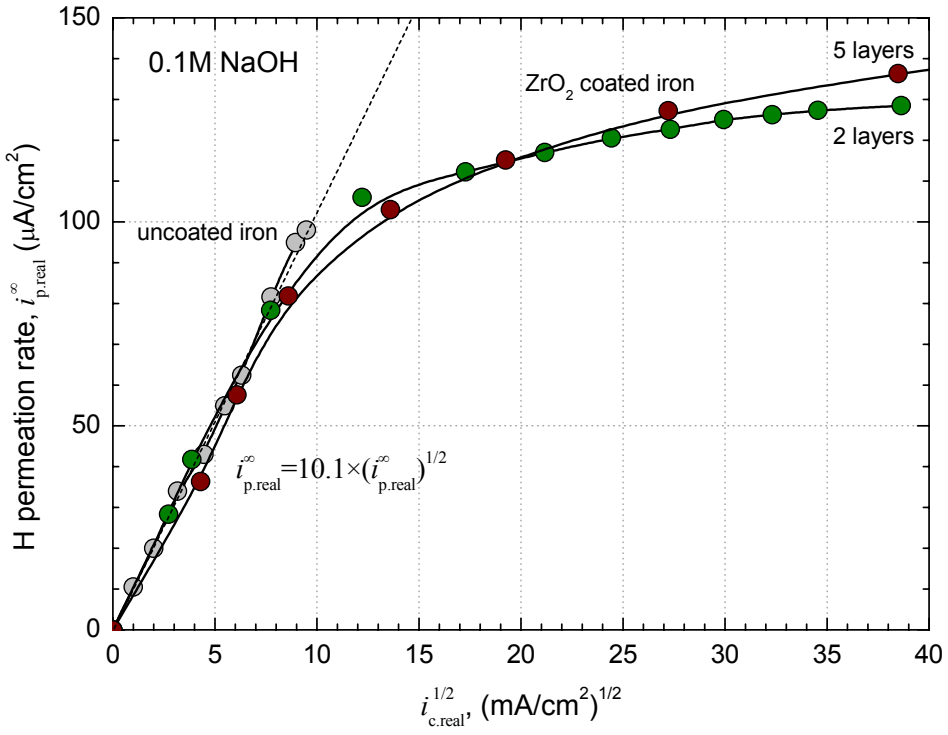

Fig. 35. Relationship between the real cathodic current density and the real permeation rate of hydrogen through the uncoated and ZrO_2 coated iron membranes.

As shown from the last figure, in the cathodic current range up to about 100 mA/cm^2, the real permeation rate of hydrogen was the same, linear function of the square root of the real cathodic current density (k = 10.1). It means that regardless of whether the iron membrane was coated with ZrO_2 or not, the entry of hydrogen into the uncovered (bare) iron proceeded according to the same mechanism. As it was mentioned earlier (equation (15)), the linear relationship between $i^{\infty}_{p,real}$ and $i^{1/2}_{c,real}$ clearly confirms that the entry of hydrogen into iron is preceded by adsorption of hydrogen atoms on its surface, and the entry rate is directly dependent on the production rate adsorbed hydrogen atoms. The same relationship between $i^{\infty}_{p,real}$ and $i^{1/2}_{c,real}$ for all membranes also confirms the assumption made that ZrO_2 partially blocked the iron surface and that both the hydrogen evolution and hydrogen entry occurred only on the ZrO_2-free iron surface.

When the $i_{c,real}$ increased more than 100 mA/cm^2, the hydrogen permeation rate grow up slower and slower (Fig. 35). It is understandable, because at the high current density range, other factors can influence on the hydrogen evolution reaction and hence

on the hydrogen entry. Among other things, one can assume that the capability of the bare iron surface to absorb hydrogen atoms (equation (1)) is limited. Unfortunately, the last assumption is difficult to verify experimentally on the uncoated membrane, because it requires extremely high applied currents, practically impossible to obtain from conventional power supplies.

5.4. Hydrogen desorption measurements

The electrochemical permeation measurements, described in the previous chapter, have focused on the entry of hydrogen into iron and on the role of ZrO_2 coating in this process. However, no less interesting is the role of this coating in the absorption of hydrogen inside the metal. This issue is complex because, as mentioned earlier, the absorbed hydrogen includes the so-called diffusible and trapped hydrogen. In quantitative terms, one should determine the amounts of these hydrogen forms, and possibly their distribution inside the metal (membrane).

The diffusible hydrogen is visible in the permeation flux (i_p). On the basis of equation (12), one could determine the steady-state concentration of the diffusible hydrogen beneath the membrane entry side (C_0), and then, assuming a linear gradient of hydrogen concentration (equation (13)), the steady state amount of the diffusible hydrogen q_{Hd} (equation (14)). However, to use equation (12), it is necessary to know the hydrogen diffusivity D. In turn, the reversibly trapped hydrogen may quantitatively determined by an analysis of the desorption rate of hydrogen from both sides of the previously charged membrane. This analysis also requires knowledge of the diffusion coefficient of hydrogen. Thus, correct determination of D is crucial.

5.4.1. Hydrogen diffusivity

After 5 days, at the end of the hydrogen charging, the successive partial build-up and decays permeation transients were recorded after changes of the cathodic current density from 10 to 20 mA/ cm^2 and then back to the previous value of 10 mA/ cm^2.

The obtained build-up and decay permeation transients for the uncoated iron membrane are shown in Fig. 36. It is seen that the experimental and computer-fitted permeation transients, using equations (7) and (8) for the build-up and decay, respectively, practically overlap each other. This indicates that the conditions required by equations (7) and (8) were fulfilled and that the obtained value of $D = 8.0\times10^{-5}$ cm^2/s,

taken as an average value of that resulted from the build-up and decay transients, may be considered as the lattice diffusivity of hydrogen in Armco iron at 30 ^{o}C. This value of D agrees with the reliable data for the lattice diffusivity of hydrogen in α iron [57,117].

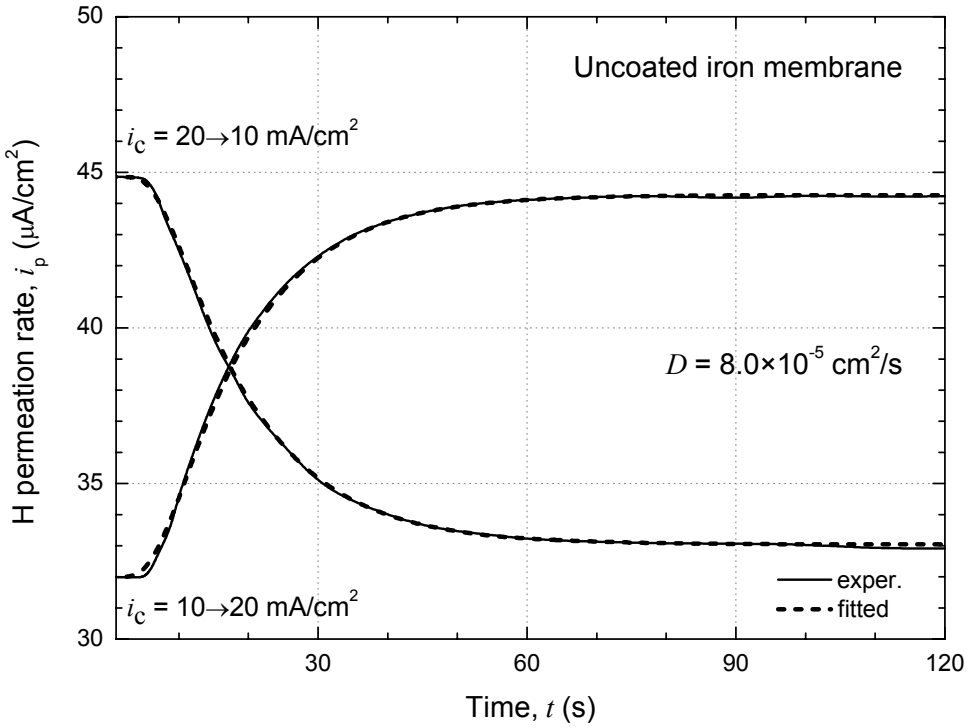

Fig. 36. Successive partial build-up and decay permeation transients for the uncoated iron membrane.

The pertinent permeation transients for the coated membranes with two and five layers of ZrO_2 are shown in Fig. 37a and Fig. 37b, respectively. In this case, there were small discrepancies between the experimental and computer-fitted permeation transients. Therefore, the resulted values of hydrogen diffusivity should be considered as the effective diffusion coefficients D_{eff}, characterizing rather the transport of hydrogen through whole given membrane, but not the mobility of hydrogen inside them. By the way, it was not surprising since the coated membranes were not homogeneous (uniform) as the uncoated membrane.

(a)

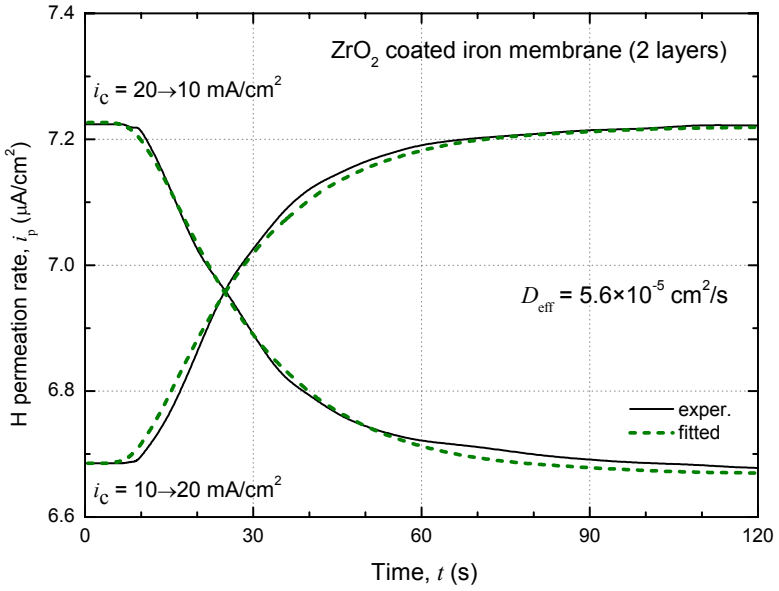

(b)

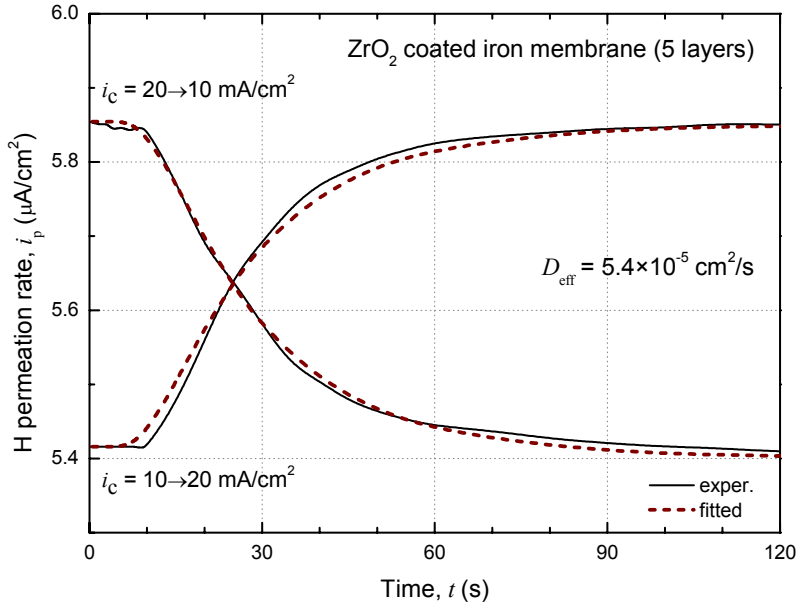

Fig. 37. Successive partial build-up and decay permeation transients for the coated iron membranes with two (a) and five (b) ZrO_2 layers.

One can note that the permeation transients for the coated membranes (Fig. 37) were somewhat delayed in relation to the transients for the uncoated one (Fig. 36), and hence $D_{eff} < D$. Formally, this fact could be considered as a contribution of the coatings to the hindrance of hydrogen transport. On the other hand, the real (lattice) diffusivity of

hydrogen in the iron substrate of the coated membrane should be the same like that in the uncoated membrane, i.e. D, and the lower values of D_{eff} are presumably caused by not sufficiently rapid change or rather settlement of the hydrogen concentration C_0 in the subsurface layer of iron of the coated membrane. As it was expected, the five-layer coating, as being thicker and probably more complex than the two-layer one, somewhat more influenced the concentration C_0.

5.4.2. Complete desorption of hydrogen

An analysis of the desorption rate of hydrogen from uncoated iron membrane, previously charged at its entry side in 0.1 M NaOH at i_c = 10 mA/cm^2 for 5 days, is shown in Fig. 38a and Fig. 38b, for the exit and formerly entry side, respectively. For both sides, the measured desorption rates ($i_{H,L}$ and $i_{H,0}$; black curves) were the sum of the pertinent desorption rates of the diffusible hydrogen ($i_{Hd,L}$ and $i_{Hd,0}$; green curves) and the trapped hydrogen ($i_{Ht,L}$ and $i_{Ht,0}$; red curves). Knowing D and assuming that the steady-state permeation rate i_p^{∞} corresponds to the initial desorption rate of the diffusible hydrogen at the exit side ($i_{Hd,L}^{o}$), the desorption rates of the diffusible hydrogen at the exit side $i_{Hd,L}$ (Fig. 38a) and at the entry side $i_{Hd,0}$ (Fig. 38b) were reconstructed using equation (16) and equation (17), respectively. Then, subtracting $i_{Hd,L}$ from $i_{H,L}$, and $i_{Hd,0}$ from $i_{H,0}$, the desorption rates of the trapped hydrogen at the exit side $i_{Ht,L}$ and at the entry side $i_{Ht,0}$, were obtained. Finally, integration of the relevant current densities in Fig. 38 gives the suitable amounts of the diffusible hydrogen ($q_{Hd,L}$ and $q_{Hd,0}$), the amounts of the reversibly trapped hydrogen ($q_{Ht,L}$ and $q_{Ht,0}$), and their appropriate sums ($q_{H,L}$ and $q_{H,0}$). The total amount of the absorbed hydrogen $q_H = q_{H,L} + q_{H,0}$. It should be noted that the amounts of the diffusible hydrogen $q_{Hd,L}$ and $q_{Hd,0}$, as well as their sum q_{Hd}, can be calculated directly using equations (18), (19) and (20), respectively.

The same analysis was performed for hydrogen desorption from the coated iron membranes with two (Fig. 39) and five (Fig. 40) layers of ZrO_2. All hydrogen amounts, originally obtained in electric charge units, were converted into molar units (mol H/cm^2) and they are summarized in Table 4.

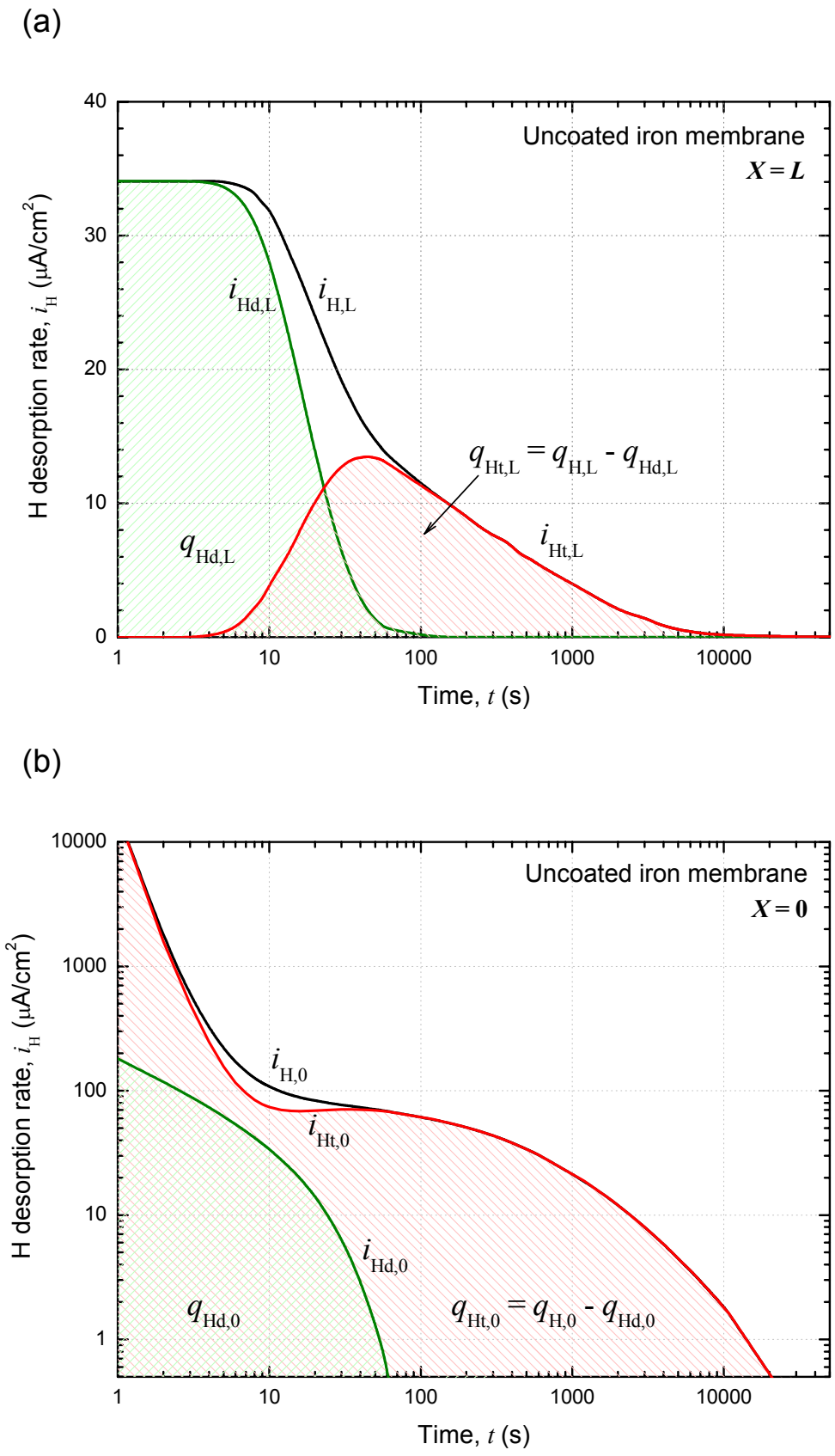

Fig. 38. An analysis of the desorption rate of hydrogen from the previously charged uncoated iron membrane at its exit (a) and entry (b) side.

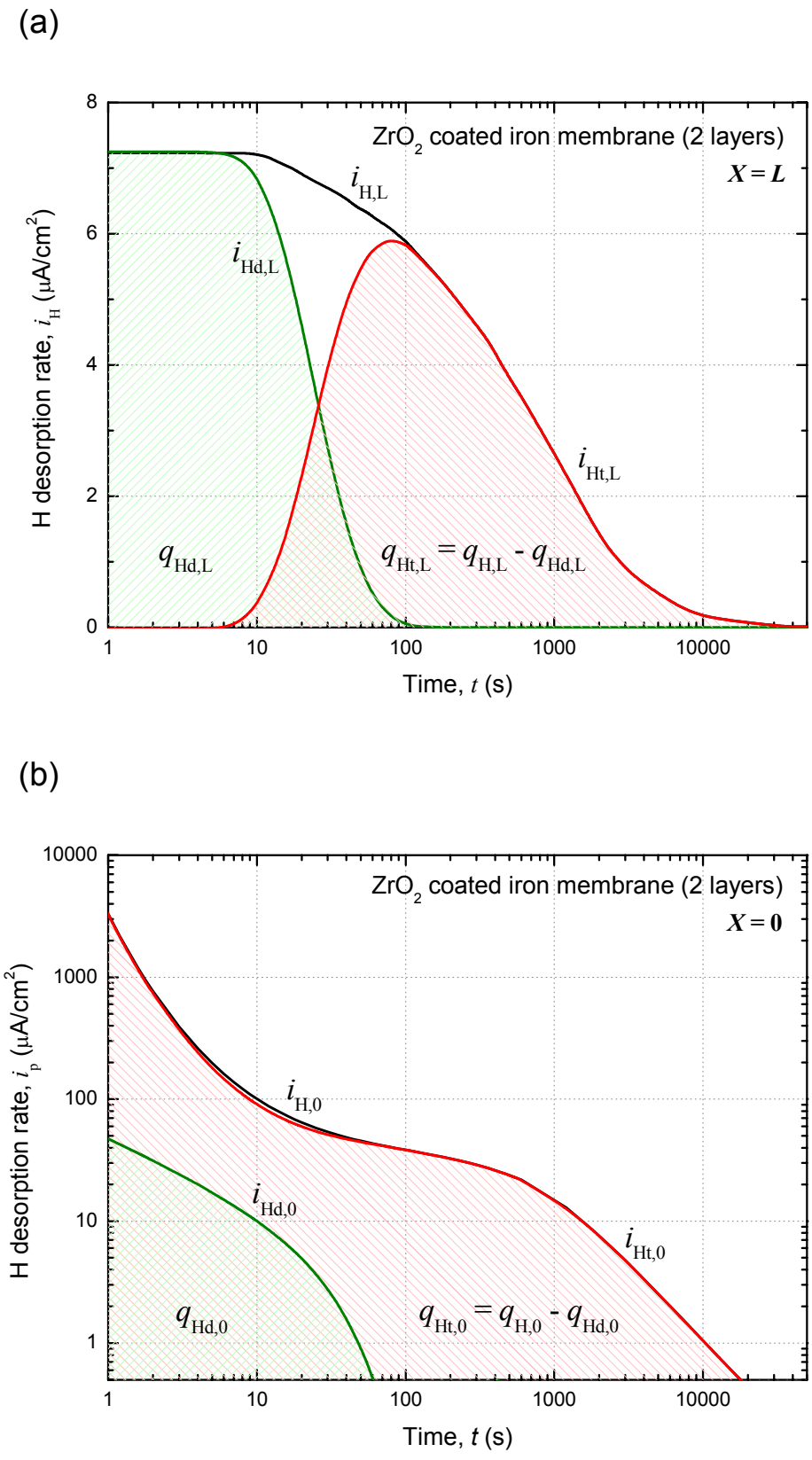

Fig. 39. An analysis of the desorption rate of hydrogen from the previously charged ZrO_2 coated (two layers) iron membrane at its exit (a) and entry (b) side.

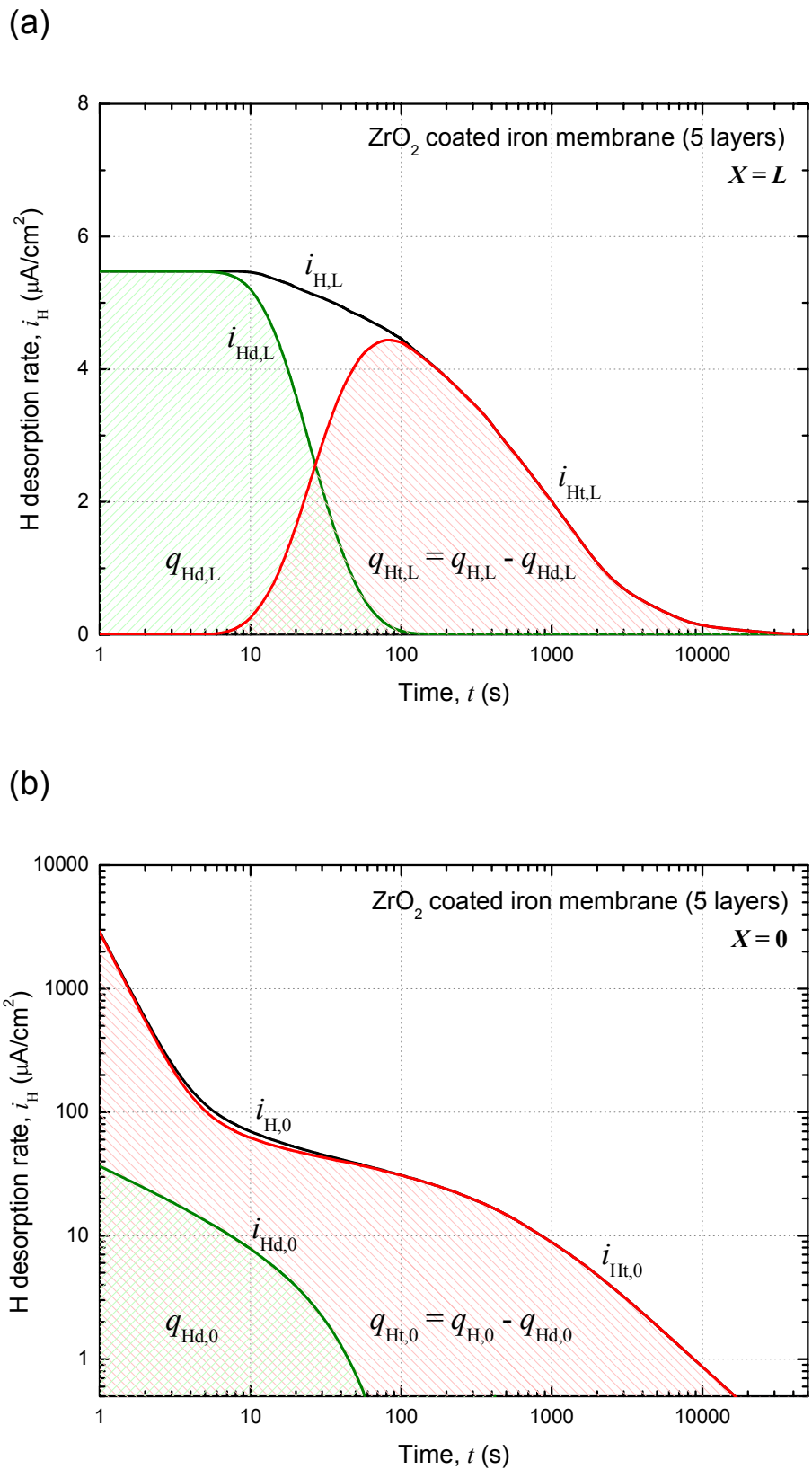

Fig. 40. An analysis of the desorption rate of hydrogen from the previously charged ZrO_2 coated (five layers) iron membrane at its exit (a) and entry (b) side.

Table 4. Partitioning of hydrogen desorbed from the previously charged uncoated and ZrO_2 coated iron membranes into their separate sides and into the different forms of the absorbed hydrogen. Charging conditions: 0.1 M NaOH, i_c = 10 mA/cm^2, t_{char} = 5 days.

	H diffusible		**H** trapped		**H** diffusible and **H** trapped	
	$q_{Hd}\times10^8$ (mol H/cm^2)	%	$q_{Ht}\times10^8$ (mol H/cm^2)	%	$q_H\times10^8$ (mol H/cm^2)	%
Uncoated iron membrane						
X=*L*	0.74	33,3	20.5	12.5	21.2	12.7
X=0	1.48	66.7	144.0	87.5	145.5	87.3
X=0 and X=*L*	2.22	100	164.5	100	166.7	100
%	**1.3**		**98.7**		**100**	
ZrO_2 coated iron membrane (2 layers)						
X=*L*	0.22	33.3	13.4	11.9	13.6	12.0
X=0	0.44	66.7	99.4	88.1	99.8	88.0
X=0 and *X*=*L*	0.66	100	112.7	100	113.4	100
%	**0.6**		**99.4**		**100**	
ZrO_2 coated iron membrane (5 layers)						
X=*L*	0.17	33.3	10.2	11.0	10.4	11.2
X=0	0.34	66.7	82.3	89.0	82.6	88.8
X=0 and *X*=*L*	0.51	100	92.5	100	93.0	100
%	**0.5**		**99.5**		**100**	

Looking at the data in Table 4, first of all, attention is drawn to the fact that the diffusible hydrogen was a very small part of the total amount of hydrogen in the membrane. Most of the absorbed hydrogen was the trapped hydrogen. With regard to the uncoated membrane it is normal since it was observed many times for iron membranes [10,118-120]. However, it is interesting that in the coated membranes, the contribution of the diffusible hydrogen in the total amount of hydrogen was even smaller.

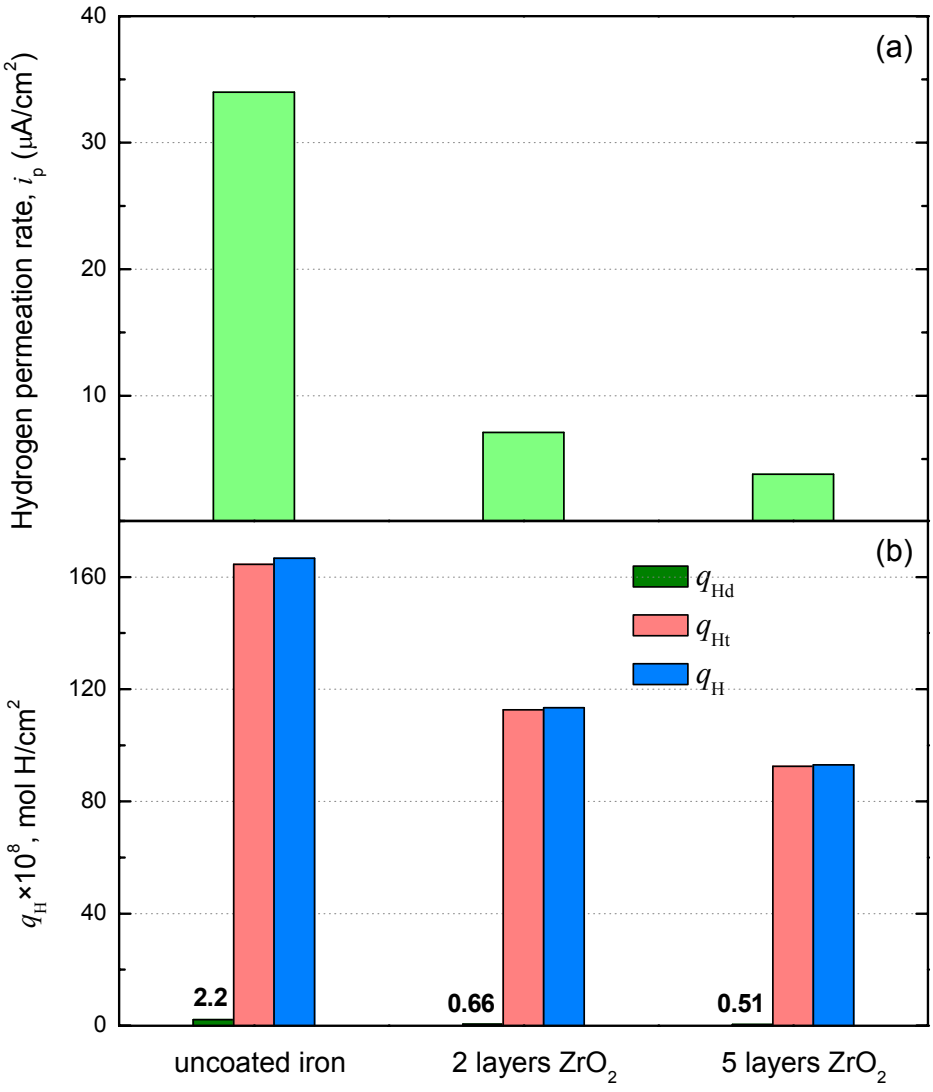

Fig. 41. Hydrogen permeation rate (a) and hydrogen balance for the cathodically charged uncoated and zirconia coated iron membranes. Charging in 0.1 M NaOH at i_c = 10 mA /cm^2 for t_{char}= 120 h.

Another conspicuous fact is that total amounts of hydrogen absorbed in the coated membranes were lower than that in the uncoated one. However, this decrease in the absorption of hydrogen was not too large - the ratio $q_H/q_{H,coat}$ was only about 1.5 and 1.8 for two and five layers of ZrO_2, respectively. In any case, the effect of the ZrO_2 coating on the entry of hydrogen was much higher - the pertinent ratio $i_p^\infty / i_{p,coat}^\infty$ was 4.8 (2 layers) and 8.9 (5 layers) – Table 3. This fact is even more perceptible in Fig. 41 comparing the permeation rate of hydrogen (a) with the hydrogen balance (b) for the cathodically charged uncoated and zirconia coated iron membranes. Since the trapped hydrogen composed a majority of the total amount of absorbed hydrogen, one can conclude that the ZrO_2 did not impede, but actually intensified hydrogen trapping.

The question is how the above behaviour of the coated membrane can be explained? It seems that the answer to this question can be found in the actual, higher values of the real cathodic current density $i_{c,real}$, and the resulting higher permeation (entry) rate of hydrogen $i_{p,real}^\infty$ at the ZrO_2-free sites of the coated membrane (Fig. 33). Namely, remembering equation (11), the steady-state permeation rate is proportional to the concentration of hydrogen beneath the entry surface (C_0), and inversely proportional to the hydrogen diffusivity D and the membrane thickness L. The actual concentration C_0 can be calculated substituting into equation (12) suitable values of the real permeation rate $i_{p,real}^\infty$ (Table 3), hydrogen diffusivities D (Fig. 36) and D_{eff} (Fig. 37). The obtained values of C_0 are given in Table 5. On this basis one can deduce that the local concentration of the diffusible hydrogen beneath the uncovered sites of the coated membranes was about 4.4 (for 2 layers) and 5.9 (for 5 layers) times higher than the concentration C_0 beneath the entry side of the uncoated membrane. Undoubtedly, higher concentration of the diffusible hydrogen means more intensive hydrogen trapping by the structural defects in the vicinity of the uncovered sites. Ultimately, although the amount of trapped hydrogen in the coated membrane was lower than that in the uncoated one (Table 4), however, this effect was smaller than expected from the measured permeation rates (referred to the geometric area).

Table 5. Real parameters characterizing the hydrogen charging ($i_{c,real}$), hydrogen transport (D, D_{eff}), hydrogen permeation ($i^{\infty}_{p,real}$) and the resulting concentration of hydrogen (C_0). Charging conditions: 0.1 M NaOH, i_c = 10 mA/cm^2, t_{char} = 5 days.

Parameter	Unit	**Uncoated iron** membrane	**ZrO_2 coated iron** membrane	
			2 layers	5 layers
$i_{c,real}$	mA/cm^2	10	147	294
D	cm^2/s	8.0×10^{-5}	-	-
D_{eff}		-	5.6×10^{-5}	5.4×10^{-5}
$i^{\infty}_{p,real}$	μA/cm^2	34	148	200
C_0	mol H/cm^3	6.29×10^{-7}	2.74×10^{-6}	3.84×10^{-6}

It is obvious that a rather weak effect of the ZrO_2 coating on the hindrance of hydrogen trapping is not beneficial for the prevention of hydrogen embrittlement. However, one should underline that the above considerations relate to hydrogen charging under the applied constant current. In this case, the cathodic evolution of hydrogen, in quantitative terms the same, was limited to a small part of the metal surface. Presumably, under different charging conditions, e.g. under potentiostatic charging, the ZrO_2 coating may be more effective.

Coming back to Table 4, one can note that a majority of the trapped hydrogen (more than 2/3 its amount) escaped from the uncoated and coated membranes their entry sides. It means that the distribution of the trapped hydrogen in the membrane was not represented by the linear concentration gradient (equation (13)), as it was for the diffusible hydrogen. One can conclude that the distribution of the trapped hydrogen, or strictly speaking the filling traps with hydrogen occurred mainly in the membrane region close to its entry side.

SUMMARY

Two-layer and five layer sol-gel zirconia coatings were deposited on one side of the Armco iron membranes by spin -coating, densified in air and annealed up to 800 ^{o}C in vacuum. The obtained ZrO_2 coatings were characterized using SEM, XPS and AFM techniques. The coatings were porous and their thickness was in the range of 120-300 nm, depending on the number of applied layers. Electrochemical examinations by the potentiodynamic polarization curves and the impedance spectroscopy (EIS) confirmed that the coatings were not completely tight, i.e. some sites on the iron surface were uncovered by ZrO_2.

According to the main goal of the work, hydrogen entry into the membranes, coated and uncoated, cathodically charged under galvanostatic control in 0.1 M NaOH solution was studied using the electrochemical permeation technique. During the initial period of charging, the effect of ZrO_2 coatings on hydrogen permeation (entry) was insignificant. However, the coatings quite efficiently prevented the iron surface become more active to hydrogen entry during a long-lasting cathodic charging. After 5 days of the uninterrupted charging, the overall permeation (entry) rate for the coated membranes was about 5 and about 9 times (for two- and five-layer coating, respectively) lower than the permeation rate through the uncoated membrane. At the same time, the cathodic potential of the ZrO_2 coated iron was much more negative than that for the uncoated iron. Both these effects strongly confirm the assumption that the ZrO_2 coatings blocked largely the iron surface for the hydrogen evolution reaction and, consequently, for the hydrogen entry into iron.

Assuming that both the hydrogen evolution and hydrogen entry occurred only on the ZrO_2-free iron surface, the effective coating coverage θ was determined by comparison of the hydrogen fluxes permeating the coated and uncoated membranes. The evaluating values of θ are ~0.93 and ~0.97 for the membranes with two and five ZrO_2 layers, respectively. Knowing θ, the real local entry rate of hydrogen and hence the real concentration of diffusible hydrogen beneath the ZrO_2-free iron site were evaluated. Under the same charging conditions, this local subsurface concentration of diffusible hydrogen was about 4 (for two-layer coating) and about 6 (for five-layer coating) times higher than the concentration of diffusible hydrogen beneath the entry side of the uncoated membrane.

The local increase in the concentration of diffusible hydrogen resulted in more intensive hydrogen trapping. Admittedly, the total amount of the trapped hydrogen, relatively to the membrane as a whole decreased, but not very strongly. Since, moreover, the trapped hydrogen accounted for almost the entire amount of absorbed hydrogen, the ZrO_2 coating was rather not very effective barrier to hydrogen absorption.

SYMBOLS

Latin symbols

A geometric area of the uncoated iron membrane, cm^2

A_{Fe} geometric area of the uncoated (free) sites on the zirconia coated membranes, cm^2

C capacitance, F/cm^2

C hydrogen concentration, mol H/cm^3

C_0 hydrogen concentration in the membrane at its entry side (X=0), mol H/cm^3

D hydrogen diffusivity, cm^2/s

D_{eff} effective hydrogen diffusivity, cm^2/s

F Faraday's constant, 96 485 C/mol

I_c cathodic (charging) current, mA

i_c cathodic (charging) current density, mA/cm^2

$i_{c,real}$ real cathodic current density, mA/cm^2

i_p hydrogen permeation rate, $\mu A/cm^2$

i_p^o initial steady-state permeation rate of hydrogen, $\mu A/cm^2$

i_p^∞ a new steady-state permeation rate of hydrogen, $\mu A/cm^2$

$i_{p,real}^\infty$ real hydrogen permeation rate, $\mu A/cm^2$

I_p^∞ steady-state hydrogen permeation current through the uncoated membrane, μA

$I_{p,coat}^\infty$ steady-state hydrogen permeation current through the zirconia coated membranes, μA

i_H desorption rate of hydrogen

$i_{H,L}$ desorption rate of hydrogen at the membrane exit side (X=L), $\mu A/cm^2$

$i_{H,0}$ desorption rate of hydrogen at the membrane entry side (X=0), $\mu A/cm^2$

$i_{Hd,L}$ desorption rate of the diffusible hydrogen at the membrane exit side, $\mu A /cm^2$

$i_{Hd,0}$ desorption rate of the diffusible hydrogen at the membrane entry side, $\mu A /cm^2$

$i_{Ht,L}$ desorption rate of the trapped hydrogen at the membrane exit side, $\mu A/cm^2$

$i_{Ht,L}$ desorption rate of the trapped hydrogen at the membrane entry side, $\mu A/cm^2$

k hydrogen permeation (entry) coefficient characterizing a given metal and charging conditions

k^* slope in the linear dependence of steady-state permeation rate on the square root of cathodic current density for the uncoated membrane

k_{coat}^* slope in the linear dependence of steady-state permeation rate on the square root of cathodic current density for the zirconia coated membrane

L	thickness of the membrane, mm
NHE	normal hydrogen electrode
R_s	electrolyte resistance, Ω/cm^2
R_p	pore resistance, Ω/cm^2
R_{ct}	charge transfer resistance, Ω/cm^2
q_H	total amount of hydrogen in the membrane, mol H/cm^2
$q_{H,coat}$	total amount of hydrogen in the for zirconia coated membrane, mol H/cm^2
q_{Hd}	total amount of the diffusible hydrogen, mol H/cm^2
q_{Ht}	total amount of the trapped hydrogen, mol H/cm^2
$q_{Hd,L}$	amount of the diffusible hydrogen leaving the membrane its exit side, mol H/cm^2
$q_{Hd,0}$	amount of the diffusible hydrogen leaving the membrane its entry side, mol H/cm^2
$q_{Ht,L}$	amount of the trapped hydrogen leaving the membrane its exit side, mol H/cm^2
$q_{Ht,0}$	amount of the trapped hydrogen leaving the membrane its entry side, mol H /cm^2
t	time, s
t_b	breakthrough time, s
t_{char}	charging time, s, h, days
X	distance in the membrane, mm
Z'	the real part of impedance (resistance), Ω cm^2
Z''	the imaginary part of impedance (reactance), Ω cm^2

Greek symbols

f	frequency, Hz
φ	phase angle, deg
θ	coating coverage

REFERENCES

1. I. Matsushima, H.H. Uhlig, Protection of steel from hydrogen cracking by thin metallic coatings, *J. Electrochem. Soc*., 113 (1966) 555.
2. S.S. Chatterjee, B.G. Ateya, H.W. Pickering, Effect of electrodeposited metals on the permeation of hydrogen through iron membranes, *Met. Trans*. A 9 (1978) 389.
3. R.H. Song, S. Pyun, Hydrogen permeation through a bilayer of Fe/electrodeposited Ni, *J. Electrochem. Soc*., 137 (1990) 1051.
4. M. Zamanzadeh, A. Allam, C. Kato, B.G. Ayeya, H.W. Pickering, Hydrogen absorption during electrodeposition and hydrogen charging of Sn and Cd coatings on iron, *J. Electrochem. Soc*., 129 (1982) 284.
5. J-M.Chen, J-K. Wu, Hydrogen diffusion through copper-plated AISI 4140 steels, *Corros. Sci*., 33 (1992) 657.
6. A.H. Bott, S.P. Bruhl, B. Gomez, M.A. Zampronio, P.E.V. Miranda, F.J. Feugeas, Pulsed-plasma-nitrided API 5L X-65 steel: hydrogen permeability and microstructural aspects, *J. Phys. D* 31 (1998) 3469.
7. T. Zakroczymski, N. Lukomski, J. Flis, Entry and transport of hydrogen in ion nitrided iron, *J. Electrochem. Soc*., 140 (1993) 3578.
8. T. Zakroczymski, N. Lukomski, J. Flis, The effect of plasma nitriding-base treatments on the absorption of hydrogen by iron, *Corros. Sci*., 37 (1995) 811.
9. T. Zakroczymski, J. Flis, N. Lukomski, J. Mankowski, Entry, transport and absorption of hydrogen in low-temperature plasma nitrided austenitic stainless steel, *Acta Mater*., 49 (2001) 1929.
10. Z. Wolarek, T. Zakroczymski, Hydrogen absorption in plasma-nitrided iron, *Acta Mater*., 54 (2006) 1525.
11. A.M. Brass, J. Chene, A. Boruty Forville, Depth profiling of cathodic deuterium in pure iron implanted with titanium or carbon, *Corros. Sci*., 39 (1997) 1469.
12. A. Kumar, B. Ravikumar, S. Mukherjee, A. Basumallick, I. Chattoray, Alteration in hydrogen absorption by and hydrogen permeation through a high-strength low-alloy steel due to plasma source ion implantation of nitrogen, *Metall. Mater. Trans. B*, 36 (2004) 1123.
13. L.C. Klein (Ed.), Sol-Gel Technology for Thin Films Fibers, Preforms, Electronics, and Specialty Shapes, Noyes Publications, Park Ridge, N.J., 1988.
14. J.D. Mackenzie, E.P. Bescher, Physical propertiws of sol-gel coatings, *J. Sol-Gel Sci. Technol*., 19 (2000) 23.
15. K. Izumi, M. Murakami, T. Deguchi, A. Morita, N. Tohge, T. Minami, Zirconia coating on stainless steel sheets from organozirconium compounds. *J. Amer. Ceram. Soc.*, 72 (1989) 1465.
16. M. Atik, J. Zarzycki, C. R' Kha, Protection of ferrite stainless steel against oxidation by zirconia coatings, *J. Mater. Sci. Lett*., 13 (1994) 266.

17. M. Atik, M. A. Aegerter, Corrosion resistance sol-gel ZrO_2 coatings on stainless steel, *J. Non-Cryst. Solids*, 147-148 (1992) 813.

18. M. Atik, S. H. Messaddeo, F. P. Luna, M. A. Aegerter, Zirconia sol-gel coatings deposited on 304 and 316L stainless steel for chemical protection in acid media, *J. Mater. Sci. Lett*., 15 (1996) 2051.

19. M. Atik, C. R' Kha, P. De Lima Neto, L. A. Avaca, M. A. Aegerter, J. Zarzycki, Protection of 316L stainless steel by zirconia sol-gel coatings in 15% H_2SO_4 solution, *J. Mater. Sci. Lett.,* 14 (1995) 178.

20. M. Atik, P. De Lima Neto, L. A. Avaca, M. A. Aegerter, Sol-gel thin films for corrosion protection, *Ceramics International.*, 21 (1995) 403.

21. I. Rotariu, G.L. Turdean, F. Kormos, D. Macarovici, G. Tolnai, I. Felhosi, P. Nagy, L. Trif, E. Kalman, The corrosion study of ZrO_2 coatings on metals, *Materials Sci. Forum.*, 537-538 (2007) 247.

22. F. Perdomo L., P. De Lima-Neto, M.A. Aegerter, L.A. Avaca, Sol-gel deposition of ZrO_2 films in air and oxygen-free atmospheres for chemical protection of 304 stainless steel: a comparative corrosion study, *J. Sol-Gel Sci. Technol.,* 15 (1999) 87.

23. L. Fedrizzi, F.J. Rodriguez, S. Rossi, F. Deflorian, R.Di Maggio, The use of electrochemical techniques to study the corrosion behaviour of organic coatings on steel pretreated with sol-gel zirconia films, *Electrochim. Acta*, 46 (2001) 3715.

24. J.F. Quinson, C. Chino, A.M. De Becdelievre, C. Guizard, M. Brunel, Deformation capability and protectiove role of zirconia coatings on stainless steel, *J. Mater. Sci*., 31 (1996) 5179.

25. J. Gluszek, *Tlenkowe Powłoki Ochronne Otrzymane Metodą Sol-Gel,* Oficyna Wydawnicza Politechniki Wrocławskiej, Wrocław, 1998.

26. M. Shane, M.L. Mecartney, Sol-gel syntesis of zirconia barrier coatings, *J. Mater. Sci*., 25 (1990) 1537.

27. A.S. Hamdy, D.P. Butt, A.A. Ismail, Electrochemical impedance studies of sol–gel based ceramic coatings systems in 3.5% NaCl solution, *Electrochim. Acta*., 52 (2007) 3310.

28. M. Fallet, H. Mahdjoub, B. Gautier, J.P. Bauer, Electrochemical behaviour of ceramic sol–gel coatings on mild steel, *J. Non-Crystal. Solids,* 293-295 (2001) 527.

29. M. Atik, P. De Lima Neto, J. Zarzycki, Protection of 316L stainless steel against corrosion by SiO_2 coatings, *J. Mater. Sci. Lett*. 13 (1994) 1081.

30. J.G. Chęcmanowski, B. Szczygieł, Właściwości ochronne powłok SiO_2 otrzymanych metodą zol-żel na stali 316L w funkcji ilości warstw oraz temperatury spiekania-badania potencjodynamiczne, *Ochronę przed korozją*, Nr 11s/A (2005)137.

31. T.P. Chou, C. Chandrasekaran, S.J. Limmer, S. Seraji, Y. Wu, M.J. Forbess, C. Nguyen, G.Z. Cao, Organic–inorganic hybrid coatings for corrosion protection, *J. Non-Cryst. Solids,* 290 (2001) 153.

32. J.G. Chęcmanowski, J. Głuszek, J. Masalski, The effect of sequence of sol-gel multilayer coatings deposited on corrosion behaviour of stainless steel 316L, *Mater. Sci*., 21 (2003) 387.

33. E. Szałkowska, J. Masalski, J. Głuszek, Electrochemical evaluation of protective properties of one-component SiO_2 and TiO_2 coatings obtained by the sol-gel method, *Mater. Sci*., 21 (2003) 367.

34. P. Galliano, J.J. Damborenea, M.J. Pascual, A. Duran, Sol-gel coatings on 316L steel for clinical applications, *J. Sol-Gel Sci. Technol*., 13 (1998) 723.

35. U. Wellbrock, W. Beier, G.H. Frischat, Preparation of SiO_2-TiO_2-ZrO_2 gel glasses and coatings by means of modified alkoxide solutions, *J. Non-Crystal. Solids,* 147-148 (1992) 350.

36. J.G. Chęcmanowski, B. Szczygieł, Własciwosci ochronne powłok ceramicznych wytworzonych metoda zol-żel w srodowisku płynów fizjologicznych, *Ochrona przed korozią*, 4-5 (2010) 201.

37. M.L. Zhelubkevich, I.M. Salvado, M.G.S. Ferreira, Sol–gel coatings for corrosion protection of metals, *J. Mater. Chem*. 15 (2005) 5099.

38. B.C. Dave, X. Hu, Y. Devaray, Sol–gel-derived corrosion-protection coatings, *J. Sol-Gel Sci. Technol.*, 32 (2004) 143.

39. N.N. Voevodin, N.T. Grebash, W.S. Soto, F.E. Arnold, M.S. Donley, An organically modified zirconate film as a corrosion-resistant treatment for aluminum 2024-T3, *Surf. Sci. Technol.*, 140 (2001) 24.

40. S.V. Lamaka, M.F. Montemor, A.F. Galio, M.L. Zhelubkevich, C. Trindade, L.F. Dick, M.G.S. Ferreira, Novel hybrid sol-gel coatings for corrosion protection of AZ31B magnesium alloy**,** *Electrochem. Acta,* 53 (2008) 4773.

41. A. Pepe, P. Galianno, M. Aparicio, A. Durán, S. Ceré, Sol-gel coatings on carbon steel: Electrochemical evaluation, *Surf. Coat. Technol*, 200 (2006) 3486.

42. M. Fallet, H. Machdjoub, B. Gautier, J. P. Bauer, Electrochemical behaviour of ceramic sol–gel coatings on mild steel, *J. Non-Cryst. Solids* 293-295 (2001) 527.

43. R.W. Staehle, A.J. Forty, D.van Rooyen, eds., Fundamental aspects of stress corrosion cracking, NACE-1, Houston, (1969).

44. I.M. Bernstein A.W. Thompson, eds., Hydrogen in metals, ASM, Metals Park, Ohio (1974).

45. A.W. Thompson, I.M. Bernstein, eds., Effect of hydrogen on behaviour of materials, TMS-AIME, New York (1976).

46. R.W. Staehle, J. Hochman, R.D. McCright, J.E. Slater, eds., Stress Corrosion Cracking Hydrogen Embrittlement of Iron Base Alloys, NACE-5, (1977).

47. R. Hanada, in Proceedings of the Second International Congress Hydrogen in Metals, Paris, (1977), Pergamon, Oxford (1978).

48. R.Gibala, R.F. Hehemann, eds., Hydrogen embrittlement and stress corrosion cracking, ASM (1984).

49. R.P. Gangloff, M.B. Ives, eds., Environment-induced cracking of metals, NACE-10, Houston (1990).

50. A.W. Thompson, R.N. Moody, eds., Hydrogen effects in materials, TMS, Moran, Wyoming (1994).

51. M. Śmiałowski, „Wodór w stali", WNT, Warszawa (1961); „Hydrogen in Steel", Pergamon, Oxford (1962).

52. J. Flis (red.) „Wodorowe i korozyjne niszczenie metali", PWN, Warszawa (1978); J. Flis, ed „Corrosion of metals and hydrogen-related phenomena", Elsevier, Amsterdam, PWN, Warszawa (1991).

53. R.A. Oriani, J.P. Hirth, M. Smialowski, eds., Hydrogen degradation of ferrous alloys, Noyes Publications (1985).

54. J.O'M, Bockris, J. McBreen, L. Nanis, The hydrogen evolution kinetics and hydrogen entry into *a*-iron, *J. Electrochem.Soc*., 112 (1965) 1025.

55. M.A.V. Devanathan, Z. Stachurski, The mechanism of hydrogen evolution on iron in acid solutions by determination of permeation rates, *J. Electrochem. Soc*., 111 (1964) 619.

56. G. Alefeld, J. Volkl eds., „Hydrogen in metals, topics in applied physics", Vol. 28, Springer-Verlag (1978), p. 321.

57. K. Kiuchi, R.B. McLellan, The solubility and diffusivity of hydrogen in well-annealed and deformed iron, *Acta Metall*., 31 (1983) 961.

58. H.. Addach, P. Bercot, M. Rezrazi, M. Wery, Hydrogen permeation in iron at different temperatures, *Mater. Lett*., 59 (2005) 1347.

59. M. Smialowski, in: R. W. Staehle, J. Hochmann, R. D. McCright, J.E. Slater (Eds.), Provc. Intern. Conf. on SCC and HE of Iron Base Alloys, NACE-5, (1997), p. 405

60. M. Devanathan, Z. Stachurski, The adsorption and diffusion of electrolytic hydrogen in palladium, *Proc. R. Soc*., 270A (1962) 90.

61. J. McBreen, L. Nanis, W. Beck, A method for determination of the permeation rate of hydrogen through metal membranes, *J. Electrochem. Soc*., 113 (1966) 1218.

62. L. Nanis, TKG. Namboodhiri, Mathematics of the electrochemical extraction of hydrogen from iron, *J. Electrochem. Soc*., 119 (1972) 691.

63. T. Zakroczymski, Electrochemical determination of hydrogen in metals, *J. Electroanal. Chem*., 475 (1999) 82.

64. T. Zakroczymski, Adaptation of the electrochemical permeation technique for studying entry, transport and trapping of hydrogen in metals, *Electrochimica Acta,* 51 (2006) 2261.

65. Z. Wolarek, T. Zakroczymski, Hydrogen absorption in plasma-nitrided iron, *Acta Mater.,* 54 (2006) 1525.

66. T. Zakroczymski, E. Owczarek, Electrochemical investigation of hydrogen absorption in a duplex stainless steel, *Acta Mater.,* 50 (2002) 2701.

67. T. Casanova, J. Crousier, The influence of an oxide layer on hydrogen permeation through steel, *Corros. Sci.*, 38 (1996) 1535.

68. Y.F.Cheng, L. Niu, Mechanism for hydrogen evolution reaction on pipeline steel in near-neutral pH solution, *Electrochem. Communicat.,* 9 (2007) 558.

69. C. Gabrielli, G. Maurin, L. Mirkova, H. Perrot, Transfer function analysis of hydrogen permeation through a metallic membrane in a Devanathan cell: Part II: Experimental investigation on iron membrane, *J. Electroanal. Chem*., 590 (2006) 15.

70. E. Owczarek, T. Zakroczymski, Hydrogen transport in a duplex stainless steel, *Acta Mater*., 48 (2000) 3059.

71. T. Zakroczymski, Z. Szklarska-Smialowska, Activation of the iron surface to hydrogen absorption resulting from a long cathodic treatment in NaOH solution, *J. Electrochem. Soc.*, 132 (1985) 2548.

72. T. Zakroczymski, Entry of hydrogen into iron alloys from the liquid phase, *Scripta Metallurgica*, 19 (1985) 521.

73. M. Bodenstein, Diffusion of cathode hydrogen through iron and platinum, *Z. Electrochem*., 28 (1922) 517.

74. T. Zakroczymski, Electrochemical determination of hydrogen in metals, *J. Electroanal. Chem*., 475 (1999) 82.

75. J.D. Wright, N.A.J.M. Sommerdijk, Sol-gel materials: chemistry and applications, CRC Press, OPA Overseas Publishers association, 2001.

76. A.C. Pierre, Introduction to sol-gel processing, Kluwer Academic Publishers, 2000.

77. C.J. Brinker, G.W. Scherer, Sol-gel Science; The Physics and Chemistry of Sol-Gel Processing, Harcourt Brace Jovanovich (Academic Press, Inc.) Boston, 1990.

78. D. Wang, Gordon P. Bierwagen, Sol–gel coatings on metals for corrosion protection, *Progress in Organic Coatings* 64 (2009) 327-338.

79. J. Livage, D. Ganguli, Sol-gel electrochromic coatings and devices: review, *Solar Energy Materials and Solar Cell,s* 68 (2001) 365-381.

80. M.L. Zheludkevich, R. Serra, M.F. Montemor, I.M. Miranda Salvado, M.G.S. Ferreira, Corrosion protective properties of nanostructured sol–gel hybrid coatings to AA2024-T3, *Surf. Coat. Technol*. 200 (2006) 3084.

81. R. Gupta, A. Kumar, Molecular imprinting in sol–gel matrix, *Biotechnology Advances,* 26 (2008) 533.

82. Y. Castro, B. Ferrari, R. Moreno, A. Duran, Silica sol-gel coatings on metals produced by EPD, *J. Sol-Gel Sci. Technol*., 26 (2003) 735.

83. T.P. Chou, C. Chandrasekaran, G.Z. Cao, Sol-gel-derived hybrid coatings for corrosion protection, *J. Sol-Gel Sci. Technol*., 26 (2003) 321.

84. D. Niznansky, J.L. Rehspringer, Infrared study of SiO_2 sol to gel evolution and gel aging, *Gel Sci. Technol*., 180 (1995) 191.

85. A.N. Khramov, N.N. Voevodin, V.N. Balbyshev, M.S. Donley, Hybrid organo-ceramic corrosion protection coatings with encapsulated organic corrosion inhibitors*, Thin Solid Films*, 447-448 (2004) 549.

86. http://www.clean.cise.columbia.edu/process/spintheory.pdf

87. C.J. Brinker, A.J. Hurd, Fundamentals of sol-gel dip-coatings, *J. Phys III France* 4 (1994) 1231.

88. http://home.wanadoo.nl/tom.peeters/Subpaginas/spin%20coating.htm

89. http://large.stanford.edu/courses/2007/ph210/hellstrom1/

90. http://www.solgel.com/articles/Nov00/mennig.htm

91. R.L. Parkhill, E.T. Knobbe, M.S. Donley, Application and evaluation of environmentally compliant spray-coated ormosil films as corrosion resistant treatments for aluminum 2024-T3, *Prog. Org. Coat*., 41 (2001) 261.

92. M. Kobayashi, C-K Jen, J-F Moisan, N Mrad, S B Nguyen, Integrated ultrasonic transducers made by the sol–gel spray technique for structural health monitoring, *Smart Materials and Structures*, 16 (2007) 317.

93. K. Watanabe, M. Sakairi, H. Takahashi, S. Hirai, S. Yamagushi, Formation of Al–Zr composite oxide films on aluminum by sol–gel coating and anodizing, *J Electroanal Chem*., 473 (1999) 250.

94. M. Sheffer, A. Groysman and D. Mandler, Electrodeposition of sol–gel films on Al for corrosion protection, *Corros. Sci*., 45 (2003) 2893.

95. M. Paunovic, M. Schlesinger, Fundamentals of Electrochemical Deposition, John Wiley & Sons, Inc, Hoboken, new jersey, 2006.

96. S. Sakka, Handbook of Sol-gel Science and Technology, Processing Characterization and Application, Kluwer Acad. Publish., Boston/Dorbrecht, London, 2005.

97. L Fedrizzi, F. J. Rodriguez, S. Rossi, F. Deflorian, R.D. Maggio, The use of electrochemical techniques to study the corrosion behaviour of organic coatings on steel pretreated with sol–gel zirconia films, *Electrochim. Acta* 46 (2001) 3715.

98. O. Lev, Z. Wu, S. Bharathi, V. Glezer, A. Modestov, J. Gun, L. Rabinovich, S. Sampath, Sol-gel materials in electrochemistry, *Chem. Mater.***,** 9 (1997) 2354.

99. M.J. Paterson, B. Ben-Nissan, Multilayer sol-gel zirconia coatings on 316 stainless steel, *Surf. Coat. Technol*., 86-87 (1996) 153.

100. T.V. Gestel, H.K. Kruidhof, D.H.A. Blank, ZrO_2 and TiO_2 membranes for nanofiltration and pervaporation Part 1. Preparation and characterization of a corrosion-resistant ZrO_2 nanofiltration membrane with a MWCO< 300, *J. Membr. Sci.*, 284 (2006) 128.

101. H. Li, K. Liang, L. Mei, S. Gu, Oxidation resistance of mild steel by zirconia sol-gel coatings, *Mater. Sci. Engineering*, A341 (2003) 87.

102. L.F. Perdomo, L.A. Avaca, M.A. Aegerter, P. De Lima-Neto, Oxygen free *J. Mater. Sci. Lett*. 17 (1998) 295.

103. M. Smialowski, in Proc. Intern. Conf. on SCC and HE of Iron Base Alloys, Unieux-Firminy, 1973, NACE-5, R.W. Staehle, J. Hochmann, R.D. McCright, J.E. Slater (Eds.), 1997 p. 405.

104. T. Zakroczymski, Z. Szklarska-Smiałowska, M. Smiałowski, Effect of arsenic on permeation of hydrogen through steel membranes polarized cathodically in aqueous solution, *Werkst. u. Korros*. 26 (1975) 617.

105. NIST X-Ray Photoelectron Spectroscopy Database. NIST Standard Reference A. Kraut-Vass, J. W. Allison, C.J. Powell, J. R. Rumble Jr.), http://srdata.nist.gov/xps.

106. A. Gajek, T. Zakroczymski, Long-lasting hydrogen evolution on and hydrogen entry into iron in an aqueous solution, *J. Electroanal. Chem*., 578, 171 (2005).

107. J. Flis, T. Zakroczymski, V. Kleshnyal, T. Kobiela, R. Duś, Changes in hydrogen entry rate in surface of iron during cathodic polarization in alkaline solutions, *Electrochim. Acta*, 44 (1999) 3989.

108. G. Grundmeier, W. Schmidt, M. Stratmann, Corrosion protection by organic coatings: electrochemical mechanism and novel methods of investigation, *Electrochem. Acta,* 45 (2000) 2515.

109. A. Pepe, P Galliano, M. Aparicio, A. Duran, S. Cere, Sol-gel coatings on carbon steel: Electrochemical evaluation, *Surf. Coat. Technol*., 200 (2006) 3486.

110. F. Mansfeld, H. Shih, H. Greene, C.H Tai, in: J.R.Scully, D.C.Silverman, M.W. Kending (Eds.), Electrochemical impedance – analysis and interpretation, ASTM, Philadelphia, 1993, p. 37.

111. K. Kiuchi, R.B. McLellan, The solubility and diffusivity of hydrogen in well-annealed and deformed iron, *Acta Matell*., 31 (1983) 961.

112. T. Zakroczymski, J. Flis, Impedance characterization of the activation of iron surface for hydrogen entry from alkaline solution, *Electrochim. Acta,* 41 (1996) 1245.

113. A. Gajek, T. Zakroczymski, Long-lasting hydrogen evolution on and hydrogen entry into iron in an aqueous solution, *J. Electroanal. Chem*., 578 (2005) 171.

114. I. Flis-Kabulska, T. Zakroczymski, J. Flis, Accelerated entry of hydrogen into iron from NaOH solutions at low cathodic and low anodic polarizations, *Electrochim. Acta,* 52 (2007) 2966.

115. I. Flis-Kabulska, J. Flis, T. Zakroczymski, Promotion of hydrogen entry into iron from NaOH solution by iron–oxygen species, *Electrochim. Ac*ta, 52 (2007) 7158.

116. P. Abélard, F.F. Baumard, The electrical conductivity of cubic stabilized zirconia: The results of an IUPAC collaborative study (Technical Report), *Pure Appl. Chem*. 67 (1995) 1891.

117. T. Zakroczymski, Z. Szklarska-Smialowska, Activation of the iron surface to hydrogen absorption resulting from a long cathodic treatment in NaOH solution, *J. Electrochem. Soc*., 132 (1985) 2548.

118. T. Zakroczymski, Electrochemical method for hydrogen determination in steel, *Corrosion,* 38 (1982) 218.

119. T. Zakroczymski, Adaptation of the electrochemical permeation technique for studying entry, transport and trapping of hydrogen in metals, *Electrochim. Acta*, 51 (2006) 2261.

120. T. Zakroczymski, Electrochemical determination of hydrogen in metals, *J. Electroanal. Chem*., 475 (1999) 82.

Results described in this dissertation were partially placed in the following publications:

1. I. Zakorchemna, N. Carmona, T. Zakroczymski
   Hydrogen permeation through sol-gel coated iron during galvanostatic charging
   Electrochimica Acta, 53 (2008) 8154.
2. G. Shul, W.Nogala, I. Zakorchemna, J. Niedziolka, M. Opallo
   Scanning electrochemical microscopy study of ion transfer process across water/2-nitrophenyloctylether interface supported by hydrophobic carbon ceramic electrode
   J. Solid State Electrochem, 12 (2008) 1285.
3. I. Zakorchemna, N. Carmona
   Hydrogen entry into iron with sol-gel coating
   Ochrona przed korozją, 11s (2006) 171.
4. I. Zakorchemna, T. Zakroczymski
   Determination of the sol-gel surface coverage on iron by electrochemical hydrogen permeation technique
   Ochrona przed korozją, 50 (11s/A) (2007) 75.
5. I. Zakorchemna, T. Zakroczymski
   Wnikanie wodoru do żelaza pokrytego powłoką ZrO_2
   Ochrona przed korozją, 51 (4-5) (2008) 127.
6. I. Voloshchuk, T. Zakroczymski
   Wpływ zol-żelowej powłoki ZrO_2 na elektrochemiczne zachowanie się żelaza w roztworze NaOH
   Ochrona przed korozją, 51 (4-5) (2008) 230.

The results were also presented at four international and six national conferences.